Al-Farabi Kazakh National University

U.A. Joldasbekov Institute of Mechanics and Engineering

UDC 004.8(043)

as manuscript

IBRAYEVA ARMAN SAYATQYZY

Synthesys of Leg Mechanism and Optimal Design of Walking Robot

8D07117 – Robotic systems

Thesis for the degree of Doctor of Philosophy (PhD)

Local supervisor: Jamalov Nutpulla,
candidate of technical sciences,
assoc. prof.

Foreign supervisor: Sarosh Patel,
PhD, assoc. prof.

Republic of Kazakhstan,
Almaty, 2023

NORMATIVE REFERENCES

The following references to standards are used in the thesis:

State Educational Standard of the Republic of Kazakhstan 5.04.034-2011: compulsory state education standard of the Republic of Kazakhstan. Postgraduate education. Doctoral studies. Basic provisions (amendments dated August 23, 2012 No. 1080);

GOST 7.32-2001. Structure and rules for preparing a report on research work.;

GOST 7.1-2003. Bibliographic record. Bibliographic description. General requirements and rules of compilation.

CONTENTS

INTRODUCTION

The proven advantages of walking mobility for traversing complex terrain have significantly fueled interest in walking-based movers (Antonov, 2018), (Ignat`ev, 2016), (Cherny`shev, 2018), (Ceccarelli, 2016). A walking robot can "step over" obstacles, which further increases its permeability. Thus, the use of a walking method of movement becomes indispensable for working in areas of destruction. In addition to high maneuverability and adaptability—the ability to move the vehicle body smoothly despite uneven terrain—another inherent advantage of walking robots is lies in the unique nature of the interaction between their supporting limbs and the load-bearing surface. This includes the capability to traverse areas with weak soil bearing capacity. Unlike a wheels or tracks, the legs of a walking robot experience minimal resistance from the environment when moving, which reduces slipping and often eliminates the wheelspin.

Increased interest in walking robots can be observed in connection with the rapid growth of agricultural robots, since walking robots cause minimal damage to the load-bearing surface. Thanks to their discrete track, as opposed to a continuous one, soil erosion is significantly reduced, and the risk of ravine formation is virtually eliminated, highlighting the positive environmental properties of walking movers. Furthermore, the walking principle of movement minimizes ground pressure, significantly lower than that of tracked or wheeled vehicles (Cherny`shev, 2018), (Wang, 2017).

As walking robots (WRs) evolve beyond the stage of laboratory models, it comes important to develop new design principles based on the requirements of optimality across various criteria. Main areas of focus include the problem of power consumption and power autonomy, speed and cost-effectiveness of the control systems, optimal technical parameters for control and traffic safety. Effectively addressing these challenges will pave the way for broader applications, enabling efficient movement over rough terrain and the execution of technological tasks in remote, hard-to-reach, or hazardous environments.

The research into walking vehicles, particularly in the context of robotics and automated systems, can be traced back to several key developments and works over the past few decades. One of the earliest examples of a walking vehicle was the "Walking truck" or "Cybernetic Anthropomorphous Machine," developed by General Electric in the 1960s. This quadrupedal machine, designed by Ralph Mosher, was an experimental project funded by the U.S. Army. (Mosher, 1969) Another early example was the "Runabout," developed by Ichiro Kato at Waseda University in Japan. This was part of the Waseda Bipedal Humanoid projects, which began in the late 1960s and continued into the 1970s. (Takanishi A., 1985) Research in bipedal robots, which are a subset of walking vehicles, saw significant growth during the 1980s and 1990s. Universities and corporations, particularly in Japan, made notable advancements. Honda's work on prototypes that eventually led to ASIMO (first revealed in 2000) is a prime example (Shigemi S., 2008).

The most famous project of Marc Raibert and his group, the BigDog project (Ignat`ev, 2016), (Ceccarelli, 2016), (International Federation of Robotics, 2017), was developed as an auxiliary robotic transport for the ground forces and was funded through DARPA. The analysis shows that leading technologically developed countries have made significant progress in the development of military robotic systems capable of conducting combat operations without human intervention with a high degree of autonomy (Serov, 2019), (Cherny`shev, 2020), (Cherny`shev, 2018). In the near future, robotic systems for various purposes will confidently take their place in the ground, sea and even space spheres of military operations. The robot is capable of moving over rugged terrain, carrying up to 150 kg of cargo at speeds of up to 7 km/h and overcoming a slope of up to 35 degrees.

Another project of the same company, the four-legged robot Cheetah, capable of reaching speeds of up to 45 km/h, was also developed with financial support from DARPA under the Maximum Mobility and Manipulation program. Cheetah has a flexible "back" that helps achieve high speed of movement.

The Russian “analogue” of a walking robot of this type is the military robot “Lynx” BPMBR400. The developer is the Kovrovsky All-Russian Scientific Research Institute “Signal” (Kovrov, Russia), conducting developments within the framework of R&D Lynx-BP (Voenny`j robot VNII Signal, 2017), (Katalog nazemnyx). It is planned to produce in various modifications, depending on the functional purpose - reconnaissance equipment, means of destroying explosive devices, a platform for transporting ammunition and ammunition, means of evacuating the dead and wounded from the battlefield, means of reconnaissance of mine-explosive barriers, weapons for fire support of units, delivery of equipment (Briskin, 2018), (Serov, 2017), (Cherny`shev, 2018). (More detailed specifications from the technical specifications can be found on the website (Ry`s`-BP, 2017)).

However, existing approaches are based on active coordination of motor operation and feature complex hierarchical control system (4 17-19). In addition, engines operate in intensive acceleration and deceleration modes and, leading to unreasonably low efficiency (Ignat`ev, 2016), (Briskin, 2019), (Mantis Hexapod, 2019). However, by placing the issues of efficiency, simplicity, and availability of technical means at the forefront, the irrationality of universal designs becomes beyond doubt. The structural solution of most WRs is also rendered irrational due to structural redundancy and multiple static uncertainties. In such systems, the number of active drives often exceeds the number of degrees of freedom. For instance, anthropomorphic WRs, which aim to replicate human bipedal walking and running, utilize a dynamic gait but are quite costly (Ceccarelli, 2016) despite achieving remarkable results (e.g., bipedal WRs like the Atlas type (Ceccarelli, 2016), (Kakiuchi, 2017), (Takasugi, 2017), etc.). This observation is equally applicable to quadrupedal (Hu, 2016), (Ding, 2015), (Da Gou, 2017) and hexapodal (Mantis Hexapod, 2019) structural schemes, which are characterized by the complexity of their multi-level control systems, significant energy expenditure to support body weight, and the reversible operating modes of engines.

An alternative to “biomorphic” designs is the use of orthogonal propulsion schemes. This separation of engines is important from the point of view of increasing efficiency and simplifying the control system. The weight load from the body falls only on the adaptation motor locking devices. However, the disadvantage of such propulsors is the use of reciprocating drives and the presence of significant lateral loads in translational pairs. The use of rectilinear guide mechanisms makes it possible to achieve kinematic decoupling of movement and separation of engine functions, when the main engine is responsible for the rectilinear translational motion of the body, another group of drives is responsible for adaptation to uneven terrain, and a third group is responsible for turning and maneuvering. Pantograph-type copying mechanisms are considered promising (Hu, 2016; Ding, 2015), which make it possible to quite simply adjust the height of trajectories and provide a linear transmission ratio between the input and output generalized coordinates. This is how, for example, the walking robot "with adaptive suspension" Adaptive Suspension Vehicle by Professor K. Waldron and others was built. The disadvantages of such designs include significant force effects on the driving organs, the use of translational pairs loaded with lateral load.

Thus, the search for alternative principles to traditional principles for designing mobile robots based on a walking platform is an urgent problem. At the same time, most existing walking robots with six (Hexapod) and four (Quadruped) supporting limbs are of the anthropomorphic type and are characterized by a complex multi-level control system, high energy consumption and low rigidity. The use of rectilinear guide mechanisms in the SLM can significantly improve these indicators, however, it is necessary to optimize the geometric parameters based on the isotropy criterion. Based on the above, the problem of optimal design of a walking vehicle and its propulsion remains **relevant** from the point of view of minimizing energy consumption and simplifying control (and, as a consequence, increasing the speed of the control system).

- Purpose of the work: development of synthesis methods for a leg mechanism and optimization of the WR parameters based on the functional decomposition method, which will simplify the control system and ensure movement over rough terrain with minimal energy consumption.

- Object of study: all-terrain walking robot;

- Subject of research: optimal structural-parametric synthesis of the kinematic scheme of a walking robot;

- Research methods: robot design methods, analytical and numerical methods for optimization synthesis of machine mechanics;

- Theoretical and practical significance of the study: optimization of the structural and kinematic parameters of a walking robot, development of a methodology and determination of the optimal structure and parameters of a walking robot;

According to the research plan, the research work consists of several **tasks**, each of which focused on certain applied and theoretical aspects of the study.

- Review and survey of research in the field of walking robots and analysis of the main types of propulsors

- Synthesis of a walking robot based on functionally independent structural modules.

- Development of synthesis/analysis methods and PC programs.
- Optimization of leg mechanism parameters.
- Development of a mechanism for adaptation to unevenness of the bearing surface
- Study of turning modes and structural-parametric synthesis of turning and maneuvering mechanisms.
- Development of design documentation
- Development and experimental study of a laboratory model of the WR.

- The novelty of the study lies in the development of methods for the synthesis and optimization of structural and metric parameters of the WR based on the functional separation of engines, which allows

- simplify the coordination of the legs and carry out movement with a minimum number of motors, the lowest energy consumption and the use of the simplest possible controls;
- solve the problem of adapting each foot to surface unevenness individually and independently of the main control unit;
- solve the problem of excessive constraints of existing structures and eliminate parasitic loads on actuators associated with multiple static uncertainties;
- eliminate additional energy costs for feet slippage and reducing the reaction in the joints when turning.

The methods of the synthesis of mechanisms with parallel topology and the methods of approximation synthesis of planar linkages were used.

The reliability and validity of the scientific provisions, conclusions and results of the dissertation are **confirmed** by the correct formulation of the problem and the use of well-known mathematical methods, methods of theoretical mechanics, methods of studying mechanisms and machines, and methods of numerical research and validated on the experimental prototype.

Connection of the dissertation work with other research works. This dissertation work was carried out under the grant scientific project of the Ministry of Education and Science of the Republic of Kazakhstan for 2020-2023 "Optimal design of an adaptive walking robot with an intelligent control system" (Grant No. AP09259589).

Publications. The author wrote 12 works on the topic of the dissertation, including 1 patent of the Republic of Kazakhstan; 5 publications in scientific journals and proceedings of international conferences included in the Scopus database; 5 publications in the proceedings of domestic and foreign scientific international conferences (Omarov et al., 2024; Ibrayev et al., 2023; Ibrayev et al., 2022; Ibrayev et al., 2023; Rakhmatulina et al., 2020; Rakhmatulina et al., 2022; Ibrayev et al., 2021; Ibrayev et al., 2021; Ibrayev et al., 2020; Tuleshov et al., 2019; Ibrayev et al., 2019; Ibrayev et al., 2019; Ibraev et al., 2018; Ibrayev et al., 2022).

Personal contribution of the author. The main results of the research carried out in dissertations were obtained by the author independently.

The thesis structure and volume. The thesis contains a Title page, Normative References, a Table of Contents, an Introduction, six Main sections, a

Conclusion, Bibliography and Appendixes. The total volume of theses is 102 pages, including illustrations and tables. Section 1 analyzes the global trends of the recent years on WRs, and indentifies promising areas of research; Section 2 introduces kinematic scheme of a WR with decoupled motion and separation of motor functions; Section 3 presents developed methods and algorythms of structural-parametric synthesis across multiple criteria, and the obtained optimal design of the leg mechanism. Section 4 presents studies on the turning/maneuring mechanism and optimization of the metric parameters of the WR on the basis of isotropy criterion. In Section 5, presented is the design of the independent adaptation mechanism to unevenness of surfaces. Section 6 describes the design and development of the physical prototype of the (AWR).

Aknowledgements

I would like to extend my deepest gratitude to my father, Sayat Ibrayev, for his unwavering support and invaluable guidance throughout my academic journey. Special acknowledgment is also reserved for my entire family, whose **enduring love** and steadfast belief in my potential have been fundamental sources of encouragement and inspiration.

Furthermore, I am immensely grateful to my supervisors, **Dr.** Jamalov Nutpulla and **Dr.** Sarosh Patel, for their insightful feedback, and constant encouragement. Their mentorship has significantly shaped my research and academic growth.

1 An examination of recent global trends in walking robot development and prospective avenues for advancement

1.1 Leading teams abroad

The leading groups in the field of research and development of walking robots are (Ignat`ev, 2016; Ceccarelli,, 2016; World Robotics, 2017): Boston Dynamics (USA), Ghost Robotics (USA, Philadelphia), Case Western Reserve University Robot Laboratory (USA), Massachusetts Institute of Technology, Institute of Mechanical Engineering named after A.A. Blagonravov RAS (Moscow), Volgograd State Technical University, FSPC "Titan-Barricades", JSC Central Design Bureau "Titan" (Russia), Tokyo Institute of Technology (Dept. Of Mechano-Aerospace Engineering, Japan, Laboratory of Professors Shigeo Hiroze and Edward Fukushima, University of Tokyo (Dept. of Mechano-Informatics, group of Professor Noriaki Takasugi), German Research Center for Artificial Intelligence (Germany, Deutsches Forschungszentrum für Künstliche Intelligenz GmbH, Robotics Innovation Center), Information Technology Research Center FZI (Karlsruhe, Germany), Chinese defense company NORINCO, Shanghai Jiao Tong University (China, Shanghai Jiao Tong University), Institute of Technology and Engineering, Changchun, China, University of Cassino (Italy, group of Professor M. Ceccarelli), Italian Institute of Technology (Genoa, Italy, Advanced Robotics Department). Detailed review material is presented in the monographs of Professor Marco Ceccarelli (University of Cassino, Italy) (Ceccarelli, 2016), Professor Kenneth Waldron (Ohio State University), G. Gent (Germany), in a number of specialized issues of the international journal “The International Journal of Robotics Research” (Figure 1.1).

The Chinese military company NORINCO has developed its version of BigDog, which they called Da Gou (Mountainous Bionic Quadruped Robot) (Da Gou, 2017). As the name suggests, this “robot mule,” like previous analogues, is also bionic, that is, based on the desire to copy biological principles of movement organization and, accordingly, is very expensive. The same applies to other well-known robots of the quadruped and hexapod type, which have a musculoskeletal mechanism of a “universal” type: the Italian four-legged WR of Professor S. Semini HyQ2max-Robot (Italian Institute of Technology, Genoa) (Semini, 2010), the ultra-modern German robot MANTIS (Multi-limbed walking robot for mobile manipulation in unstructured environments) (Mantis, 2019), “Multi-limbed walking robot for mobile manipulation in unstructured environments”, developed by the German Research Center for Artificial Intelligence, Robotics Innovation Center (Germany) (Carrió, 2018; Ceccarelli, 2016), Finnish MECANT and Plustech machines for real transport and technological operations weighing more than one ton (Tam, 2020; Li, 2012), the German six-legged WR LAURON V, developed by the Research Center for Information Technologies FZI (Karlsruhe, Germany) and others (Ceccarelli, 2016; Kim, 2017; Mantis, 2019; Briskin, 2018; Chen, 2017; Fernández, 2018).

However, it should be remembered that existing approaches based on active coordination of motor motion use a complex hierarchical control system (Ceccarelli, 2016; Kim, 2017; Sharbafi, 2017; Yang, 2017), and the operation of motors in intensive acceleration and deceleration modes causes unreasonably low efficiency (Ignat`ev, 2018; Briskin, 2019; Mantis, 2019). Anthropomorphic walking robots that seek to replicate human bipedal walking and running and use a dynamic gait (statically unstable) are extremely expensive (Ceccarelli, 2016) (despite the fantastic results demonstrated by bipedal (bipedal) robots such as Atlas (Boston Dynamics) and others (Kakiuchi, 2017; Takasugi, 2017; etc.)).

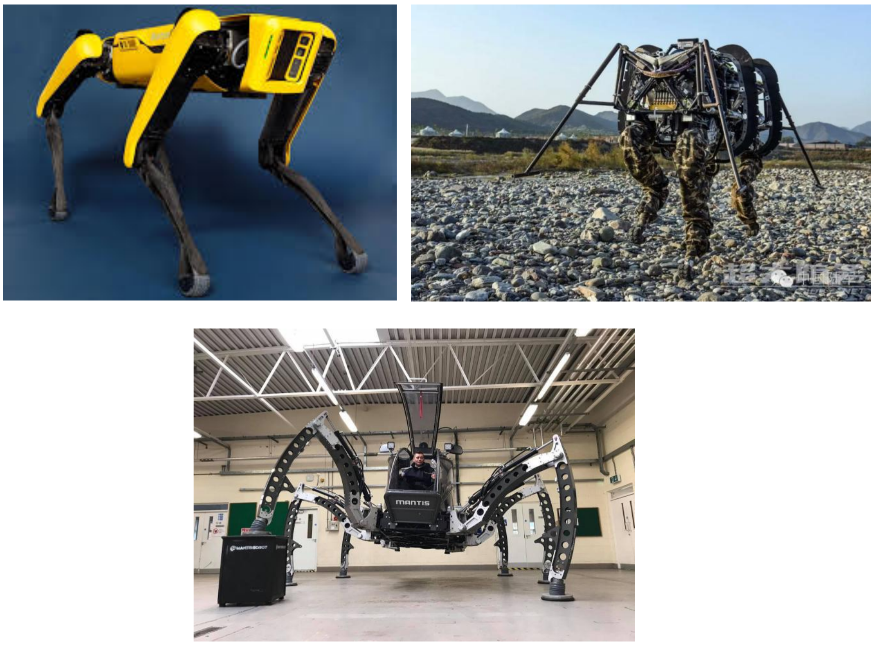

Figure 1.1 – a) Spot, Boston Dynamics (USA) (frobotsguide.com);
b) – Quadruped robot Da Gou, NORINCO (China) (army-guide.com) ;
b) – Hexapod-robot MANTIS, German Research Center for Artificial Intelligence, Center for Innovation in Robotics (Germany) (laughingsquid.com)

The same largely applies to Quadruped (Hu, 2016; Ding, 2015; Da Gou, 2017) and Hexapod (Mantis, 2019) structural patterns. Such robots have virtually unlimited maneuvering capabilities and high maneuverability. Therefore, it is most advisable to use them, for example, in destruction zones to move cargo and technological equipment over extremely difficult terrain. However, the complexity of the multi-level control system, high energy consumption to maintain the weight of the hull and reverse operating modes of the engines in such machines impose restrictions on transport speed and payload. The irrationality of the structural solution of most walking robots is also associated with structural redundancy and multiple static uncertainty. The number of active drives in such systems is much greater than the number of degrees of freedom of the system. So, for example, in robots like Hexapod (Mantis, 2019) (in which each leg is driven by three actuators), when gaiting in a three-step manner, the number of degrees of freedom is six, while the active actuators are 9. (This is taking into account only the “supporting” legs; if all legs are in the support phase, then the number of active drives is 18, and the number of degrees of freedom of the system is 6). As a result, parasitic loads arise in the engines (motors work “against each other”), reactions in the joints increase, foot slipping, etc. Thus, one can observe, on the one hand, the virtuoso abilities of robots in performing complex movements, at the same time, the irrationality of most existing anthropomorphic and biomorphic robot designs from a mechanical point of view.

This state of affairs is explained by the fact that advanced research teams, such as Boston Dynamics and others, pursued the main goal of copying the biological principles of organizing limb movement and demonstrating the “ultimate” capabilities of the robot (Sharbafi, 2017), and the issue of optimal mechanical design remained in the background. The main result of these studies and full-scale tests is a brilliant answer to the question: what mobility tasks can be performed by technical controls and how far can one go when implementing the principles of bionics based on modern robotics technologies. However, at this stage, the main trend is the search for alternative concepts to traditional concepts for creating robots, taking into account the requirements of efficiency, simplicity and availability of low-cost technical means (Briskin, 2019; Miroshkina, 2018; Komoda, 2017; Wang, 2018; Zang, 2017).

1.2 Comparative analysis of the main ideas in the design of walking robots

Modern trends clearly show that it is the rational mechanics of the designed system that largely determines its future operational characteristics, significantly affects the quality of the control system, and allows reducing the cost of the robot. The implementation of the traditional principle, of course, can be justified by the specifics of the functional task being performed. For example, for working in a destruction zone, when the main criterion is a high degree of maneuverability. However, in most cases, the problem can be solved by cheaper, simpler and more reliable means - primarily due to the developed mechanical part of the robot. Walking robots are not widely used due to the complexity of the movers and low energy efficiency (Komoda, 2017; Briskin, 2020; Kalinin, 2019; Miroshkina, 2018).Therefore, one of the main tasks of increasing the operating efficiency of walking robots is to reduce power losses: since for walking robots the power expended to set them in motion, in the general case, is proportional to the cube of the speed, and energy losses, accordingly, to the square. Some methods for solving this problem are also known: by introducing energy recuperators, by abandoning the uniform movement of the center of mass of the robot body while maintaining the average speed, and others.

Therefore, for example, the use of orthogonal-type support-locomotion mechanisms (SLM) makes it possible to achieve kinematic decoupling of movement and separation of engine functions, when the main engine is responsible for the rectilinear translational motion of the body, another group of drives is responsible for adapting to uneven terrain, and the third group is responsible for turning and maneuvering. The implementation of this principle makes it possible to build a significantly cheaper control system, achieve optimal motion characteristics, increase the efficiency of the system and, thus, forms the basis of an alternative principle for designing walking robots in relation to “biomorphic” designs (Ignat`ev, 2016; Mantis, 2019; Miroshkina, 2018; Komoda, 2017).

Providing the required movement characteristics is largely determined by the rational choice of the propulsion system and the corresponding organization of gaits (Ceccarelli, 2016; Briskin, 2018; Chen, 2017; Briskin,, 2019).

Thus, copying or orthogonal propulsors have all the advantages of insectomorphic type propulsors (which are open kinematic chains), at the same time, they have a number of additional advantages. In such propulsors, the main linear translational movement of the machine body is carried out by the main engine, and the weight load from the body falls only on the engine locking device. Such “gravitational independence” of the main drive of horizontal movement is important from the point of view of increasing efficiency and simplifying the control system. However, the disadvantage of such propulsors is the use of reciprocating drives, as well as the presence of significant lateral loads in translational pairs. The use of pantograph-type copying mechanisms is considered promising: the advantages of such a scheme are a fairly simple solution for adjusting the height of trajectories, a linear gear ratio between the generalized coordinates of the mechanism and the Cartesian coordinates of the reference point. Based on such a mechanism, for example, the legs of the walking robot of Professor Marco Ceccarelli, the Adaptive Suspension Vehicle (a six-legged model) of the Ohio State University (Figure 1.2), the walking apparatus of Professor Shigeo Hiroze (Tokyo Institute of Technology), etc. are built. However, the disadvantage of such designs are significant force impacts on the driving organs, the use of translational pairs loaded with transverse load. Translational kinematic pairs can again be eliminated by using articulated rectilinear guide mechanisms (Ceccarelli, 2016), however, as already indicated, the presence of a similarity coefficient leads to a deterioration in positioning accuracy. More preferable, as mentioned above, is the approximate Cartesian mechanism proposed by scientists from the IMMash Ministry of Education and Science of the Republic of Kazakhstan, which is a hinge-lever mechanism (Figure 1.3).

These factors explain the increased interest in trajectory-type movers that provide a given step cycle, and therefore interest in the problems of synthesizing musculoskeletal mechanisms is being revived (Wang, 2018; Zang, 2017; Buskiewicz, 2018; Geonea, 2019; Ghassaei, 2016; Savin, 2017; Selvi, 2017; Shen, 2019; Soh, 2015; Veerendrakumar, 2016). How important the advantages of such mechanisms are is clearly demonstrated by the project of the four-legged robot “The Ghost Minitaur” (developed by the Philadelphia startup Ghost Robotics), one of the most successful in terms of maneuverability (Ghost Robotics, n.d.; Blackman et al., 2016). Despite the fact that the robot has shown the advantages of the walking method of movement over tracked and wheeled ones, the robot propulsion does not have the ability to adapt to uneven supporting surfaces and therefore does not provide horizontal uniform movement of the body. Thus, the main purpose of the automatic suspension is not fulfilled. Therefore, the use of lever mechanisms, especially hinged-lever mechanisms - generators of rectilinear trajectories (approximate or accurate) can significantly simplify the leg drive (Gao et al., 2017; Geonea and Tarnita, 2017; Pop et al., 2016;

Selvi and Ceccarelli, 2020; Shao et al., 2016; Shen et al., 2018; Tsuge et al., 2016; Xu et al., 2020).

Figure 1.2 – Pantograph Leg Mechanism of Adaptive Suspension Vehicle. Ohio State University, USA, Courtesy of Professor Kenneth Waldron (cyberneticzoo.com)

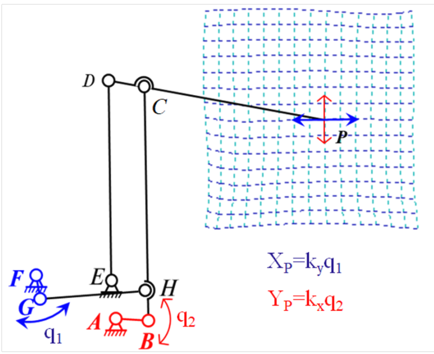

Figure 1.3 – Cartesian 7R robot with the decoupled motion of end-effector coordinates

Trajectory-type propulsors have advantages over other types of walking propulsors due to lower energy consumption, the absence of motor reversal, a simpler control system, and high speed of movement. The very idea of using rectilinear guiding mechanisms is not new (A.P. Bessonov, N.V. Umnov, K. Hunt, K. Waldron, etc.) (Figure 1.4), however, a number of problems remain unresolved; here we will only point out the main difficulties. Thus, many authors have studied in detail Theo Jansen's mechanism (Gao et al., 2017; Geonea and Tarnita, 2017; Pop et al., 2016; Selvi and Ceccarelli, 2020; Shao et al., 2016; Shen et al., 2018; Tsuge et al., 2016; Xu et al.,

2020) and attempts have been made to improve its various characteristics from the point of view of use in walking machines. Thus, work (Xu et.al, 2020) describes a method for synthesizing a mechanism based on two criteria, which made it possible to improve the quality and accuracy of reproducing the step cycle of the natural movement of a human leg. Komoda tried to achieve adjustability of the foot trajectory of the Jansen mechanism by changing the position of the fixed axis (Komoda et al., 2017), and also conducted a comparative study of the Chebyshev and Klann mechanisms. Similar studies were also carried out by Nansai, Zang H.B. (Zang et.al, 2017), Wang C.Y. (Wang et.al, 2018) and other researchers, by changing the lengths of binary links, they were able to obtain adaptive mechanisms with two or more degrees of freedom, significantly expanding the possibility of practical use of the prototype - Theo Jansen mechanism. Wang C.Y. created a mathematical model that allows us to study the influence of leash lengths on the kinematic and dynamic characteristics of the leg mechanism. However, the range of adjustment of the foot trajectory is quite small compared to the length of the straight section of the trajectory. In the following sections it will be shown that these results can be significantly improved by using approximation synthesis methods: even with the help of simple four-bar hinges it is possible to achieve a significant range of adaptation.

a)

Figure 1.4 – a) Federal Research and Production Center "Titan-Barricades" (based on trajectory-generator), JSC CDB "Titan" (Russia) ; b) Walking machine with a trajectory generator developed by Bauman Moscow State Technical University

1.3 Study of trajectory propulsors

Despite the wide variety of rectilinear guide mechanisms, the requirement for adaptability to uneven terrain makes most of them unsuitable for practical use as propulsors of walking machines. Thus, the precise rectilinear guiding mechanisms of the Pocelle-Lipkin, Hart and more complex inverters are difficult to adjust. It is possible to implement approximately rectilinear parallel trajectories over a fairly wide range of control using articulated four-bar links (for example, modifications of the Roberts mechanism, etc.). However, all these mechanisms do not ensure the constancy of the speed analogs of the reference point along straight sections of trajectories over the entire range of changes in the adaptation height (on different straight trajectories, the speed of movement of the reference point should be the same at the same value of the angular velocity of rotation of the input link). Other articulated four-bars (the Watt mechanism and its modifications, Evans mechanisms related to the Watt mechanism, crane mechanisms, modifications of the Roberts mechanism, etc.) also do not satisfy this requirement and are mainly double-rocker arms.

Much attention has been paid to straight-line crank mechanisms from the “lambda-shaped” family, but their main disadvantage is that the straight section is internal to the mechanism. Strictly speaking, such mechanisms with an internal transfer site exist, and even two solutions are known. However, in the first of them, the crank-rocker mechanism, the height of the transfer section is unacceptably low and the accuracy is poor. Another solution is a two-crank mechanism from the “lambda-shaped” family, described by E. Dykesman. However, they reproduce straight ones less accurately than crank-rocker lambda-shaped mechanisms. This is due to the property of the connecting rod curve (in this case, a cardioid): every straight line perpendicular to the symmetry axis of the connecting rod curve intersects it at no more than four points, whereas in the crank-rocker group there are six such intersections. In addition, in these mechanisms the connecting rod curve “describes” the entire mechanism (all hinges of the mechanism are inside the trajectory) and the transfer section is characterized by significant accelerations. It should also be noted that in these works, the possibilities of regulating the position of the reference point on the connecting rod plane are mainly considered, and the possibilities of regulating any other dimensions have practically not been studied. Leg mechanisms based on a fourth-class mechanism with an adjustable crank length, propulsion schemes in the form of gear-lever and six-link guide mechanisms, mechanisms with non-circular gear transmission, various modifications of crank-slider mechanisms, etc. have also been proposed. Analysis shows that the most difficult thing is to satisfy the conservation condition speeds when adjusting height.

Thus, the question of the capabilities of multi-movement lever systems from the point of view of their applicability in the propulsors of walking vehicles remains open. The capabilities of the simplest four-bar mechanisms have also not been fully explored.

1.4 Developments of Kazakh scientists: the most promising areas of research

The most significant achievements of Kazakh scientists in the development of walking-type mobile robots should be considered the development of analytical and numerical methods for optimization synthesis of walking robot propulsors, taking into account a set of quality criteria, the main of which are minimizing energy costs when moving over rough terrain and simplifying the control system, increasing speed (Ibraev et al., 2019a; Ibraev et al., 2019b; Tuleshov et al., 2020a; Tuleshov et al., 2020b; Ibrayev, 2002; Omarov et al., 2024; Ibrayev et al., 2023; Ibrayev et al., 2023; Rakhmatulina et al., 2020; Rakhmatulina et al., 2022; Ibrayev et al., 2021; Ibrayev et al., 2021; Ibrayev et al., 2020; Tuleshov et al., 2019; Ibrayev et al., 2019c; Ibrayev et al., 2018; Ibrayev et al., 2022). In existing designs of "biomorphic" type walking robots, the main engine power is spent on intensive acceleration and deceleration, which causes low system efficiency. In addition, coordinating the operation of a large number of drives leads to an unreasonably complex control system (for example, in the most famous design of the Hexapod type, the number of such drives reaches 18!), and significant variability of the structure and redundant connections create parasitic loads on the motors and lead to an increase in reactions in the hinges. All these shortcomings are eliminated through rational structural synthesis of a walking robot, optimal design of the structural and geometric parameters of the robot based on motion decomposition and functional separation of motors.

The problem of synthesizing the musculoskeletal mechanisms of walking robots was solved in the works of scientists from the IMMash named after academician U.A. Dzholdasbekov of the Ministry of Education and Science of the Republic of Kazakhstan by two methods:

1) by developing methods for approximation synthesis of adjustable mechanisms, allowing to generate rectilinear horizontal trajectories of the foot at different heights relative to the chassis using an adjustable parameter, i.e. introduction of an additional drive for adaptation to unevenness of the supporting surface;

2) by synthesizing musculoskeletal mechanisms with rectilinear translational movement of the supporting limb, which allows for an unlimited range of adaptation to uneven terrain with obstacles; in this case, the method allows you to generate the required step cycle of the foot, taking into account the optimal transmission of force.

Optimal synthesis of walking robot propulsors made it possible to develop a control system in which the adaptation system for unevenness of the bearing surface operates independently of the main control unit. This leads to significant unloading of the control system, because adaptation of each leg is carried out individually and coordination of their work is not required. As a result of structural optimization, the number of main motors involved in control is minimized, which also has a positive effect on minimizing energy costs for moving over uneven terrain.

Based on the developed methods, a Cartesian pedipulator was obtained for the first time, based on the musculoskeletal mechanism of the leg with complete kinematic decoupling of movement in degrees of freedom, when one drive is responsible for the horizontal movement of the foot, and the other for the vertical lifting/lowering. The only existing analogue is the Sylvester pantograph mechanism, first used by Professor

K. Waldron in the so-called. “car with adaptive suspension” - a five-ton walking robot from Ohio State University (Adaptive suspension vehicle, Professor Kenneth Waldron) (Song Shin-Min and Waldron Kenneth J., 1989). However, difficulties arise here with the manufacture of the drive translational kinematic pair due to large lateral loads on the guides, with limited service life of the hydraulic cylinder. The uniqueness of the mechanism proposed by the Kazakhstanis is that it uses only rotational kinematic pairs (Ibrayev, 2002).

Methods have been developed for the synthesis of an exoskeleton of the lower limb, operating on the principle of gravitational independence of engines, in which the main drive of horizontal movement operates with minimal energy consumption for moving the body and payload (Ibrayev et al., 2023; Ibrayev et al., 2021). An additional drive for adjusting the height of the foot and adapting to unevenness of the bearing surface is equipped with a locking mechanism that holds the weight of the body and payload. Thanks to this, the height drive also consumes minimal power and the exoskeleton as a whole has the simplest control system.

1.5 The most promising areas of research

Modern trends in the development of automation and robotics make it urgent to develop "modern concepts for the analysis and synthesis of mechanisms, machines and their complexes in relation to solving problems of robotics and biomechanics, mathematical modeling when conducting research in the field of machine mechanics and robotics" (academician K.V. Frolov). Research conducted at the IMMash named after academician U.A. Joldasbekov is of significant importance in light of the growing trend of abandoning blind copying of "biological" principles when designing robotic systems and searching for alternative ways to design robots with optimal mechanics of actuators. A new class of mechanisms for manipulators and robots with closed kinematic chains has been developed, allowing to achieve the most rational combination of mechanical and electronic control components of a robotic system.

The fundamental directions developed by Kazakh scientists correspond to global trends in the field of service robotics and require further development. In contrast to the traditional principle of constructing walking robots of the anthropomorphic and insectomorphic type, using active suspension and characterized by low efficiency, the concept proposed by IMMash scientists is based on the decomposition of the robot's movement into functional components and separation of the functions of the motors, which makes it possible to obtain optimal structural and metric parameters of the robot from the point of view energy consumption and building the most efficient control system.

Most foreign robots such as Quadruped and Hexapod, including American robots Boston Dynamics (BigDog, MITCheetah), despite the demonstration effect, were developed according to the principles of bionics, which is inherently expensive, since how the main engine power is spent on intense acceleration and braking. The Russian walking robot "Lynx," like the Chinese DaGou, the Italian HyQ-Robot, etc., also belong to the "biomorph" category and largely repeat the project of the Boston Dynamics company. Rather, these robots are built to demonstrate the extreme capabilities of robotics technology, i.e. show what complex movements and maneuvers can be performed using existing technical controls. However, in practical use, these designs do not meet the requirement of optimality, primarily from the point of view of efficiency and due to the need to coordinate a huge number of drives. At the same time, significant variability in the structure of walking robots and redundant connections create parasitic loads on the motors and lead to an increase in reactions in the joints.

The IMMash research team proposes to eliminate all these shortcomings primarily through rational design of the mechanical structure of the robot. Methods for optimal synthesis of walking robot mechanisms based on decomposition of movement into functional components and separation of motor functions are significantly new and meet global development trends, allowing the robot to move and rotate with a minimum number of motors, with the least energy consumption and using the most effective robot motion control system, to solve the problem of redundant connections of existing structures and eliminate parasitic loads on engines associated with multiple static indeterminacy, eliminate additional energy costs for slipping legs and reduce reactions in the joints of the legs when turning.

The research being carried out is important on a national scale, because For the first time, a Kazakh walking robot will be created for locomotion in rough terrain and areas with weak bearing capacity of the soil. The results open up broad prospects in the development of service and agricultural robotics, in the development of domestic robots for emergency departments when working in destruction zones, for mining and rescue work, in railway track machines, in medical robots, and in mobile robots for military purposes.

According to the International Federation of Robotics (IFR), a steady increase in the ratio of service robots to industrial robots can be observed. This trend in global robotics is important for Kazakhstan with undeveloped industrial robotics. Kazakhstan is not even represented in the annual IFR ranking of the number of robots used per 10 thousand workers, so in order to at least equal Russia, Kazakhstan needs to have several thousand robots. But at the same time, the Science Fund mainly supports completed developments and technologies that are ready for commercialization; Kazakh scientists do not have to finance these promising developments in the field of robotics.

Based on the above, comprehensive support from the state for key participants in the robotics platform, including increased investment in fundamental and applied research in the field of robotics, adaptation of the best world experience in this industry should be considered a priority for increasing the competitiveness of the Republic of Kazakhstan.

1.6 Conclusions on Section 1

Among the various ideas considered for the design of the WR legs, three main types can be identified, each with different advantages. The advantage of WRs of biomorphic and anthropomorphic types is their versatility, i.e., the ability to move in any desired direction and a high degree of maneuverability, making this robot very convenient, for example, in areas of destruction. In this sense, orthogonal-type propellers of walking robots have all the advantages of a universal biological design (Hexapod type or four-legged Quadruped), which also refers to the type of propulsion system with a gravitationally independent suspension. However, the motors perform swinging movements, and propellers based on trajectory-generating mechanisms are more preferable in terms of energy consumption for translational movement of the body/hull due to the rotation of the main crank motors with constant angular velocity.

2. Kinematic scheme of a walking robot with decoupling of movements by degrees of freedom and separation of motor functions

The question of the organization of locomotion on artificial limbs has long attracted the attention of researchers (N. Umnov, 1996; Baigunchekov et al., 2017; Baigunchekov et al., 2018; Kim and Wensing, 2017; Tedeschi and Carbone, 2014). Traditional designs of biological walking robots are based on the desire to blindly copy the musculoskeletal functions of living organisms and are characterized by a complex, multi-level control architecture. An alternative to "insectomorphic" designs is an approach based on the abandonment of universality in favor of optimal motion characteristics and ease of control by separating the functions of the motors, when each drive has a specific functional purpose (Serov et al., 2019; Chernyshev et al., 2020; Chernyshev and Arykantsev, 2018; Voennyj robot VNII Signal, 2017; Briskin et al., 2018; Serov et al., 2018; Serov et al., 2017). For example, the use of SLMs of an orthogonal type makes it possible to achieve kinematic decoupling of movement and separation of engine functions, when the main engine is responsible for the rectilinear translational motion of the body, another group of drives is responsible for adapting to uneven terrain, and the third group is for turning and maneuvering. The objective of this work is to show that a rational block diagram of the design being developed can significantly simplify the control of the movement of a WR by minimizing the number of motors responsible for turning the machine. A method for turning the WR, carried out by a minimum number of drives, and a kinematically equivalent scheme of the WR are proposed to simplify the study of motion when turning.

2.1 Decoupling of movements and separation of functions of the walking robot motors.

In traditional designs of universal-type walking robots, all drives are simultaneously involved in organizing movement both during rectilinear translational movement of the body, and during rotation/maneuvering and adaptation to unevenness of the load-bearing soil. The work (Wettergreen & Thorpe, 1992) is devoted to the study of the modes of rotation of the WR during the “three-point” gait, when two main gaits are used for turning: circular and rotating. A similar approach for various types of gaits was also used in works (Ryan & Hunt, 1985; Song et al., 1984) within the framework of the traditional insectomorphic robot design. However, the irrationality of the structural solution of most WR is associated not only with the complexity of management, but also with structural redundancy and multiple static uncertainty (Figure 2.1). The number of active drives in such systems is much greater than the number of degrees of freedom of the system. Most of the standard structures (quadrupeds and hexapods) have three or four motors on each leg (Table 2.1). So, for example, in a Hexapod-type WR (in which each leg is driven by three motors), during so called “tripod gate”, the number of degrees of freedom is six, while the active actuators are 9. (This is taking into account only the “supporting” legs; if all legs are in the support phase, then the number of active drives is 18, and the number of degrees of freedom of the system is 6). As a result, parasitic loads arise in the engines (motors work “against each other”), reactions in the joints increase, foot slipping, etc.

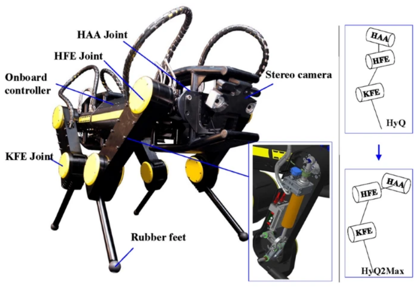

a)

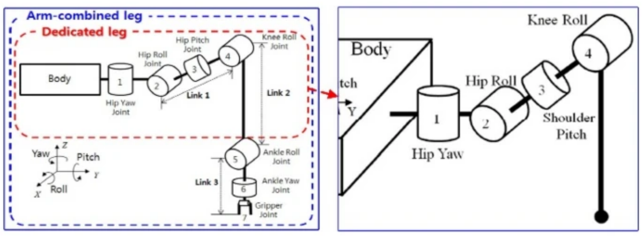

b)

Figure 2.1 – Structure of classical WR legs: a) – quadruped: 3 motors per leg;

b) – hexapod: 4 motors per leg (He & Gao, 2020).

Table 2.1 – Parameters of the most well-known WR (He & Gao, 2020)

Name of the Robot	*D* (m)	*G*	*V* (m/s)	*W* (kg)	*PL* (kg)	*DOF*	*Fr*	*f*	*A*
BIONIC QUADRUPED [61]	1.2 × 0.38 × 1 *(L × W × H)*	Trot	0.83	120	–	4/ leg	–	0.7	Hy
SCALF-I [62]	1 × 0.4 × 0.68 *(L × W × H)*	Trot	1.8	123	80	3/ leg	–	1.8	Hy
HyQ [65]	1 × 0.5 × 0.98 *(L × W × H),0.68(l)*	Trot	2	80	–	3/ leg	0.6	2	Hy/ E
Star1ETH [70]	0.6(L),0.49(*l*)	Bound	1	23	25	3/ leg	0.21	1.6	E
ANY mal [73]	–	Free gait	1	30	10	3/ leg	–	–	E
MIT cheetah I [74]	–	Trot-running	6.1	33	–	2/ leg	–	–	E
Quadro [58]	0.9*(L)*	–	0.2	35	3	–	–	0.23	E
HUBODOG [58]	0.8 *(L)*, 0.6 *(l)*	Trot	0.55	42	24	3/ leg	0.05	0.69	E
Big Dog −1 [58]	1 × 0.3 × 0.8 *(L × W × H)*	Trot Run	1.8	90	50	4/ leg	–	1.8	Hy
Big Dog −2 [58]	1.1 × 0.3 × 1 *(L × W × H)*	Bound	3.5	109	154	4/ leg	–	3.18	Hy
LS3 [81]	1.7*(H)*	Trot	–	590	181	3/ leg	–	–	Hy
LittleDog [84]	0.3 *(L)*		0.25	2.85		3/ leg	–	0.84	E
Cheetah [85]	1.7*(H)*	Gallop Run	12.5	–	–	3/ leg	–	–	–
Wild cat [86]	1.17*(H)*	Trot, bound Gallop,	8.8	154		3/ leg	–	–	Hy
SPOT [87]	1.1 × 0.5 × 0.84 *(L × W × H)*	–	1.6	30	14	3/ leg	–	–	E

D: Dimension(m); *L*: Length(m); *W*: Width(m); *H*: Height(m); *l*: Leg Length(m); *G*: Gait; *v*: Speed(m/s); *W*: Weight(kg); *PL*: Pay Load(kg); *DOF*: Degree of Freedom; *A*: Actuator, *m*: meter, *m/s*: meter per second, *Normalized Speed(NS)* : Speed/Body length, *Payload Capacity(PLC) (%)* $=\frac{Payload}{Weight}$, *Normalized Work Capacity(NWC)* : Normalized Speed × Payload Capacity, f_r: Froude No $= v^2/2gl$,*Hy*: Hydraulic, *E*: Electric , *F* :Stride per Second.

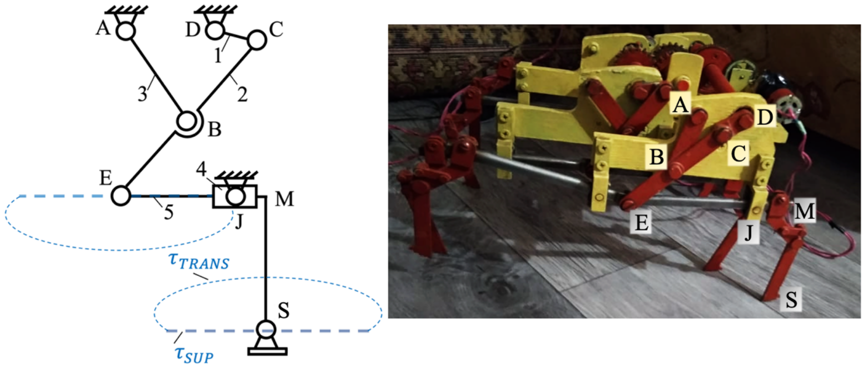

a)

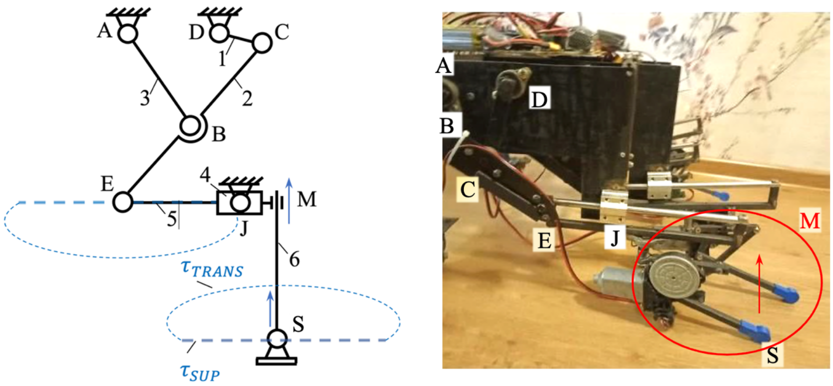

b)

Figure 2.2 – Model of a walking apparatus using a straight-line guide mechanism as a propulsion device.

In Figure 2.2a, depicted is an initial prototype developed to demonstrate the capability of providing rectilinear translational motion of the body. An additional linkage *EJM* was incorporated into the 4-bar mechanism *ABCD*. As the crank's rotation angle φ_{AB} varies within the limits of $\varphi_0 \leq \varphi_{AB} \leq \varphi_0 + \Phi_{sup}$, $\Phi_{sup} > \pi$, where Φ_{sup}, defining the "duration" of the support phase (SPh), the connecting rod *EM* undergoes rectilinear translational motion. Consequently, all points on this linkage trace identical trajectories.

By connecting a vertical pair *M* to this 5th link, adaptability to uneven surfaces is ensured without compromising the rectilinearity of the body's motion. Figure 2.2b illustrates another leg mechanism of the walking apparatus with an adaptation mechanism. To adjust the height h and enable vertical lifting and lowering of the foot

S, an additional straight-line guiding mechanism is affixed to the connecting rod, conventionally represented as a prismatic pair M in Figure 2.2b.

It is noteworthy that if the body moves horizontally at a speed V, then the connecting rod EM, along with the foot, moves relative to the body at a speed $V_S = -V$. Consequently, with respect to the fixed coordinate system associated with the load-bearing surface, the connecting rod remains stationary. During strictly vertical lifting and lowering of the foot, the horizontal speed of the foot S relative to the ground remains zero.

To carry out the rotation of the body, we propose to introduce additional joints O_i, rotating around the vertical axis $O_i z_i'$ (Figure 2.4a). To simplify the study of the turning modes, an equivalent kinematic scheme of the WR is also presented (Figure 2.4b, 2.4c), where entire STMs of the robot were modeled as prismatic pairs $\boldsymbol{P_i}(i = 1, \dots, 6)$**.** Actuating the joints O_i to turn the robot will lead to structural redundancy that mentioned above. Thus, turning is carried out due to the difference in velocities of $\boldsymbol{P_i}$**.**

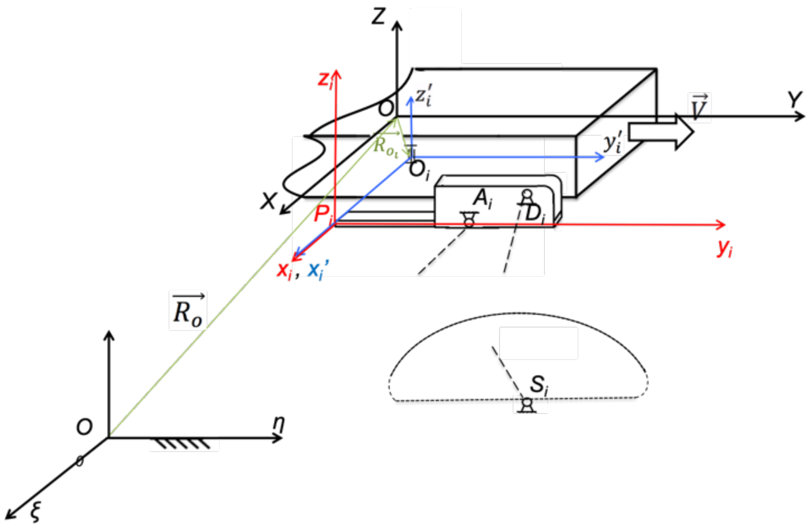

a)

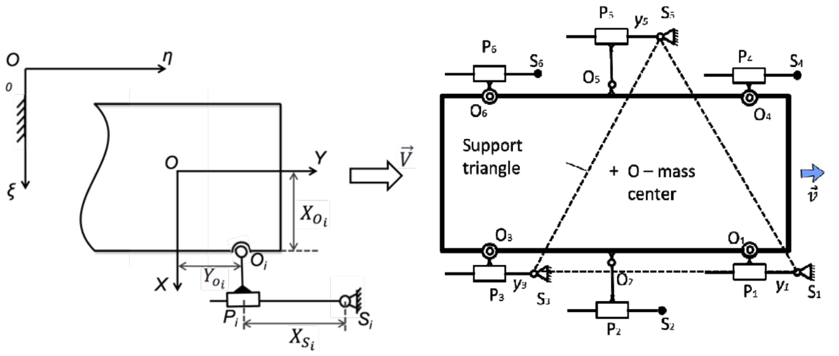

b) c)

Figure 2.4 – WR structural scheme on the plane $O\xi\eta$ with equivalent 2D kinematics [18] ("tripod" gate)

2.2 Substantiation of WR structure

The kinematic equivalent schemes mentioned above are introduced for the analysis of turning modes, and are presented in a two-dimensional manner. This choice is made because the vertical motion of the legs — adaptation to surface irregularities — does not affect the horizontal motion of the robot, as further expounded in subsequent chapters. Figure 2.5 illustrates the kinematic equivalent scheme in three-dimensional space. Notably, only supporting legs are depicted in the Figure 2.5, as legs in the transference phase do not contribute to the overall motion of the robot. In the subsequent sections, the rationality of the proposed structural configuration will be proven for both planar and spatial schemes.

Commented [MOU1]:

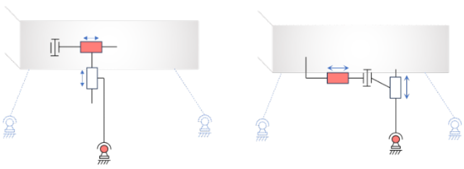

Figure 2.5 – Spatial kinematic equivalent scheme of the WR, featuring only the supporting legs during "tripod" gate

Note, that the mentioned above kinematic equivalent schemes are introduced for studying turning modes, and presented in 2D, since the vertical motion of the legs (adaptation to the irregularities of the surface) does not affect the horizontal motion of the robot (see next chapters). Figure 2.5 presents the kinematic equivalent scheme in space. Only supporting legs are depicted there, since the legs on the transference phase are not involved in the overall motion of the robot. Further the rationality of the proposed structure will be proven for both planar and spatial schemes.

An experimental prototype shown in Figure 2.2b correspond to the kinematic-equivalent scheme in Figure 2.6a, Figure 2.6b.

The equivalent mechanism (Figure 2.4c) has 3 DoF, since the number of moving links is n = 7, and p_5 = 9, then the number of DoF, W

$$W = 3n - 2p_5 = 21 - 18 = 3,$$

where p_5 is the number of kinematic pairs with five constraints.

For spatial case

$$p_5 = 3(\text{legs}) \cdot 3(\text{per leg}); W = 6(n+1) - 3p_3 - 5p_5 = 6(3 \cdot 3 + 1) - 3 \cdot 3 - 5 \cdot 9 = 6 = \text{number of input joints.}$$

Thus, the number of degrees of freedom is equal to the number of active drives, which meets the requirement of rational structural synthesis of the kinematic diagram of the robot. Due to rational mechanics, the problem of redundant connections is eliminated, parasitic loads on motors and deformation of links associated with multiple static indeterminacy are eliminated, and slippage of the robot's feet is eliminated.

For a kinematic diagram of another type, presented in Figure 2.6 the same structural formulas are valid.

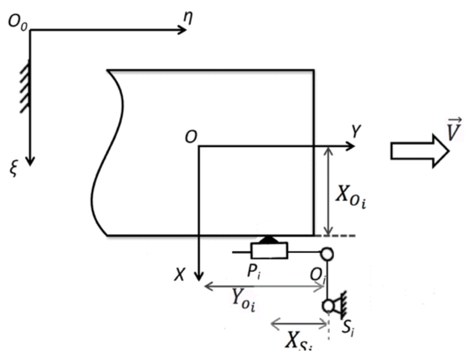

a)

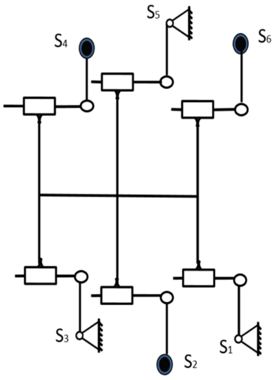

b)

Figure 2.6 – 2D Kinematic-equivalent scheme of the WR with regular “tripod” gate

Figure 2.7 shows a kinematically equivalent scheme of an eight-legged robot with a regular four-legged gait (at each moment of time, four legs are in the support phase). To obtain a rational structural scheme of the robot in this case, the robot must have a dissected body. To prove this statement, it is necessary to show that the number of DoF of such a system with a regular four-legged gait is equal to the number of active power drives (conventionally shown by arrows), i.e. the number of input joints of all legs in the support phase. Only moving links that ensure movement of the body are considered, i.e. legs in the swing phase are excluded.

The following structural formula shows “irrationality” of the structure shown in Figure 2.7a:

$$p_5 = 4\ (\text{supporting legs}) \cdot 3; W = 6(n+1) - 3p_3 - 5p_5 = 6(4 \cdot 3 + 1) - 3 \cdot 4 - 5 \cdot 12 = 6 \neq \text{ number of input links } = 12$$

After partition of the robot body:

$$p_5 = 4\ (\text{supporting legs}) \cdot 3 + 2; W = 6(n+1) - 3p_3 - 5p_5 = 6 \cdot 15 - 3 \cdot 4 - 5 \cdot 14 = 8 = \text{ number of input links}$$

Thus, the following decomposition of the robot’s movement is proposed:

a) generating rectilinear-forward motion of the robot through the use of a trajectory SLM;

b) the introduction of additional drives to adapt to uneven terrain (so that these drives operate independently and coordination of their work is not required);

c) turning control due to the difference in the angular velocities of the SLM cranks.

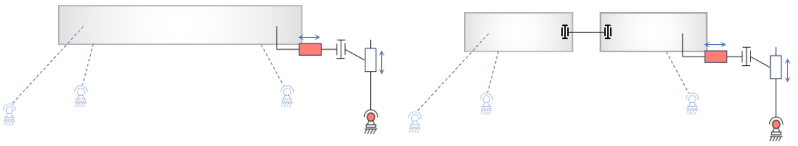

a) b)

Figure 2.7 – Kinematic equivalent scheme of the WR during regular 4-legged gait. a) – overconstrained structure; b) – "rational" structure

Let's introduce the following coordinate systems:

- $\boldsymbol{O_0\xi\eta\zeta}$ – absolute (fixed) coordinate system, rigidly connected to the supporting (bearing) surface, the WR body moves along the $\boldsymbol{O_0\eta}$ axis with a speed $\vec{\boldsymbol{V}}$.
- $\boldsymbol{OXYZ}$ – coordinate system rigidly connected to the WR body.
- $\boldsymbol{O_i x_i' y_i' z_i'}$ – local coordinate system associated with the i-th leg, the beginning of which $\boldsymbol{O_i}$ coincides with the center of the joint $\boldsymbol{O_i}$.
- $\boldsymbol{P_i x_i y_i z_i}$ – also a local coordinate system, rigidly connected to the leg mechanism with number *i*; the plane $\boldsymbol{P_i y_i z_i}$ coincides with the plane of the leg mechanism, the axes are parallel to the axes of the coordinate system $\boldsymbol{O_i x_i' y_i' z_i'}$, the beginning of $\boldsymbol{P_i}$ is shifted along the axis $\boldsymbol{x_i'}$ by a distance $\boldsymbol{x_{P_i}'}$.

Let the foot S_i be in support, so that $\xi_{S_i} = const$, $\eta_{S_i} = const$, $\zeta_{S_i} = const$. With uniform rotation of the crank A_iB_i with a constant angular velocity $\dot{q}_i = \dot{\varphi}_i = \omega_i = const$, the foot S_i moves relative to the coordinate system *OXYZ* uniformly and rectilinearly with a speed $\vec{V}_{S_i} = -\vec{V}$, i.e. parallel to the $P_i y_i$ axis. Neglecting minor deviations, we can assume that the coordinate at the foot S_i depends linearly on the generalized coordinate q_i:

$$y_{S_i} = y'_{S_i} = A_i + B_i q_i, \tag{2.1}$$

and the coordinates of *X* and *Z* remain constant:

$$x_{S_i} = 0, x'_{S_i} = x'_{P_i} = const, \tag{2.2}$$

$$z_{S_i} = z'_{S_i} = -h_i \tag{2.3}$$

For rectilinear and uniform movement of the body, the cranks $\boldsymbol{A_iB_i}$ of all legs located in the support must rotate with the same angular velocity $\dot{\boldsymbol{q}}_i = \boldsymbol{\omega_i} = \boldsymbol{\omega}$. Then, differentiating expression (2.2), we obtain

$$\dot{y}_{S_i} = V^y_{S_i} = B_i \dot{q}_i = B_i \omega_i, \tag{2.4}$$

whence follows

$$B_i = B = -\frac{V}{\omega} = const, \tag{2.5}$$

where V – is the velocity of translational motion of the body: $V_{S_i}^{y} = -V$.

Further, for the convenience of studying the rotation of the WR, we will take the coordinates $\boldsymbol{y_i} = \boldsymbol{y_{S_i}}$ instead of $\boldsymbol{q_i}$ as conditional generalized coordinates.

Another important limitation is the absence of singular positions when the lines S_iO_i intersect at one point, or all S_iO_i are parallel (for supporting legs) (Figure 2.8a, b).

Remark 1. Note that if, when designing the WR, we take all O_iP_i=0, then during the rectilinear translational movement of the WR, the configuration would be in a special position (Figure 2.8c) and when rotating from this position, an ambiguity in the WR configuration would arise.

Remark 2. When designing the WR, it is necessary to take into account that the hinges O_i (Figure 2.4) were introduced not as drive ones, but to eliminate redundant connections. Rectilinear translational motion of the body is possible without them, but then the structural diagram will be irrational, since the number of degrees of freedom will be zero ($W = 3 \cdot 4 - 2 \cdot 6 = 0$). Rotation of such a mechanism will not be possible.

Remark 3. In the swing phase, the feet S_i are raised from the surface and then the hinges O_i will be passive (hinges O_2, O_4 and O_6 in Figure 2.4). However, in reality, we only need to return the link O_iP_i (the plane of the mechanism, see Figure 2.2) to its original ("neutral") position: to the position where the angle $(\widehat{OY, O_iP_i})$, formed by the link O_iP_i axis OY_ξ is equal to 90^0. Thus, in the hinges O_i in place of the active drives, it is enough to place a "return link" (for example, springs).

Remark 4. And thus the six-legged WR will have six main active drives working together (instead of twelve in a flat design and eighteen in a Hexapod-type spatial robot). The task of the control system will be to ensure the coordinated operation of these drives, so reducing the number of drives to six leads to a significant simplification of the control system. Note that due to the separation of motor functions, the robot's movement is controlled independently of the system for adapting to unevenness. The latter includes six more drives, but coordination of their work is not required, because adaptation of each leg is carried out individually.

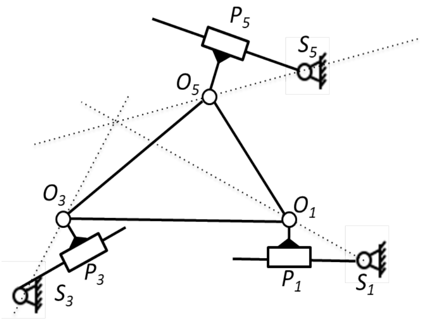

a)

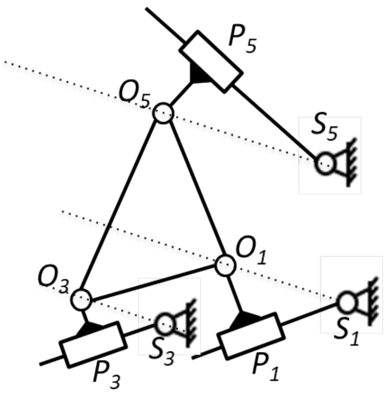

b)

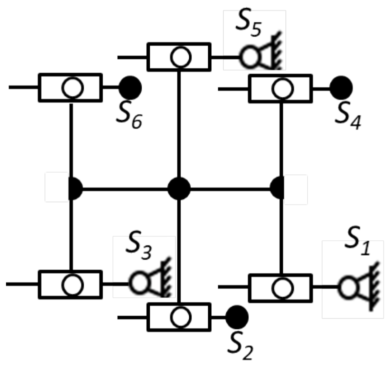

c)

Figure 2.8 – Configurations of WR in singular positions

2.3 Conclusions on the Section 2

The application of the principle of separation of drive functions in the rational design of a walking robot is shown. As a result, the robot moves in an optimal mode from a mechanical point of view, with minimal energy consumption and using a simplified control system. Rational structural synthesis of the WR made it possible to eliminate the problem of redundant connections and multiple static uncertainty in the structure of traditional “universal” robots such as Hexapod, and also made it possible to get by with a minimum number of active drives. As a result of structural optimization, the number of main motors has been reduced to six, while the additional six adaptation drives are not involved in the main movement, coordination of their work is not required, because adaptation of each leg is carried out individually (independent of the others). Finally, the use of this approach makes it possible to perform parametric synthesis of WR based on well-known methods of multicriteria synthesis of parallel manipulators (based on such criteria as manipulability, isotropy, etc.).

3 Development of methods for analysis, structural-parametric synthesis and optimal design of leg mechanisms

In connection with the increased interest in trajectory type propulsion devices (Gavrilov, Golubev, and Danshin 2013; Kim, Jung, Shin, and Seo 2014; Plecnik and McCarthy 2016; Pop et al 2016; Selvi and Samet 2017; Wang and Hou 2018; Geonea 2019) that provide a given step cycle, increases the relevance of the problem of leg mechanism synthesis. In recent years, different approaches have been proposed for the dimensional synthesis of linkage mechanisms of walking robot (WR) leg (Umnov 1996; Xu 2019; Briskin et al. 2018; Komoda and Wagatsuma 2017; Özgun and Ceccarelli 2019; Gavrilov, Golubev, and Danshin 2013; Kim, Jung, Shin, and Seo 2014; Plecnik and McCarthy 2016; Pop et al 2016; Selvi and Samet 2017; et al.). For example, (Selvi and Samet 2017; Wang and Hou 2018; Geonea 2019; Funabashi 1987; McGovern and Sandor 1973) are devoted to adjustable trajectory generators synthesis. However, most of the existing methods of synthesis suffer from so-called "branching defect" (Krishnamurty and Turcic, 1988), when one part of the desired motion is generated by one assembly of the mechanism, while another one is reproduced by another one. Moreover, the proposed mechanisms have a poor range of adaptation to irregularities of the supporting surface. It is obvious that the solution of the last problem can be the use of the mechanism with output-link, all points of which generate straight-line trajectory. However, increasing the adaptation range this way leads to another problem: decreased transmission angle (Ibrayev 2014). The main reason for drawbacks mentioned is that the "traditional" methods of synthesis are based on the minimization of structural error, implying the compliance to specific geometric constraints, such as circle fitting (matching a circular point on a coupler) etc. Therefore, synthesized mechanism often has unfavorable force transmission or even doesn't work at all due to the break of the mechanism kinematic chain (Wang and Sodhi 1996).

The method of synthesis proposed in this paper doesn't suffer from these disadvantages due to minimizing directly the error of the mechanism output. The results of optimal design of six-link leg-linkage with straight-line and translatory motion of the output point and with unlimited adaptation range on the rough terrain are presented. (Ibrayev et al., 2020) proposed another mechanism with a "shin-link", all points of which performs a rectilinear and translational movement. The optimal step cycle parameter of the leg is attained by maximizing the duration ratio of support and transference phases and, at the same time, the best transmission angle is achieved without loss of accuracy. Increasing the transmission angle (from $12° - 15°$ in existing prototypes to 25° (Artobolevsky, 1979) ensures higher efficiency and lower power consumption (Levitsky, 1990). This paper is an extended version of the conference paper published in (Ibrayev et al., 2020). The previous work is enhanced by changes and extension in analytical synthesis method, complemented with discussions, functionality studies of the lambda mechanism; numerical solutions supplemented on the basis of an improved synthesis method are provided in current work. New prototypes of WR are developed using the synthesized straight-line generator as propellers.

3.1 Description of six link leg mechanism structure

A rational structure of a WR based on kinematic decoupling of movement is proposed by (Song et al., 1984; Ryan and Hunt, 1985), which allows to simplify the control system of the robot, as well as to reduce power consumption due to:

a) the rotation of the main crank motors with constant angular velocity during the translational movement of the body/hull;
b) the absence of structural redundancy.

The simplicity of the control system is explained by the independence of the work of each group of actuators. A mechanism structure with translatory motion of the output link *EJ* is plotted in Figure 3.1. Here the basic straight-line generating mechanism *ABCD* is the "lambda-type mechanism", the link 5 (*EJ*) of the additional kinematic chain 4-5 copies the trajectory of the coupler point *E* due to the translational motion of this link. Thus, with the additional input link 6 and the input joint *M* we obtain the adjustable leg mechanism for multiple straight-line generation: now one can easily change the foot height and adjust the foot position on uneven surface. Note that the additional actuator at the joint *M* is used just to fix the foot position on the output link 5 (to fix link 6 relative to link 5), so the joint *M* is passive on the support phase of the step cycle.

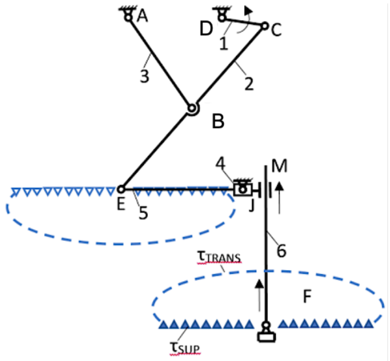

Figure 3.1– Leg linkages with translational output motion based on P. Chebyshev's "lambda mechanism"

On the support phase τ_{SUP} (that correspond to the crank angle (φ_{AB}) change within the range $\varphi_0 \le \varphi_{AB} \le \varphi_0 + \Phi_{SUP}$, where φ_0 is a crank angle at the start of the support phase and $\varphi_0 + \Phi_{SUP}$ – corresponds to the end of the support phase. (Figure 3.3)

- the leg foot *F* has to trace straight-line with nearly constant velocity relative to the robot chassis while the angular velocity of crank *AB* is constant (the relation between the input and output velocities has to be nearly linear;

and, for the robot stable motion,

- the duration of the support phase has to be longer than the duration of the transfer phase τ_{TRANSF} (when foot is off ground, that correspond to crank angle φ_{AB} values within the range $\varphi_0 + \Phi_{SUP} \leq \varphi_{AB} \leq \varphi_1$, where $\varphi_1 = \varphi_0 + 360°$).

If crank AB angular velocity is constant, then the ratio $\nu = \Phi_{SUP}/\Phi_{TRANSF}$ is equal to the duration ratio of two phases. This ratio is referred to as the parameter of step cycle. In classical Chebyshev's lambda mechanism with $\Phi_{SUP} = 184°, \Phi_{TRANSF} = 176°$ (Φ_{TRANSF} is a magnitude of the angle corresponding to the transfer phase), this ratio υ is equal to 1,045.

The prototype of the legged robot horizontal propulsion mechanism was designed in the Institute of Mechanics and Mechanical Engineering of Kazakhstan Ministry of Sciences (Figure 3.2). For stable motion of the vehicle, two legs should occur alternately in the support/transference phases while the crank angles of these mechanisms are shifted by 184°. To overlap support phases of these two mechanisms, support phase should be longer than transference phase: $\Phi_{SUP} > 180°$ and, thus, the parameter $\nu \geq 1$ should be as greater as possible. However, according to the previous studies (Funabashi, 1987), increasing this parameter leads to poor solutions in terms of both accuracy and transmission angle. A new method of synthesis proposed in the next section does not have these inherent drawbacks due to minimizing the deviation of the output motion from the desired/prescribed one directly, i.e., instead of minimizing the residual error, derived from geometric constraints, such as circle fitting, etc.

Figure 3.2 – Prototype of the legged robot horizontal propulsion mechanism

3.2 Approximate Synthesis of the Path Generator by Minimizing Directly the Output Accuracy

3.2.1 Analytical Synthesis by four Parameters

Let us consider a four-bar linkage *ABCD* that is described by the linkage dimensions $X_A = Y_A = 0, X_D, Y_D, r_{AB}, l_{BC}, l_{CD}$ (Figure 3.3), where X_A, Y_A, X_D, Y_D are the absolute coordinates of the frame pivots *A* and *D* relative to the absolute reference frame *OXY*. The crank angle φ_{AB} is varied within the range $\varphi_0 \leq \varphi_{AB} \leq \varphi_0 + \Phi_{\text{SUP}}$ as

$$\varphi_i = \varphi_0 + \Phi_{\text{SUP}} k_i, \text{where } k_i = \frac{i-1}{N-1}, i = 1, 2, \ldots, N.$$

and for each crank angle $\varphi_{AB} = \varphi_i$ position analysis is supposed to be carried out; thus, *N* positions of the coupler *BC* are supposed to be determined.

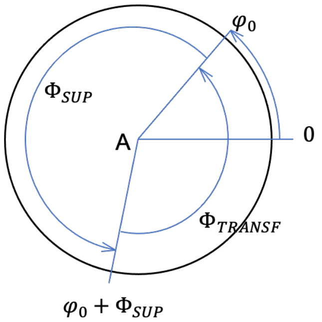

Figure 3.3 – A step cycle of the leg: φ_0 is a crank angle corresponding to the beginning of the support phase, $\varphi_0 + \Phi_{SUP}$ – end of the support phase; Φ_{TRANSF} – corresponds to the transfer phase

If *Bxy* is the local moveable reference frame fixed on the coupler *BC*, with the axis *Bx* lying along the link *BC*, so we know the coordinates X_{B_i}, Y_{B_i} of the origin *B* and inclination angles $\beta_i = \beta_{BC}$. Now the coupler point (end-effector) *E* with the local coordinates x_E, y_E relative to *Bxy* is sought, that most accurately reproduces the trace through *N* prescribed points $E_1^*, \ldots, E_N^*$ with the given absolute coordinates $X_{E_i}^*, Y_{E_i}^*$ $(i = 1, \ldots, N)$. In Figure 3.4, $\overrightarrow{R_{E_i}^*}$ is a radius-vector of the points on the program trajectory, and $\overrightarrow{R_{E_i}}$ – on real trajectory. If the given (program) trajectory is horizontal,

$$\begin{cases} X_{E_i}^* = X^0 + Lk_i, \; i = 1, 2, \ldots, N \\ Y_{E_i}^* = Y^0, \end{cases} \tag{3.1a}$$

where L is a length of the given trajectory (straight-line), X^0, Y^0 – absolute coordinates of the point E_1^*.

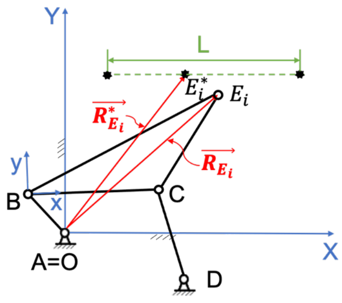

Figure 3.4 – Kinematic scheme of the linkage $ABCD$: $\overrightarrow{R_{E_i}^*}$ is a radius-vector of the points on the program trajectory, and $\overrightarrow{R_{E_i}}$ – on real trajectory

In general case, if the trajectory is a straight line at angle α with horizontal and with length L, then

$$\begin{cases} X_{E_i}^* = X^0 + L_X k_i, i = 1, 2, \dots, N \\ Y_{E_i}^* = Y^0 + L_Y k_i \end{cases} \tag{3.1b}$$

where $L_X = L\cos\alpha, L_Y = L\sin\alpha$ (Figure 5).

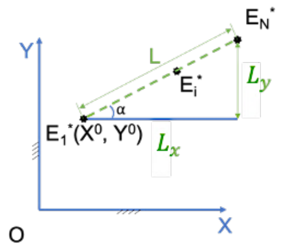

Figure 3.5 – Program (prescribed) trajectory of the coupler point

The absolute coordinates of the points $E_i(X_{E_i}, Y_{E_i})$ of the joint E are given by

$$\overrightarrow{R_{E_i}} = \overrightarrow{R_{B_i}} + \Gamma(\beta_i)\overrightarrow{r_E}$$

$$
\begin{cases} X_{E_i} = X_{B_i} + x_E cos\beta_i - y_E sin\beta_i \\ Y_{E_i} = Y_{B_i} + x_E sin\beta_i + y_E cos\beta_i, \end{cases} \tag{3.2}
$$

where $\overrightarrow{R_{B_i}}$ is a radius vector of the joint *B* with absolute coordinates X_{B_i}, Y_{B_i}. $\Gamma(\beta_i)$ is a rotation matrix of dimension 2×2, $\overrightarrow{r_{E_i}}$ is a radius-vector of the coupler point (*E*) on real trajectory relative to *Bxy*.

The synthesis task consists of satisfying approximately the following conditions:

$$
\overrightarrow{R_{E_i}} - \overrightarrow{R^*_{E_i}} = \vec{0} \tag{3.3}
$$

That is

$$
\begin{cases} X_{B_i} + x_E cos\beta_i - y_E sin\beta_i = X^0 + L_x k_i \\ Y_{B_i} + x_E sin\beta_i + y_E cos\beta_i = Y^0 + L_y k_i \end{cases} \tag{3.4}
$$

The designing task is formulated as the following minimization problem

$$
\delta = \sum_{i=1}^{N} \delta_i^2 \quad => \min_{x_E, y_E, X^0, Y^0} \tag{3.5}
$$

where δ is a design error – the distance between actual positions E_i and the desired ones E_i^*,

$$
\delta_i^2 \equiv \|E_i E_i^*\|_2^2 = \left(X_{E_i} - X^0 - X_i^*\right)^2 + \left(Y_{E_i} - Y^0 - Y_i^*\right)^2 \tag{3.6}
$$

where $X_i^* = L_X k_i, Y_i^* = L_Y k_i, X^0, Y^0$ are shifting of the prescribed points (E_i).

If L and α are given, the design parameters are $x_1 = x_E$, $x_2 = y_E, x_3 = X^0$, $x_4 = Y^0$ (note that the coordinates of the crank pivot *A* were specified above to be $X_A = Y_A = 0$). From equations (3.2), δ is written as follows

$$
\delta = \sum_{i=1}^{N} \Big\{ (X_{B_i} + x_1 cos\beta_i - x_2 sin\beta_i - X_i^* - x_3)^2 + (Y_{B_i} + x_1 sin\beta_i + x_2 cos\beta_i - Y_i^* - x_4)^2 \Big\} \tag{3.7}
$$

Here $X_{B_i}, Y_{B_i}, \beta_i, X_i^*, Y_i^*$ are known. The necessary condition of minimum $\partial\delta / \partial x_j = 0, j = 1, \dots, 4,$ yield 4 linear equations with 4 unknowns

$$
\boldsymbol{AX} = \boldsymbol{b}. \tag{3.8}
$$

The matrix $\boldsymbol{A}$ can be written in the form [19] $\boldsymbol{A} = \boldsymbol{B^T B}$, where $\boldsymbol{B^T} = [\mathbf{C}_1, \mathbf{C}_2, \dots, \mathbf{C}_N]$,

$$\boldsymbol{C}_i = \begin{bmatrix} cos\beta_i & -sin\beta_i & -1 & 0 \\ sin\beta_i & cos\beta_i & 0 & -1 \end{bmatrix}.$$

Thus, the matrix $\boldsymbol{A}$ is non-negatively determined and it's all main minors as well, hence linear equations (3.8) yield single solution. It should be noted that the main advantage of this technique is that there is no branching defect and, moreover, the designer can specify the desired transmission angle.

3.2 Analytical Synthesis by six Parameters

The number of determined analytically variables can be increased by another two if we introduce into the number of variables the parameters $x_5 = L\cos\alpha$ and $x_6 = L\sin\alpha$. The meaning of these parameters is the rotation and scaling of the mechanism as a whole. But now we have to consider a "normalized mechanism" with a unit length of the axle spacing of the bases (frame) $AD = 1$ and $X_A = Y_A = 0, X_D = 1, Y_D = 0$. Then the minimized approximation function in new variables $x_1, x_2, x_3,\ x_4, x_5, x_6$ has the form

$$\sum_{i=1}^{N} \left\{ (X_{B_i} + x_1 cos\beta_i - x_2 sin\beta_i - x_3 - x_5 k_i)^2 + (Y_{B_i} + x_1 sin\beta_i + x_2 cos\beta_i - x_4 - x_6 k_i)^2 \right\} \tag{3.9}$$

Then, similarly to the previous case, from the necessary minimum condition for the variables $x_1, \ldots, x_6$ we obtain the system of six linear equations of type (8), where

$$\mathbf{A} = \begin{bmatrix} \mathbf{E} & \mathbf{A}_1 & \mathbf{A}_2 \\ \mathbf{A}_1^{\mathrm{T}} & \mathbf{E} & 1/2\mathbf{E} \\ \mathbf{A}_2^{\mathrm{T}} & 1/2\mathbf{E} & \frac{1}{N}\sum_{i=1}^{N} k_i^2\,\mathbf{E} \end{bmatrix},$$

$$\mathbf{E} = \begin{bmatrix} 1 & 0 \\ 0 & 1 \end{bmatrix}, \tag{3.10}$$

$$\mathbf{A}_1 = \begin{bmatrix} -\dfrac{1}{N}\displaystyle\sum_{i=1}^{N} cos\beta_i & -\dfrac{1}{N}\displaystyle\sum_{i=1}^{N} sin\beta_i \\ \dfrac{1}{N}\displaystyle\sum_{i=1}^{N} sin\beta_i & -\dfrac{1}{N}\displaystyle\sum_{i=1}^{N} cos\beta_i \end{bmatrix},$$

$$\mathbf{A}_2 = \begin{bmatrix} -\frac{1}{N}\sum_{i=1}^{N} k_i \cos\beta_i & -\frac{1}{N}\sum_{i=1}^{N} k_i \sin\beta_i \\ \frac{1}{N}\sum_{i=1}^{N} k_i \sin\beta_i & -\frac{1}{N}\sum_{i=1}^{N} k_i \cos\beta_i \end{bmatrix}$$

$\mathbf{b}=[b_1, b_2,\ldots, b_6]^{\mathrm{T}}$, $b_1 = -\frac{1}{N}\sum_{i=1}^{N}(X_{B_i}cos\beta_i + Y_{B_i}sin\beta_i)$,

$$b_2 = \frac{1}{N}\sum_{i=1}^{N}(X_{B_i}sin\beta_i - Y_{B_i}cos\beta_i),$$

$$b_3 = \frac{1}{N}\sum_{i=1}^{N} X_{B_i},$$

$$b_4 = \frac{1}{N}\sum_{i=1}^{N} Y_{B_i},$$

$$b_5 = \frac{1}{N}\sum_{i=1}^{N} k_i X_{B_i},$$

$$b_6 = \frac{1}{N}\sum_{i=1}^{N} k_i Y_{B_i}$$

3.3 Testing the results

To test the method proposed in previous sections let us use well known Chebyshev's lambda mechanism (Figure 3.1) with the following link lengths:

$$r_{AB} = 0.5,\ l_{BC} = 0.625, l_{CD} = 0.625,$$

frame pivot coordinates:

$$X_A = 0, Y_A = 0, X_D = -0.5,\ Y_D = 0,$$

initial crank angle $\varphi_{AB} = 90°$.

With these parameters the coupler point *E* generates approximately horizontal straight-line, specified by points $E_1(2,2)$ and $E_N(0,2)$. The step cycle parameters of this mechanism are $\Phi_{SUP} = 184°, \Phi_{TRANSF} = 176°$, and $\nu = \Phi_{SUP}/\Phi_{TRANSF} = 1.045$.

The desired motion is given by *N* prescribed equidistant points $(X_i, Y_i), i = 1, \dots, N$ horizontal straight-line segment of length *L=1* determined by

$$Y_0^* = 0, \mathrm{X}_0^* = 0, X_N^* = 1,$$

as follows:

$$Y_i^* = Y_0^*,\ X_i^* = X_0^* + (X_N^* - X_0^*)k_i.$$

So, the coupler point has to trace equidistant horizontal points (X_i^*, Y_i^*) while the crank angle φ_i is changed by constant increment $\Delta_\varphi = \varphi_i - \varphi_{i-1} = \Phi_{SUP}/(N - 1)$, thus, the relation between input and output velocities (coupler point horizontal velocity and crank angular velocity) will be nearly linear.

The mechanism synthesis parameters are determined to be:

$$x_1 = x_E = 1.23218,$$

$$x_2 = y_E = -0.02180,$$

$$x_3 = X^0 = 2.04035,$$

$$x_4 = Y^0 = 1.95574.$$

Minimum of the Euclidean norm is achieved with these parameters. The real accuracy (maximal error on the output) achieved is

$$\varepsilon = \max_{i=1,\dots,N} \sqrt{\left\|E_i E_i^*\right\|_2^2} = 0.002,$$

i.e., 0.2%, trajectory height $Y_E^0 = -0.9827$ (Figure 3.6)

In six-parameter case, desired movement is also given by *N* finitely distant points (X_i^*, Y_i^*), i =1, …, *N*, lying on a horizontal segment of length *L=1*:

$$\begin{cases} Y_i^* = Y_0^*, \\ X_i^* = X_0^* + (X_N^* - X_0^*)k_i, i = 1, 2, \dots, N. \end{cases} \quad (3.11)$$

The synthesis parameters found are following:

$$r_{AB} = 0.24743,$$

$$l_{BC} = 0.61857,$$

$$l_{CD} = 0.61857,$$

$$X_D = -0.49479,$$

$$Y_D = -0.00768,$$

$$x_1 = x_E = 1.23218,$$

$$x_2 = y_E = -0.02180,$$

$$x_3 = X^0 = 2.04035,$$

$$x_4 = Y^0 = 1.95574,$$

$$x_5 = L\cos\alpha =- \ 2.02056\ ,$$

$$x_6 = L\sin\alpha = 0.03138.$$

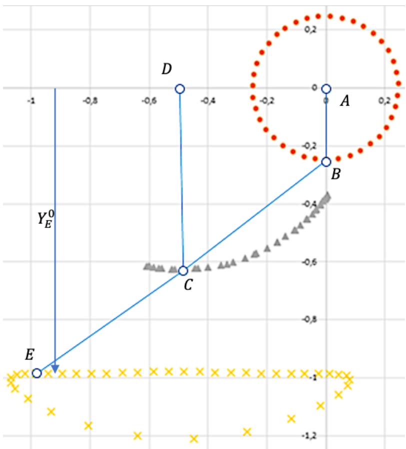

Figure 3.6 – Synthesized mechanism – method test

3.4 Functionality Study of the Chebyshev Mechanism

The variable parameters of the search area were given by

- $0.15 \leq r_{AB} \leq 0.750$
- $0.400 \leq l_{BC} \leq 1.200$
- $0.400 \leq l_{CD} \leq 1.200$
- $15° \leq \varphi_0 \leq 150°$ (initial angle of the crank).
- $190° \leq \Phi_{SUP} \leq 220°$

The mechanism link dimensions are varied by Sobol-Statnikov random LP$_\tau$-sequence method (Statnikov, 1999), for each value of the variable parameters, the parameters $x_1, x_2, \ldots, x_6$ were determined by analytical synthesis.

For the accuracy ε < 0.015 (1.5% from step length) and the worst value of the pressure angle μ_e>30° ($\mu_e = \min(\mu_i, 180 - |\mu_i|)$, μ_i is the pressure angle of the mechanism at *i*-th position, the parameters lie within the boundaries:

- $0.15 \leq r_{AB} \leq 0.670$
- $0.410 \leq l_{BC} \leq 1.200$
- $0.450 \leq l_{CD} \leq 1.200$
- $24° \leq \varphi_0 \leq 113°$.

The mechanism with the maximum Φ_{SUP} value and minimum of links constant dimensions $S = \Sigma l_i$ is shown in Figure 3.7a. The mechanism with the best accuracy is shown in Fig.7b. The accuracy of all of the obtained mechanisms can be improved by local search.

The mechanisms with the best μ_e values are shown in Figure 3.7c,d, however, these mechanisms have very huge dimensions: the better the transmission angle, the worse the mechanism dimensions. More compact mechanisms are presented in Figure 7e-h. Table 3.1 corresponds to the mechanisms shown in Figure 3.7.

The possibility of increasing of the parameter Φ_{SUP} up to 270° was studied. The mechanism with $\Phi_{SUP} = 270°$ is shown in Figure 3.8a. As expected, the larger the angle Φ_{SUP} the worse the accuracy and transmission angle: the mechanism has the accuracy 1.3%, whereas the angle $\mu_e = 12.4°$, which is, of course, unacceptable. At the same time, we observe the compact mechanism dimensions. Nevertheless, the compromise solution is shown in Figure 3.8b with $\Phi_{SUP} = 265°$, the accuracy 1.3% and $\mu_e = 19°$. Finally, trying to improve transmission angle up to $\mu_e = 25°$ leads to compromise solution with further decrease in the value of the $\Phi_{SUP} = 232°$ (see Figure

3.8d), the accuracy is 0.8%. Table 2 represents the parameters of the mechanisms in Figure 3.8.

Table 3.1 – Parameters of the mechanisms in Figure 3.7.

LP$_\tau$	**r$_{AB}$**	**BC**	**CD**	X_D	Y_D	φ_0	x_P	y_P	S_x	S_y	**accuracy**
254	0,30475	0,52602	0,68496	-0,53957	0,45021	207,38226	0,75118	0,30410	0,68594	1,50257	0,01017
958	0,27495	0,65352	0,64086	-0,65392	0,30159	240,98711	1,06360	0,51025	0,93311	1,78113	0,00564
2832	0,31933	1,25004	1,59662	-1,27288	1,53606	214,92422	1,31896	1,07583	0,13555	1,02718	0,00657
716	0,31510	0,83516	0,94771	-0,84873	0,85434	204,87726	0,93535	0,68031	0,36470	1,21463	0,00983
4418	0,32059	0,66452	0,84780	-0,67283	0,72679	208,80739	0,78034	0,52378	0,37129	1,26668	0,01043
970	0,28325	0,66814	0,69291	-0,68768	0,48731	218,04003	0,90721	0,57621	0,62916	1,53021	0,00959
938	0,32344	0,61929	0,87601	-0,63433	0,69395	204,79524	0,78459	0,39617	0,40168	1,27153	0,00929
158	0,28327	0,59856	0,70411	-0,61246	0,40861	219,77593	0,90648	0,37549	0,74094	1,59605	0,00915

LP_τ	Y_P	μ_e, **deg.**	$d\varphi$	ΣL	**Fig.6**
4254	-0,49956	35,4	219,7	2,5	a)
5958	-0,88176	40,2	190,8	3,1	b)
12832	-1,09865	**70,9**	199,9	6,1	c)
9716	-0,71626	59,4	217,1	4,0	d)
14418	-0,58001	**50,8**	207,5	3,2	e)
9970	-0,74289	48,5	216,5	3,2	f)
4938	-0,52557	44,8	211,5	3,0	g)
5158	-0,67388	39,7	215,1	2,9	h)

Table 3.2 – Parameters of the mechanisms in Figure 3.8.

LPτ	**r$_{AB}$**	**BC**	**CD**	X_D	Y_D	φ_0	x_P	y_P	S_x	S_y	**accuracy**
26239	0,22215	0,34980	0,35020	-0,29672	-0,02400	-118,38177	0,70725	-0,05224	2,66504	1,38452	0,01340
10539	0,24757	0,38280	0,40521	-0,37030	0,09351	209,42744	0,69700	0,09750	1,94367	1,70734	0,01350
16867	0,22768	0,42761	0,43076	-0,36849	0,01137	229,38446	0,82319	-0,00133	2,34719	1,67886	0,00755
8277	0,24247	0,46252	0,46239	-0,43410	0,08361	229,47388	0,86981	0,14968	1,82675	1,81800	0,00811

LP_τ	Y_P	μ_e, deg.	$d\varphi$	ΣL	Fig.7
26239	-0,47478	12,40006	269,84407	1,40310	a)
10539	-0,44707	19,36943	265,24292	1,71184	b)
16867	-0,58996	18,91090	248,18298	1,77158	c)
8277	-0,63424	24,92673	232,44507	2,06778	d)

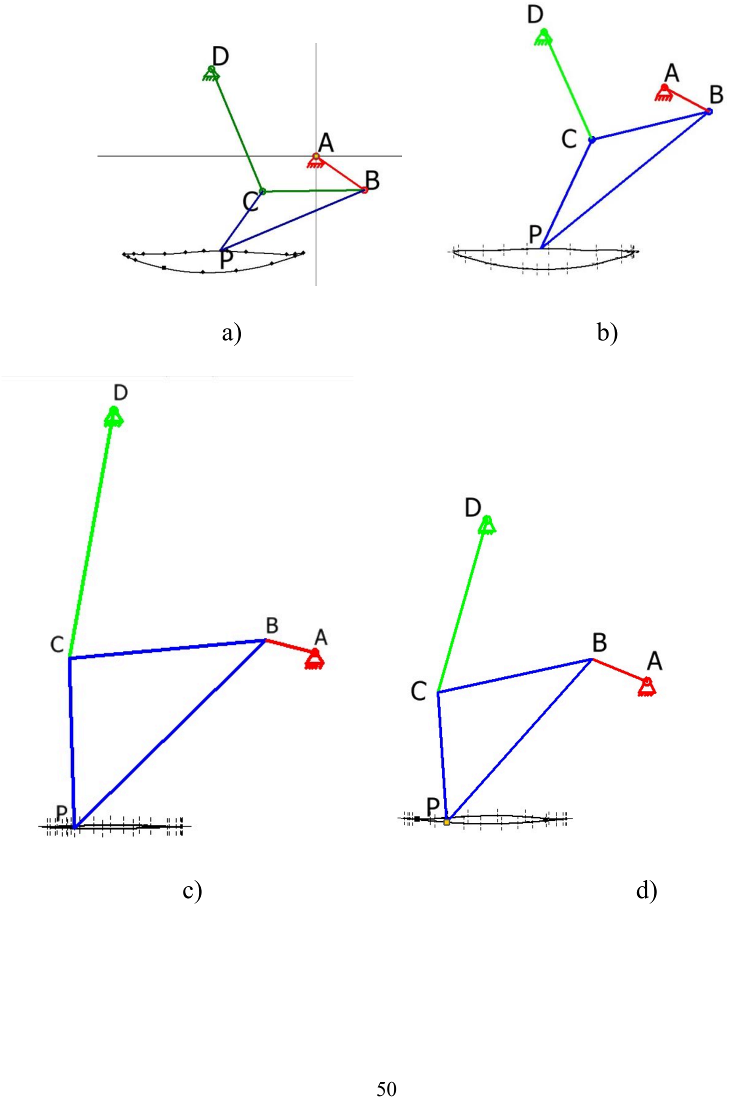

a) b)

c) d)

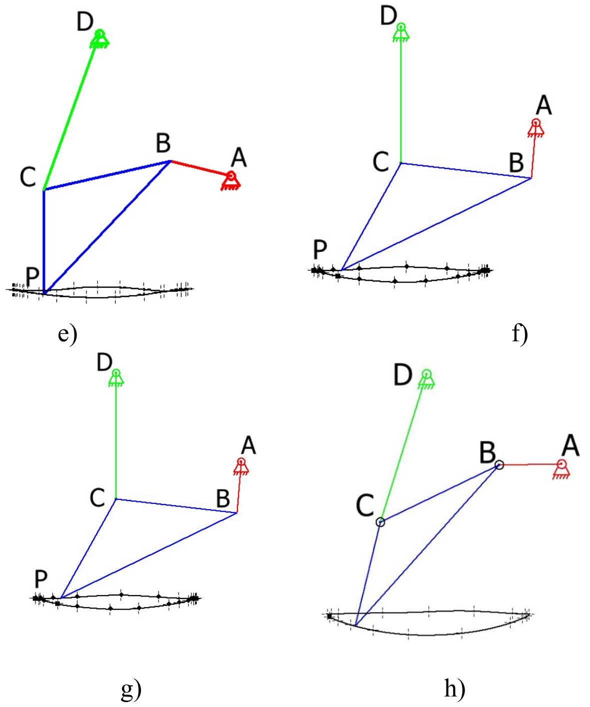

Figure 3.7 – Functionality study of the Chebyshev mechanism

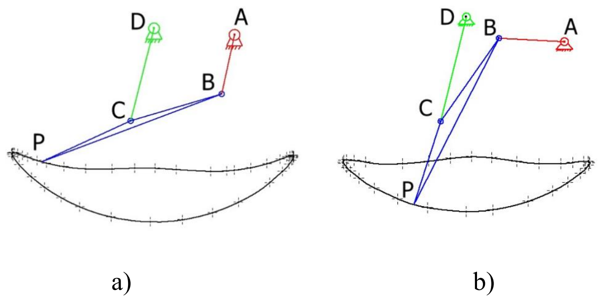

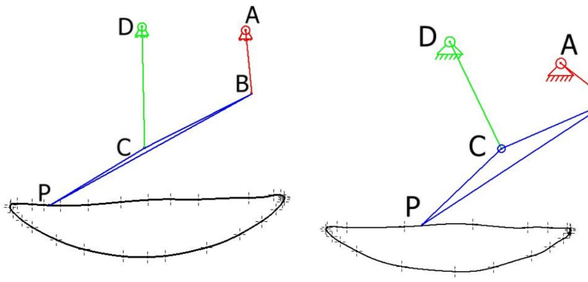

c) d)

Figure 3.8 – Functionality study of the Chebyshev mechanism

3.5 Optimal Leg Design

Each of the solutions discussed above can be improved by the local search in the surrounding area. On the first stage the lengths of normalized mechanism (when $X_A = Y_A = 0, X_D = 1, Y_D = 0$) and the value of Φ_{SUP} (which is the third criteria) are varied by Sobol-Statnikov random LP_τ-sequence method (Statnikov, 1999], the boundaries of the search were set:

- $0.150 \le \mathrm{r_{AB}} \le 0.750$,
- $0.400 \le l_{BC} \le 1.200$,
- $0.400 \le l_{CD} \le 1.200$,
- $15° \le \varphi_0 \le 150°$,
- $190° \le \varphi_{SUP} \le 220°$ (the third criterion).

For each value of the mentioned varying parameters we

- obtain the worst value of the pressure angle $\mu_e = \min\,(|\mu_i|, 180° - |\mu_i|)$;
- determine 6 synthesis parameters X= $[x_1, \dots, x_6]^T$ by solving the linear equations (3.10);
- determine the worst deviation – the accuracy of reproduction of the program trajectory (approximation error) $\varepsilon = \max_{i=1,\dots,N} \sqrt{\|E_i E_i^*\|_2^2}$;
- record the results in the Test Table.

The Test Tables are analyzed and truncated 1) by accuracy ($\varepsilon < 0.015$), 2) by pressure angle ($\mu_e > 18$). Figure 3.9 shows the solutions corresponding to the best accuracy, whereas the solutions with the best pressure angles are shown in Figure 3.10.

On the next stage duration of the support phase is chosen on the basis of previous analyses Φ_{SUP}=220^0, then the ratio is $\nu = \Phi_{SUP}/\Phi_{TRANSF} = 1.57$. The ranges of the lengths of the normalized mechanism are now narrowed down to

- $0.175 \le \mathrm{r_{AB}} \le 0.5$,
- $0.410 \le l_{BC} \le 1.200$,
- $0.530 \le l_{CD} \le 1.200$,
- $40° \le \varphi_0 \le 100°$

On the next stage duration of the support phase is chosen on the basis of previous analyses Φ_{SUP}=220^0, then the ratio $\upsilon=\Phi_{SUP}/\Phi_{TRANSF}$ is υ=1.57. The ranges of the lengths of the normalized mechanism are now narrowed down to

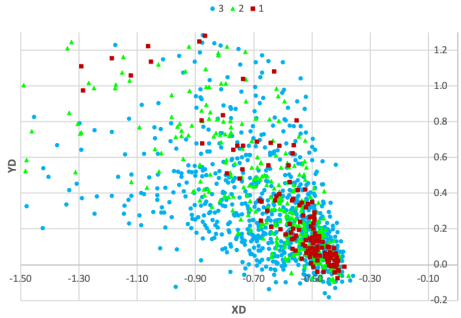

a)

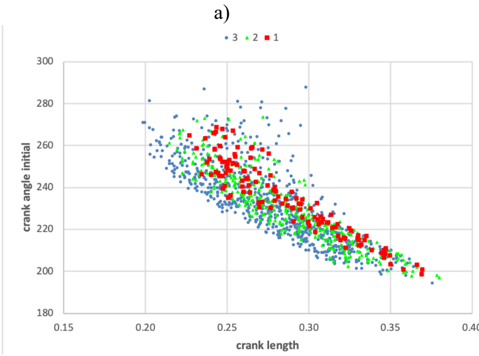

b)

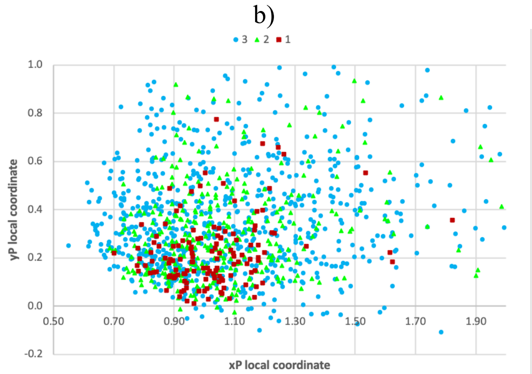

c)

Figure 3.9 – Scatter of solutions with the best accuracy ε (first stage): ‘1’ – $\varepsilon \leq 0{,}0075$ (the best accuracy on the truncated (by accuracy) table); ‘2’ – $0{,}0075 < \varepsilon \leq 0{,}01$; ‘3’ – $0{,}01 < \varepsilon \leq 0{,}015$ (the worst accuracy on the truncated (by accuracy) table)

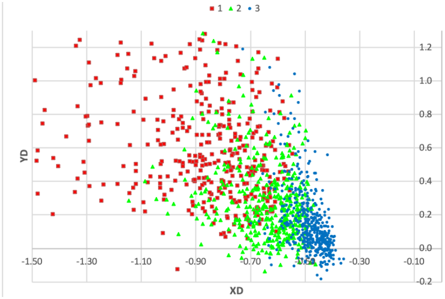

a)

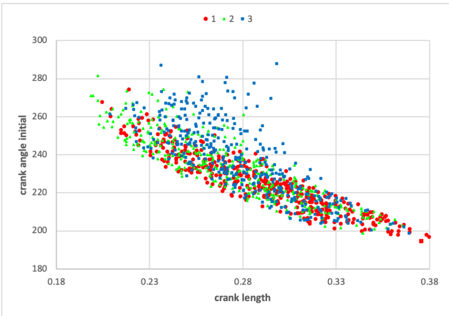

b)

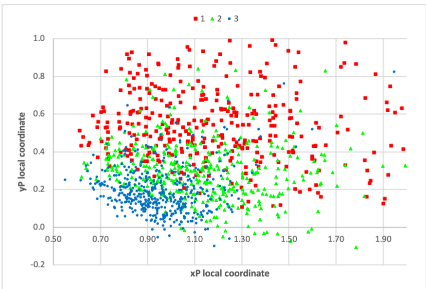

c)

Figure 3.10 – Scatter of solutions with the best motion transfer μ_e (first stage):
'1' – μ_e>40° the best motion transfer on the truncated (by μ_e) table;
'2' – 30°≤ μ_e<40°;'3' – 18°≤ μ_e<30°

- $0.175 \leq r_{AB} \leq 0.5$,
- $0.410 \leq l_{BC} \leq 1.200$,
- $0.530 \leq l_{CD} \leq 1.200$,
- $40° \leq \varphi_0 \leq 100°$

On this stage truncated are Test Tables with the accuracy limit ε<0.006 (0.6% of the trajectory length) and the pressure angle μ_e>22°. Table 3 shows the link sizes with the best accuracy (ordered by increasing approximation error), and Table 4 shows the mechanisms with the best motion transfer (ordered by decreasing pressure angle μ_e).

The scatter of acceptable solutions under the indicated restrictions (Figure 3.11, 3.12 and Table 3.3, Table 3.4) show that the considering criteria are conflicting: as the accuracy improves, the pressure angle decreases and vice versa. For example, it can be seen from the resulting figures that the best parameter values $X_D - Y_D$ in terms of accuracy (red dots) lie in the lower right corner (Figure 3.11a), while acceptable solutions $X_D - Y_D$, corresponding to good pressure angles, lie in the upper left corner (red dots in Figure 3.12a). The best parameter values $r_{AB} - \varphi_0$ in terms of accuracy lie in the upper left corner (red dots in Figure 3.11b), while the best solutions $r_{AB} - \varphi_0$, corresponding to good pressure angles lie in the lower right corner (Figure 3.12b). Finally, the best parameters $x_E - y_E$ lie at the bottom in terms of accuracy (red dots in Figure 3.11c), and are shifted upward in terms of pressure angle (red dots in Figure 3.12c).

Table 3.3 – The mechanism dimensions with the best accuracy

r_{AB} [m]	l_{BC} [m]	l_{CD} [m]	X_D [m]	Y_D [m]	φ_0, ***[deg]***
0,2335	0,4926	0,5037	-0,4243	0,0301	245
x_1=x_E	x_2=y_E	x_3=S_x	x_4=S_y	δ	μ_e
0,9568	0,0271	2,0543	1,8465	0,0049	22,2

Working with truncated Test Tables, further we discard solutions with restrictions μ_e < 24°. and ε > 0.0057, compromise solutions were found that satisfy all of the considered conflict criteria. The best solutions in terms of accuracy are shown in Table A1 (Appendix 1), in terms of pressure angle – in Table A2 (Appendix 1). As a result of the analysis of these Tables, the first line of Table A2 with the LP_τ -sequence number 10995 was chosen as the optimal solution; best pressure angle μ_e = 25.1°; however, the loss in accuracy is not significant: the accuracy ε = 0.0057 is very close to the best accuracy $\varepsilon = 0.0052$ obtained from Table A1 (Appendix A).

Table 3.4 – The mechanism dimensions with the best transmission angle

r_{AB} [m]	l_{BC} [m]	l_{CD} [m]	X_D [m]	Y_D [m]	φ_0 [deg]
0,2445	0,4867	0,5002	-0,4531	0,0925	238
$x_1=x_E$	$x_2=y_E$	$x_3=S_x$	$x_4=S_y$	δ	μ_e
0,9230	0,1457	1,7207	1,8693	0,0060	25,5

Noteworthy are 3 more solutions included in the Top 14 of both Tables A1 and A2: these are solutions with LP_τ -sequence numbers 29755, 23207 and 10823.

The final mechanism is shown in Figure 3.13, the mechanism structural scheme corresponds to the scheme in Figure 3.1. Instead of prismatic pair M in Figure 3.1, we used another straight-line generator driven by a servo, that provides a set of infinite vertical-line trajectories which allow the robot to adopt to unevenness of the surface. The study of the adaptation mechanism of the WR is out of scope of this work. As a part of the design work, an operational prototype of the WR was developed (Figure 3.13) using the synthesized mechanism as a propeller. Directions for the future research include investigation and experimental studies of the adaptation mechanism.

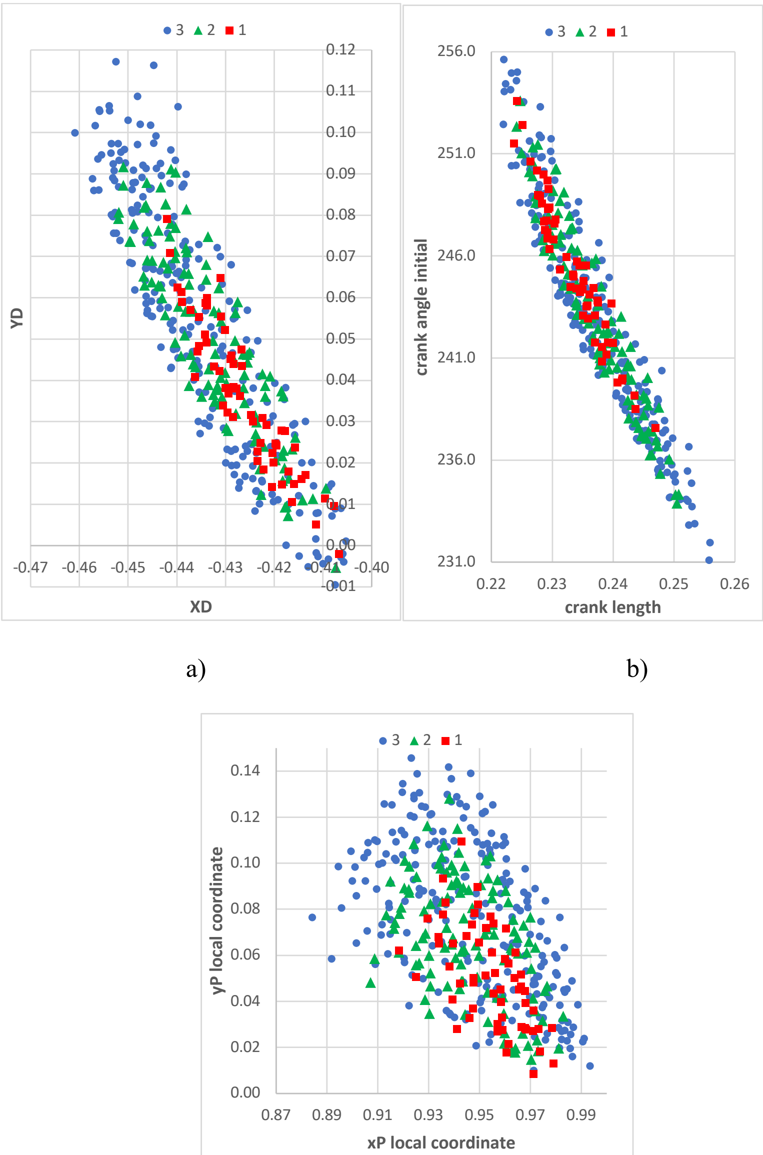

a) b)

c)

Figure 3.11 – Scatter of solutions with best accuracy: ‘‘1’ – $\varepsilon \leq 0{,}0054$; ‘2’ – $0{,}0054 < \varepsilon \leq 0{,}0057$;‘3’ – $0{,}0057 < \varepsilon \leq 0{,}006$

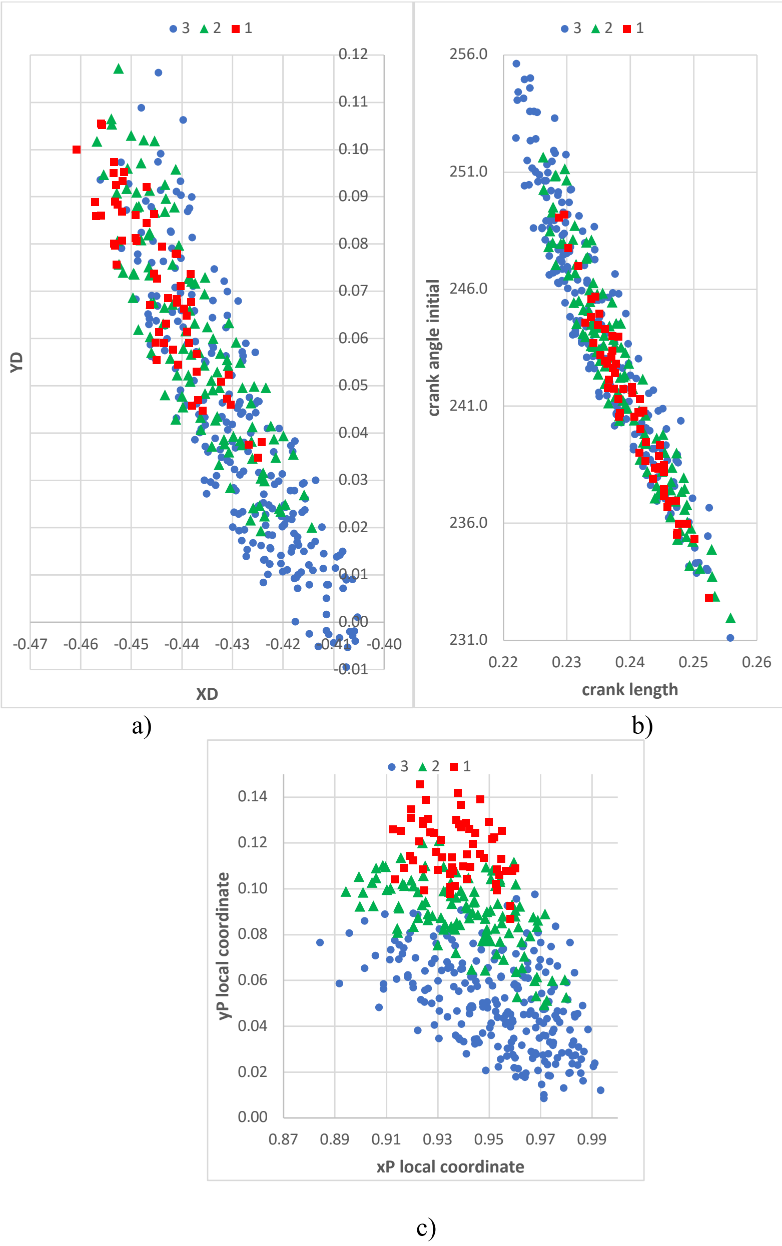

Figure 3.12 – Scatter of solutions with the best motion transfer: ‘1’ – $\mu_e \geq 24$grad.; ‘2’ – $23{,}5 \leq \mu_e < 24$ (grad) ; ‘3’ – $22 \leq \mu_e < 23{,}5$ (grad)

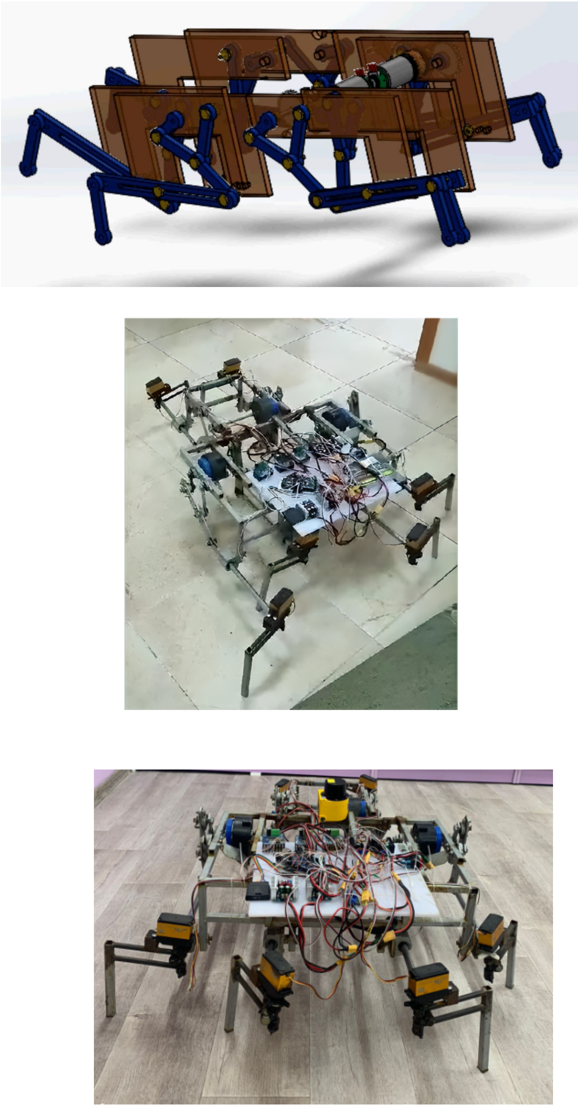

Figure 3.13 – 3D model of the WR and the experimental prototype

3.6 Conclusions on Section 3

An optimal design of walking robot leg mechanism is proposed that allows to reduce the power consumption and simplifies the control system of the robot. Open-ended неограниченный range of foot adaptation to unevenness of a supporting surface is reached due to the use of the “shin-link” that performs rectilinear and translational motion. The analytical synthesis methods based on the least-square approximation are presented that eliminates “the branching defect” that occurs in the most of the existing methods. The method of multicriteria design using Sobol – Statnikov LP-tau sequences allowed to find the mechanism with desired accuracy of the output motion, transmission angle and step cycle parameter. Transmission angle increased from $12° - 15°$ in existing prototypes to 25°. The step cycle parameter $\nu = \Phi_{SUP}/\Phi_{TRANSF}$ of the synthesized mechanism is 1.59, the duration of the support phase is increased up to 221°, whereas the values of these parameters in prototype are $\nu = 1.045$ and $\Phi_{SUP} = 184°$.

4 Optimization of the metric parameters of the WR

Various "measures" have been proposed to estimate how far the position of the mechanism is "remote" from the nearest singular position of the second kind. In Mechanisms and Machines Theory, for example, there is the concept of the quality of motion transmission (the closest concept in German literature is "Uebertragungsguete"). In the English-language literature, there are a number of concepts that are close in meaning, such as manipulability, the ability of force and motion transfer, the kinematic performance index, etc.

So, in work (Kraynev & Glazunov, 1994), as such a measure, the "transfer coefficient" is proposed as the product of the sines of the pressure angles related to the output and input links. Funabashi, H. *et al*. (Takeda & Funabashi, 1995; Takeda et al., 1997) propose to use the sine of the pressure angle related to the output link, wherein consider the angle formed by the direction of motion of a rotational or spherical kinematic pair on the platform and the direction of the relative motion of this pair around the joint on the input link. Despite the fact that the equality of the named angle to zero is a sufficient condition of singularity, its magnitude is not linear with respect to the force transmission.

Yoshikava, T. (Yoshikawa, 1985) uses the determinant of the Jacobian matrix as a criterion of manipulability, which transforms the generalized velocities at the input into the generalized velocities at the output object, and the determinant is a measure that reflects the transformation of a unit sphere into an ellipsoid, more precisely, the change in its dimensions along the principal axes. In other words, this measure indicates some integrated value of the velocity that is achieved by the generalized output velocities in different directions. Considering special cases of symmetric planar and spatial manipulators, Duffy, J. (Lee et al., 1996) also introduced a measure based on the determinant of the Jacobian matrix. It is obvious that these measures are local criteria and depend on the configuration of the manipulator. Tsai, K.Y. in the work (Tsai & Huang, 1998) introduces a global criterion that is the integral of the square of the determinant (of a matrix that is the product of the Jacobian matrix and its transposition) over the entire working volume of the manipulator.

A clearer interpretation of the transfer criterion was described in the works of Angeles, J. (Angeles, 2003; Angeles & López-Cajún, 1992), who proposed to consider as the measure the condition number k of the Jacobian matrix, which is equal to the ratio of the largest and smallest eigenvalues. If we consider the ellipsoids of generalized velocities and generalized forces, then the number k reflects the uniformity of the motions and forces transmission. The maximum reciprocal value $1/k$ over the entire working volume (which varies from zero to one), is called the kinematic conditioning index of the manipulator. In addition to the Chebyshev norm, the root mean square criterion is also introduced as an integral of the Euclidean norm over the entire working volume.

The most complete to date is the method of optimal synthesis of parallel manipulators, proposed by representatives of the German school. In the works of Schoenherr, J. (Schoenherr & Bemessen, 1998; Schoenherr, 1999; Schoenherr & Weidermann, 1998) a generalized functional (Guetefunktional) is introduced based on

the use of the product of the weighted norm of the Jacobian matrix and the weighted norm of the inverse matrix and a method of optimal synthesis is presented.
The monograph (Ibraev, 2014) presents the results of researches on developing of synthesis methods and new kinematic schemes of planar manipulators, which are isotropic (in terms of force transfer) in the entire working area.

Consider a robot/manipulator with $W_q = n$ d.o.f. and generalized coordinates $q = [q_1, q_2, \dots, q_n]^T$. Assume that the output object also has $W_x = n$ d.o.f. Then the singular positions of the manipulator or robot, which are important in the analysis and synthesis of manipulators, are determined by the Jacobian matrix ($\boldsymbol{J}$): in such positions, its determinant is equal to zero: $\det\boldsymbol{J} = 0$. In the vicinity of such configurations, there is no unique solution to the direct and inverse kinematics. These positions define the boundaries of the working area of the manipulator (Sefrioui & Gosselin, 1995; Chablat et al., 1999) and are worst in terms of force transfer. The same Jacobian matrix is used in (Ibraev, 2014) to define the best configurations in terms of force and motion transfer:

$$\boldsymbol{J}^T\boldsymbol{J} = \alpha^2\boldsymbol{E}, \tag{4.1}$$

or

$$\boldsymbol{J}\boldsymbol{J}^{\boldsymbol{T}} = \alpha^2\boldsymbol{E}. \tag{4.2}$$

The configurations, satisfying (4.1) or (4.2), where E is the identity matrix and α is some real number, are called “isotropic”, which are the furthest configurations from singularity.

In Section 4.2 provided are the brief description of a walking robot (WR) structure and its kinematic-equivalent scheme that simplifies the study of turning modes. The isotropy criterion (4.2) is applied to the quasi-planar WR in Section 4.3 and on its basis, in Section 4.4, the optimal geometrical parameters of the robot were defined. An experimental prototypes of the WR with decoupled motion are presented. The experimental studies of the synthesized turning mechanism will be provided in the future. In this research we considered only one structural scheme of the WR. Future directions include also investigation of different structural schemes.

4.1 Derivation of the Isotropy Criterion

This section is devoted to defining criteria for the WR, which ensure optimal movement of the robot in terms of force/motion transmission. Consider a tripod gait, i.e., a common method, when three legs are in the support, three are in the transfer (lifted up) phase at all times. In the equivalent scheme (Figure 4.1) the first, third and fifth legs are in the support phase (feet S_1, S_3, S_5), *C* is the center of mass of the robot body/hull, $O_0\xi\eta\zeta$ is a global coordinate system fixed with the bearing surface, *CXY* is a coordinate system fixed with the robot body/hull. O_iP_i $(i = 1, 3, 5)$ is a local coordinate system, fixed with a link O_iP_i. The local coordinates of the joint S_i in this coordinate system are $x_{S_i} = a_i, y_{S_i} = q_i$, where q_i are generalized coordinates, $i = 1, 3, 5$.

For each foot S_i the following vector equation holds:

$$\overrightarrow{O_0S_i} = \overrightarrow{O_0C} + \overrightarrow{CO_i} + \overrightarrow{O_iS_i}, \quad i = 1, 3, 5, \tag{4.1}$$

or in terms of radius vectors of the joint centers,

$$\overrightarrow{R_{S_i}} = \overrightarrow{R_C} + \Gamma(\theta)\overrightarrow{r_{O_i}} + \Gamma(\theta + \alpha_i)\overrightarrow{r_{S_i}}, \tag{4.2}$$

where $\Gamma(\theta)$ is a rotation matrix:

$$\Gamma(\theta) = \begin{bmatrix} \cos(\theta) & -\sin(\theta) \\ \sin(\theta) & \cos(\theta) \end{bmatrix},$$

and

$$\overrightarrow{R_{S_i}} = \left[\xi_{S_i}, \eta_{S_i}\right]^T,$$

$$\overrightarrow{R_C} = [\xi_C, \eta_C]^T, \quad \overrightarrow{r_{O_i}} = \left[X_{O_i}, Y_{O_i}\right]^T, \ \overrightarrow{r_{S_i}} = [a_i, q_i]^T$$

are the radius-vectors of the mass center C of the body/hull, and the centers of the joints O_i, S_i in the coordinate systems $O_0\xi\eta\zeta, CXY, O_ix_iy_iz_i$respectively. θ is a rotation angle of the robot body/hull with respect to the absolute coordinate system $O_0\xi\eta\zeta$.

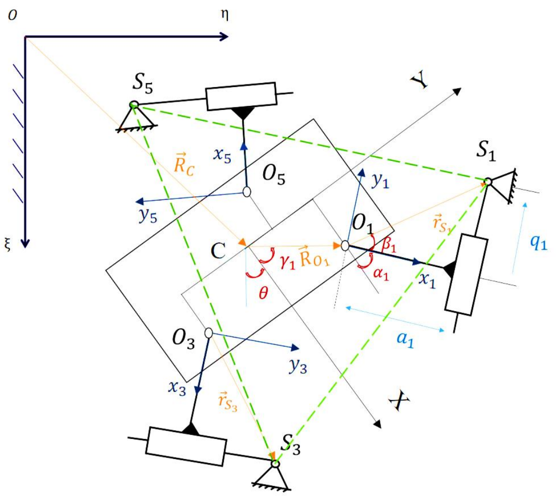

Figure 4.1 – Kinematic-equivalent scheme of the WR with a “tripod”-gate

Differentiation of (4.2) with respect to time gives the following correlation:

$$\vec{0} = \dot{\vec{R_C}} + \dot{\theta}\Gamma\left(\theta + \frac{\pi}{2}\right)\vec{r_{O_i}} + \left(\dot{\theta} + \dot{\alpha}_i\right)\Gamma\left(\theta + \alpha + \frac{\pi}{2}\right)\vec{r_{S_i}} +$$

$$+\Gamma\left(\theta + \alpha_i\right) \cdot \dot{\vec{r_{S_i}}}, \tag{4.3}$$

since $\frac{d\vec{R_{S_i}}}{dt} = \vec{0}$.

From (4.3) a Jacobian matrix J_q of the system can be found, which is defined as

$$\dot{\mathbf{x}} = J_q \dot{\mathbf{q}}$$

or

$$J_q = \frac{d\mathbf{x}}{d\mathbf{q}}, \tag{4.4}$$

$\mathbf{x} = \left[\vec{R_C}^T, L_\theta \theta\right]^T = \left[\xi_C, \eta_C, L_\theta \theta\right]^T$ – output coordinates, where L_θ – characteristic length, and input coordinates are $\mathbf{q} = \left[q_1, q_3, q_5\right]^T$.

To eliminate α_i, from the equation (4.3), we multiply the equation from the left by the vector $\vec{O_i S_i} = \Gamma\left(\theta + \alpha_i\right)\vec{r_{S_i}}$. Then since,

$$\left(\theta+\alpha_i\right)\overrightarrow{r_{S_i}}^T\cdot\Gamma^T(\theta+\alpha_i)\cdot\Gamma\left(\theta+\alpha_i+\frac{\pi}{2}\right)\cdot\overrightarrow{r_{S_i}}=0,$$

the equation (4.3) can be rewritten as follows:

$$\overrightarrow{r_{S_i}}^T\cdot\Gamma^T(\theta+\alpha_i)\cdot\dot{\overrightarrow{R_C}}+\dot{\theta}\cdot\overrightarrow{r_{S_i}}^T\cdot\Gamma^T\left(\frac{\pi}{2}-\alpha_i\right)\cdot\overrightarrow{r_{O_i}}=$$

$$=-q_i\dot{q}_i,\quad i=1,3,5. \tag{4.5}$$

Then the Jacobian matrix

$$J_q=A^{-1}B, \tag{4.6}$$

where

$$A=\begin{bmatrix}\overrightarrow{r_{S_1}}^T\cdot\Gamma^T(\theta+\alpha_1) & \frac{1}{L_\theta}\overrightarrow{r_{S_1}}^T\cdot\Gamma^T\left(\frac{\pi}{2}-\alpha_1\right)\cdot\overrightarrow{r_{O_1}}\\ \overrightarrow{r_{S_3}}^T\cdot\Gamma^T(\theta+\alpha_3) & \frac{1}{L_\theta}\overrightarrow{r_{S_3}}^T\cdot\Gamma^T\left(\frac{\pi}{2}-\alpha_3\right)\cdot\overrightarrow{r_{O_3}}\\ \overrightarrow{r_{S_5}}^T\cdot\Gamma^T(\theta+\alpha_5) & \frac{1}{L_\theta}\overrightarrow{r_{S_5}}^T\cdot\Gamma^T\left(\frac{\pi}{2}-\alpha_5\right)\cdot\overrightarrow{r_{O_5}}\end{bmatrix},$$

$$B=-\begin{bmatrix}q_1 & 0 & 0\\ 0 & q_3 & 0\\ 0 & 0 & q_5\end{bmatrix}.$$

The isotropy condition (1.1) can be transformed to another form [12]:

$$\left(J_q^{-1}\right)^T\cdot J_q^{-1}=\frac{1}{\lambda^2}E, \tag{4.7}$$

where E is the identity matrix, $\dim E=3\times 3$, and

$$J_q^{-1}=$$

$$\begin{bmatrix}\frac{1}{q_1}\overrightarrow{r_{S_1}}^T\cdot\Gamma^T(\theta+\alpha_1) & \frac{1}{q_1L_\theta}\overrightarrow{r_{S_1}}^T\cdot\Gamma^T\left(\frac{\pi}{2}-\alpha_1\right)\cdot\overrightarrow{r_{O_1}}\\ \frac{1}{q_3}\overrightarrow{r_{S_3}}^T\cdot\Gamma^T(\theta+\alpha_3) & \frac{1}{q_3L_\theta}\overrightarrow{r_{S_3}}^T\cdot\Gamma^T\left(\frac{\pi}{2}-\alpha_3\right)\cdot\overrightarrow{r_{O_3}}\\ \frac{1}{q_5}\overrightarrow{r_{S_5}}^T\cdot\Gamma^T(\theta+\alpha_5) & \frac{1}{q_5L_\theta}\overrightarrow{r_{S_5}}^T\cdot\Gamma^T\left(\frac{\pi}{2}-\alpha_5\right)\cdot\overrightarrow{r_{O_5}}\end{bmatrix} \tag{4.8}$$

The following equation can be derived from (4.8):

$$\frac{1}{q_i}\overrightarrow{r_{S_i}}^T \cdot \Gamma^T(\theta+\alpha_i) =$$

$$= \frac{1}{q_i}\left[\overrightarrow{e_\xi}^T \Gamma(\theta+\alpha_i)\overrightarrow{r_{S_i}} \quad \overrightarrow{e_\eta}^T \Gamma(\theta+\alpha_i)\overrightarrow{r_{S_i}}\right],$$

$$\frac{1}{q_i L_\theta}\overrightarrow{r_{S_i}}^T \cdot \Gamma^T\left(\frac{\pi}{2}-\alpha_i\right)\cdot \overrightarrow{r_{O_i}} = \frac{1}{q_i L_\theta}\overrightarrow{e_\zeta}^T\left[\overrightarrow{r_{O_i}} \times \Gamma(\alpha_i)\overrightarrow{r_{S_i}}\right],$$

where $\overrightarrow{e_\xi}, \overrightarrow{e_\eta}, \overrightarrow{e_\zeta}$ are the basis vectors of the coordinate system $O_0\xi\eta\zeta$.

Thus,

$$J_q^{-1} = \tag{4.9}$$

$$-\begin{bmatrix} \frac{1}{q_1}\overrightarrow{e_\xi}^T\Gamma(\theta+\alpha_1)\overrightarrow{r_{S_1}} & \frac{1}{q_1}\overrightarrow{e_\eta}^T\Gamma(\theta+\alpha_1)\overrightarrow{r_{S_1}} & \frac{1}{q_1 L_\theta}\overrightarrow{e_\zeta}^T\left[\overrightarrow{r_{O_1}}\times\Gamma(\alpha_1)\overrightarrow{r_{S_1}}\right] \\ \frac{1}{q_3}\overrightarrow{e_\xi}^T\Gamma(\theta+\alpha_3)\overrightarrow{r_{S_3}} & \frac{1}{q_3}\overrightarrow{e_\eta}^T\Gamma(\theta+\alpha_3)\overrightarrow{r_{S_3}} & \frac{1}{q_3 L_\theta}\overrightarrow{e_\zeta}^T\left[\overrightarrow{r_{O_3}}\times\Gamma(\alpha_3)\overrightarrow{r_{S_3}}\right] \\ \frac{1}{q_5}\overrightarrow{e_\xi}^T\Gamma(\theta+\alpha_5)\overrightarrow{r_{S_5}} & \frac{1}{q_5}\overrightarrow{e_\eta}^T\Gamma(\theta+\alpha_5)\overrightarrow{r_{S_5}} & \frac{1}{q_5 L_\theta}\overrightarrow{e_\zeta}^T\left[\overrightarrow{r_{O_5}}\times\Gamma(\alpha_5)\overrightarrow{r_{S_5}}\right] \end{bmatrix}.$$

The isotropy condition can be represented in a more compact form, using the variable β_i, the angle between the vectors $\overrightarrow{O_iP_i}$ and $\overrightarrow{r_{S_i}}$, i.e. $tg\beta_i = \frac{q_i}{a_i}$ (see figure 1). To this end we can obtain

$$\frac{1}{q_i}\Gamma(\theta+\alpha_i)\overrightarrow{r_{S_i}} =$$

$$= \frac{r_{S_i}}{q_i}\Gamma(\theta+\alpha_i)\cdot\begin{bmatrix}\cos\beta_i \\ \sin\beta_i\end{bmatrix} = \frac{1}{\sin\beta_i}\begin{bmatrix}\cos(\theta+\alpha_i+\beta_i) \\ \sin(\theta+\alpha_i+\beta_i)\end{bmatrix},$$

where $r_{S_i} = \sqrt{a_i^2+q_i^2}$ – magnitude of the vector $\overrightarrow{r_{S_i}}$, and $\cos\beta_i = \frac{a_i}{r_{S_i}}, \sin\beta_i = \frac{q_i}{r_{S_i}}$. Hence,

$$\frac{1}{q_i}\overrightarrow{e_{\xi_i}}^T\cdot\Gamma(\theta+\alpha_i)\overrightarrow{r_{S_i}} = \frac{\cos(\theta+\alpha_i+\beta_i)}{\sin\beta_i};$$

$$\frac{1}{q_i}\vec{e}_{\eta_i}^{\,T}\cdot\Gamma(\theta+\alpha_i)\vec{r}_{S_i}=\frac{\sin(\theta+\alpha_i+\beta_i)}{\sin\beta_i};$$

Also, the right column in the expression (4.9) can be simplified as follows:

$$\frac{1}{q_i L_\theta}\vec{e}_\zeta^{\,T}\left[\vec{r}_{O_i}\times\Gamma(\alpha_i)\vec{r}_{S_i}\right]=$$

$$\frac{r_{S_i}}{L_\theta q_i}\vec{e}_\zeta^{\,T}\cdot\begin{vmatrix} X_{O_i} & Y_{O_i} \\ \cos(\alpha_i+\beta_i) & \sin(\alpha_i+\beta_i)\end{vmatrix}\vec{e}_\zeta=$$

$$\frac{r_{O_i}}{L_\theta\sin\beta_i}\sin(\alpha_i+\beta_i-\gamma_i),$$

r_{O_i}, γ_i – polar coordinates of the center of the joint O_i:

$$r_{O_i}=\sqrt{X_{O_i}^2+Y_{O_i}^2}, tg\gamma_i=\frac{Y_{O_i}}{X_{O_i}}.$$

Then the expression (4.9)

$$J_q^{-1}=$$

$$\begin{bmatrix} \dfrac{cos(\theta+\alpha_1+\beta_1)}{sin\,\beta_1} & \dfrac{sin(\theta+\alpha_1+\beta_1)}{sin\,\beta_1} & \dfrac{r_{O_1}}{L_\theta sin\,\beta_1}sin(\alpha_1+\beta_1-\gamma_1) \\ \dfrac{cos(\theta+\alpha_3+\beta_3)}{sin\,\beta_3} & \dfrac{sin(\theta+\alpha_3+\beta_3)}{sin\,\beta_2} & \dfrac{r_{O_3}}{L_\theta sin\,\beta_2}sin(\alpha_3+\beta_3-\gamma_3) \\ \dfrac{cos(\theta+\alpha_5+\beta_5)}{sin\,\beta_5} & \dfrac{sin(\theta+\alpha_5+\beta_5)}{sin\,\beta_5} & \dfrac{r_{O_5}}{L_\theta sin\,\beta_5}sin(\alpha_5+\beta_5-\gamma_5)\end{bmatrix}. \quad (4.10)$$

Now, from (4.7)

$$\left(J_q^{-1}\right)^T\cdot J_q^{-1}=\begin{bmatrix} j_{11} & j_{12} & j_{13} \\ j_{21} & j_{22} & j_{23} \\ j_{31} & j_{32} & j_{33}\end{bmatrix}=\frac{1}{\lambda^2}E, \quad (4.11)$$

where

$$j_{11}=\sum_{i=1,3,5}\frac{\cos^2(\theta+\alpha_i+\beta_i)}{\sin^2\beta_i};$$

$$j_{12} = \sum_{i=1,3,5} \frac{\sin 2(\theta + \alpha_i + \beta_i)}{2\sin^2\beta_i};$$

$$j_{13} = \sum_{i=1,3,5} \frac{r_{O_i}\cos(\theta + \alpha_i + \beta_i)\sin(\alpha_i + \beta_i - \gamma_i)}{L_\theta \sin^2\beta_i};$$

$$j_{21} = \sum_{i=1,3,5} \frac{\sin 2(\theta + \alpha_i + \beta_i)}{2\sin^2\beta_i};$$

$$j_{22} = \sum_{i=1,3,5} \frac{\sin^2(\theta + \alpha_i + \beta_i)}{\sin^2 i};$$

$$j_{23} = \sum_{i=1,3,5} \frac{r_{O_i}\sin(\theta + \alpha_i + \beta_i)\sin(\alpha_i + \beta_i - \gamma_i)}{L_\theta \sin^2\beta_i};$$

$$j_{31} = \sum_{i=1,3,5} \frac{r_{O_i}\cos(\theta + \alpha_i + \beta_i)\sin(\alpha_i + \beta_i - \gamma_i)}{L_\theta \sin^2\beta_i};$$

$$j_{32} = \sum_{i=1,3,5} \frac{r_{O_i}\sin(\theta + \alpha_i + \beta_i)\sin(\alpha_i + \beta_i - \gamma_i)}{L_\theta \sin^2\beta_i};$$

$$j_{33} = \sum_{i=1,3,5} \frac{r_{O_i}\sin^2(\alpha_i + \beta_i - \gamma_i)}{L_\theta^2 \sin^2\beta_i}.$$

Therefore, we get 6 **isotropy conditions**:

$$\sum_{i=1,3,5} \frac{\cos^2(\theta + \alpha_i + \beta_i)}{\sin^2\beta_i} = \frac{1}{\lambda^2}; \tag{4.12}$$

$$\sum_{i=1,3,5} \frac{\sin^2(\theta + \alpha_i + \beta_i)}{\sin^2\beta_i} = \frac{1}{\lambda^2}; \tag{4.13}$$

$$\sum_{i=1,3,5} \frac{r_{O_i}\sin^2(\alpha_i + \beta_i - \gamma_i)}{\sin^2\beta_i} = \frac{1}{\lambda^2}; \tag{4.14}$$

$$\sum_{i=1,3,5} \frac{\sin 2(\theta + \alpha_i + \beta_i)}{\sin^2\beta_i} = 0; \tag{4.15}$$

$$\sum_{i=1,3,5} \frac{r_{O_i} \cos(\theta + \alpha_i + \beta_i) \sin(\alpha_i + \beta_i - \gamma_i)}{\sin^2 \beta_i} = 0; \tag{4.16}$$

$$\sum_{i=1,3,5} \frac{r_{O_i} \sin(\theta + \alpha_i + \beta_i) \sin(\alpha_i + \beta_i - \gamma_i)}{\sin^2 \beta_i} = 0. \tag{4.17}$$

For convenience in the further studies the derived conditions were used in different forms. From (4.1), (4.12)

$$\frac{1}{\lambda^2} = \frac{1}{2}\left(\frac{1}{\sin^2 \beta_1} + \frac{1}{\sin^2 \beta_3} + \frac{1}{\sin^2 \beta_5}\right). \tag{4.18}$$

since,

$$\sum_{i=1,3,5} \frac{\cos^2(\theta + \alpha_i + \beta_i)}{\sin^2 \beta_i} = \sum_{i=1,3,5} \frac{\sin^2(\theta + \alpha_i + \beta_i)}{\sin^2 \beta_i}\ , \tag{4.19}$$

$$\sum_{i=1,3,5} \frac{\cos 2(\theta + \alpha_i + \beta_i)}{\sin^2 \beta_i} = 0\,. \tag{4.20}$$

And from (4.15), (4.20)

$$\begin{aligned} &\sum_{i=1,3,5} \frac{1}{\sin^2 \beta_i} \begin{bmatrix} \cos 2(\theta + \alpha_i + \beta_i) \\ \sin 2(\theta + \alpha_i + \beta_i) \end{bmatrix} = \\ &= \sum_{i=1,3,5} \frac{1}{\sin^2 \beta_i} \Gamma(2\theta) \cdot \begin{bmatrix} \cos 2(\alpha_i + \beta_i) \\ \sin 2(\alpha_i + \beta_i) \end{bmatrix} = 0 \end{aligned} \tag{4.21}$$

Since the last equality holds for any θ, the angle θ can be eliminated from the conditions (4.12) and (4.13):

$$\frac{\cos 2(\alpha_1 + \beta_1)}{\sin^2 \beta_1} + \frac{\cos 2(\alpha_3 + \beta_3)}{\sin^2 \beta_3} + \frac{\cos 2(\alpha_5 + \beta_5)}{\sin^2 \beta_5} = 0 \tag{4.22}$$

$$\frac{\sin 2(\alpha_1 + \beta_1)}{\sin^2 \beta_1} + \frac{\sin 2(\alpha_3 + \beta_3)}{\sin^2 \beta_3} + \frac{\sin 2(\alpha_5 + \beta_5)}{\sin^2 \beta_5} = 0 \tag{4.23}$$

Similarly, the rotation angle can be excluded from the equations (4.16), (4.17).

If we denote $u_i = r_{O_i} \sin(\alpha_i + \beta_i - \gamma_i)$, $i = 1,3,5$, then the equations (4.14), (4.16), (4.17), taking into account (4.18) will get the following forms:

$$\sum_{i=1,3,5} \frac{u_i^2}{sin^2 \beta_i} = \frac{L_\theta^2}{2} \sum_{i=1,3,5} \frac{1}{sin^2 \beta_i}; \tag{4.24}$$

$$\begin{aligned} &\begin{bmatrix} \displaystyle\sum_{i=1,3,5} \frac{u_i \, cos(\theta + \alpha_i + \beta_i)}{sin^2 \beta_i} \\ \displaystyle\sum_{i=1,3,5} \frac{u_i \, sin(\theta + \alpha_i + \beta_i)}{sin^2 \beta_i} \end{bmatrix} = \\ &= \sum_{i=1,3,5} \frac{u_i}{sin^2 \beta_i} \Gamma(\theta) \cdot \begin{bmatrix} cos(\alpha_i + \beta_i) \\ sin(\alpha_i + \beta_i) \end{bmatrix} = 0. \end{aligned} \tag{4.25}$$

$$\begin{aligned} &\sum_{i=1,3,5} \frac{u_i \, cos(\alpha_i + \beta_i)}{sin^2 \beta_i} = 0, \\ &\sum_{i=1,3,5} \frac{u_i \, sin(\alpha_i + \beta_i)}{sin^2 \beta_i} = 0. \end{aligned} \tag{4.26}$$

And from (4.22), (4.23)

$$\frac{\cos^2 2(\alpha_5 + \beta_5)}{\sin^4 \beta_5} = \frac{\cos^2 2(\alpha_3 + \beta_3)}{\sin^4 \beta_3} + \frac{\cos^2 2(\alpha_1 + \beta_1)}{\sin^4 \beta_1} + $$
$$+2 \frac{\cos 2(\alpha_3 + \beta_3) \cos 2(\alpha_1 + \beta_1)}{\sin^2 \beta_3 \sin^2 \beta_1};$$

$$\frac{\sin^2 2(\alpha_5 + \beta_5)}{\sin^4 \beta_5} = \frac{\sin^2 2(\alpha_3 + \beta_3)}{\sin^4 \beta_3} + \frac{\sin^2 2(\alpha_1 + \beta_1)}{\sin^4 \beta_1} + $$
$$+2 \frac{\sin 2(\alpha_3 + \beta_3) \sin 2(\alpha_1 + \beta_1)}{\sin^2 \beta_3 \sin^2 \beta_1}.$$

Hence,

$$\frac{1}{\sin^4\beta_5} =$$

$$= \frac{1}{\sin^4\beta_3} + \frac{1}{\sin^4\beta_1} + 2\frac{\cos 2(\alpha_3 + \beta_3 - \alpha_1 - \beta_1)}{\sin^2\beta_3 \sin^2\beta_1}. \tag{4.27a}$$

$$\cos 2(\alpha_3 + \beta_3 - \alpha_1 - \beta_1) =$$

$$= \frac{\sin^2\beta_3 \sin^2\beta_1}{2}\left(\frac{1}{\sin^4\beta_5} - \frac{1}{\sin^4\beta_3} - \frac{1}{\sin^4\beta_1}\right). \tag{4.27b}$$

Due to the symmetricity of equations (4.22), (4.23), using the cyclic permutation of indices (1 – 3 – 5 – 1),

$$\cos 2(\alpha_5 + \beta_5 - \alpha_1 - \beta_1) =$$

$$= \frac{\sin^2\beta_5 \sin^2\beta_1}{2}\left(\frac{1}{\sin^4\beta_3} - \frac{1}{\sin^4\beta_5} - \frac{1}{\sin^4\beta_1}\right). \tag{4.28}$$

4.2 Study of the Isotropy Conditions

4.2.1 Deserve more attention the symmetric solutions. Let's consider the case $\beta_i = \frac{\pi}{2}, i = 1,3,5$. From (3.18),

$$\frac{1}{\lambda^2} = \frac{3}{2}, \tag{4.1}$$

The following can be derived from (3.12), (3.13):

$$\sin^2 \alpha_1 + \sin^2 \alpha_3 + \sin^2 \alpha_5 = \frac{3}{2}; \tag{4.2}$$

$$\cos^2 \alpha_1 + \cos^2 \alpha_3 + \cos^2 \alpha_5 = \frac{3}{2}. \tag{4.3}$$

And (3.14) gives

$$\sin 2\alpha_1 + \sin 2\alpha_3 + \sin 2\alpha_5 = 0. \tag{4.4}$$

From (4.2) and (4.3) it follows

$$\cos 2\alpha_1 + \cos 2\alpha_3 + \cos 2\alpha_5 = 0. \tag{4.5}$$

A simple solution can be found from last formulas:

$$\cos 2(\alpha_3 - \alpha_1) = -\frac{1}{2};$$

Analogically, we can get

$$\cos 2(\alpha_i - \alpha_j) = -\frac{1}{2}, \qquad i,j = 1,3,5, i \neq j. \tag{4.6}$$

The parameters r_{O_i}, γ_i can be found using (3.14), (3.16) and (3.17):

$$\sum_{i=1,3,5} r_{O_i} \cos^2(\alpha_i - \gamma_i) = \frac{L_\theta^2}{\lambda^2}$$

Knowing that (see equation (4.1)

$$\sum_{i=1,3,5} r_{O_i} \cos^2(\alpha_i - \gamma_i) = \frac{3L_\theta^2}{2}, \tag{4.7}$$

we find

$$\sum_{i=1,3,5} r_{O_i} \sin\alpha_i \cos(\alpha_i - \gamma_i) = 0, \tag{4.8}$$

and

$$\sum_{i=1,3,5} r_{O_i} \cos\alpha_i \cos(\alpha_i - \gamma_i) = 0. \tag{4.9}$$

The last equations are also true for $\beta_i = -\frac{\pi}{2}$.
Denote $r_{O_i}\cos(\alpha_i - \gamma_i) = x_i$, then

$$\begin{cases} x_1^2 + x_3^2 + x_5^2 = \dfrac{3}{2} L_\theta^2 \\ x_1 \sin\alpha_1 + x_3 \sin\alpha_3 + x_5 \sin\alpha_5 = 0 \\ x_1 \cos\alpha_1 + x_3 \cos\alpha_3 + x_5 \cos\alpha_5 = 0 \end{cases} \tag{4.10}$$

According to the Cramer's rule, the solution of the last two equations:

$$\Delta = \sin(\alpha_3 - \alpha_5),$$

$$x_3 = -\frac{x_1 \begin{vmatrix} \sin\alpha_1 & \sin\alpha_5 \\ \cos\alpha_1 & \cos\alpha_5 \end{vmatrix}}{\Delta} = \frac{x_1 \sin(\alpha_5 - \alpha_1)}{\sin(\alpha_3 - \alpha_1)} \tag{4.11}$$

$$x_5 = -\frac{x_1 \begin{vmatrix} \sin\alpha_3 & \sin\alpha_1 \\ \cos\alpha_3 & \cos\alpha_1 \end{vmatrix}}{\Delta} = \frac{x_1 \sin(\alpha_1 - \alpha_3)}{\sin(\alpha_3 - \alpha_5)} \tag{4.12}$$

Thus,

$$x_1^2 = \frac{L_\theta^2}{2}. \tag{4.13}$$

For example, when $L_\theta = 1\frac{m}{rad}$,

$$r_{O_i}\cos(\alpha_i - \gamma_i) = \pm\frac{1}{\sqrt{2}}\ m;$$

Or if $L_\theta = \sqrt{2}\frac{m}{rad}$,

$$r_{O_i}\cos(\alpha_i-\gamma_i)=\pm 1\,.$$

4.2.2 Consider a more general case: $\beta_1=\beta_3=\beta_5$.

Rewrite the equations (3.22), (3.23) as follows:

$$\left(\frac{\cos x_1}{\sin^2\beta_1}+\frac{\cos x_3}{\sin^2\beta_3}\right)^2=\left(-\frac{\cos x_5}{\sin^2\beta_5}\right)^2, \tag{4.14}$$

$$\left(\frac{\sin x_1}{\sin^2\beta_1}+\frac{\sin x_3}{\sin^2\beta_3}\right)^2=\left(-\frac{\sin x_5}{\sin^2\beta_5}\right)^2. \tag{4.15}$$

Then we get

$$\cos(x_1-x_5)= \tag{4.16}$$

$$=\frac{\sin^2\beta_5\sin^2\beta_1}{2}\left(\frac{1}{\sin^4\beta_3}-\frac{1}{\sin^4\beta_5}-\frac{1}{\sin^4\beta_1}\right)$$

And making cyclic permutation (1 – 3 – 5 – 1),

$$\cos(x_1-x_5)= \tag{4.17}$$

$$=\frac{\sin^2\beta_5\sin^2\beta_1}{2}\left(\frac{1}{\sin^4\beta_3}-\frac{1}{\sin^4\beta_5}-\frac{1}{\sin^4\beta_1}\right).$$

The case of equal angles $\beta_1=\beta_3=\beta_5$ will lead to a simple solution, which coincides with (4.6):

$$\begin{cases}\cos 2(\alpha_3-\alpha_1)=-\dfrac{1}{2},\\ \cos 2(\alpha_5-\alpha_1)=-\dfrac{1}{2}.\end{cases} \tag{4.18}$$

Hence,

$$\begin{cases}\alpha_3=\alpha_1\pm\dfrac{\pi}{3}+2\pi n, n=0,1,\\ \alpha_5=\alpha_1\mp\dfrac{\pi}{3}+2\pi k, k=0,1\end{cases} \tag{4.19}$$

This solution gives 8 combinations of $\{\alpha_3-\alpha_1,\alpha_5-\alpha_1\}$, each of which satisfies (3.22) and (3.23):

$$\left\{\frac{\pi}{3},-\frac{\pi}{3}\right\};\left\{\frac{\pi}{3},-\frac{2\pi}{3}\right\};\left\{-\frac{\pi}{3},\frac{\pi}{3}\right\};\left\{-\frac{\pi}{3},-\frac{2\pi}{3}\right\};$$
$$\left\{-\frac{2\pi}{3},-\frac{\pi}{3}\right\};\left\{-\frac{2\pi}{3},\frac{2\pi}{3}\right\};\left\{\frac{2\pi}{3},\frac{\pi}{3}\right\};\left\{\frac{2\pi}{3},-\frac{\pi}{3}\right\}, \tag{4.20}$$

Fig.5a illustrates 1-, 2-, 3-, 4-, 5-, 7-th solutions and the Fig.5b represents combinations $\{\alpha_3-\alpha_1,\alpha_5-\alpha_1\}=\left\{-\frac{2\pi}{3},\frac{2\pi}{3}\right\}$, and $\{\alpha_3-\alpha_1,\alpha_5-\alpha_1\}=\left\{\frac{2\pi}{3},-\frac{\pi}{3}\right\}$.

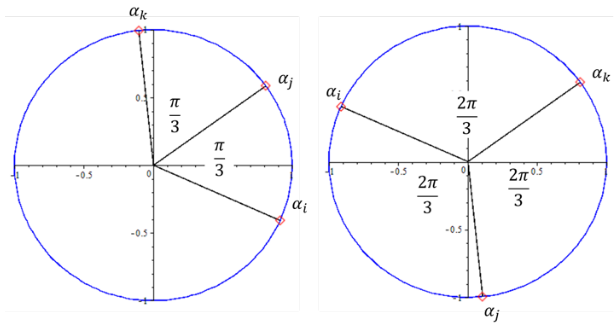

a) b)

Figure 4.2 – Illustration of combinations $\{\alpha_3-\alpha_1,\alpha_5-\alpha_1\}$

To search for the parameters β_i, r_{O_i}, we set $\beta_1=\beta_3=\beta_5=\beta$ again. Equation (24) in this case will take the form:

$$\sum_{i=\cancel{1,2},3} u_i^2=\frac{3L_\theta^2}{2}, \tag{4.21}$$

where

$$u_i=r_{O_i}sin(\alpha_i+\beta-\gamma_i).$$

Equations (3.25) and (3.26) give a system of two linear equations in the unknowns $\{u_3,u_5\}$:

$$\sum_{i=\cancel{1,3},5} u_i\Gamma(\beta)\cdot\begin{bmatrix}\cos(\alpha_i)\\ \sin(\alpha_i)\end{bmatrix}=0,$$

from where

$$\sum_{i=1,3,5} u_i \cos(\alpha_i) = 0, \qquad i = 1,3,5; \tag{4.22}$$

$$\sum_{i=1,3,5} u_i \sin(\alpha_i) = 0, \qquad i = 1,3,5. \tag{4.23}$$

Solving the last equations by Cramer's method with respect to u_3 and u_5,

$$u_3 = u_1 \frac{\sin(\alpha_1 - \alpha_5)}{\sin(\alpha_5 - \alpha_3)},$$
$$u_5 = u_1 \frac{\sin(\alpha_3 - \alpha_1)}{\sin(\alpha_5 - \alpha_3)}. \tag{4.24}$$

It is known from (3.18) that

$$\sin^2(\alpha_i - \alpha_j) = \frac{1 - \cos 2(\alpha_i - \alpha_j)}{2} = \frac{3}{4}. \tag{4.25}$$

Then the solution of (4.21) is

$$u_i = \pm \frac{L_\theta}{\sqrt{2}}, i = 1,3,5. \tag{4.26}$$

or

$$sin(\alpha_i + \beta - \gamma_i) = \pm \frac{L_\theta}{\sqrt{2} r_{O_i}}, i = 1,3,5. \tag{4.27}$$

The equality $u_1^2 = u_3^2 = u_5^2$ follows from (4.20) and (4.21). The solutions correspond to 8 combinations of $\{u_1, u_3, u_5\}$:

$$\begin{gathered}
\left\{\frac{L_\theta}{\sqrt{2}}, \frac{L_\theta}{\sqrt{2}}, \frac{L_\theta}{\sqrt{2}}\right\}, \left\{\frac{L_\theta}{\sqrt{2}}, \frac{L_\theta}{\sqrt{2}}, -\frac{L_\theta}{\sqrt{2}}\right\}, \\
\left\{\frac{L_\theta}{\sqrt{2}}, -\frac{L_\theta}{\sqrt{2}}, \frac{L_\theta}{\sqrt{2}}\right\}, \left\{\frac{L_\theta}{\sqrt{2}}, -\frac{L_\theta}{\sqrt{2}}, -\frac{L_\theta}{\sqrt{2}}\right\}, \\
\left\{-\frac{L_\theta}{\sqrt{2}}, \frac{L_\theta}{\sqrt{2}}, \frac{L_\theta}{\sqrt{2}}\right\}, \left\{-\frac{L_\theta}{\sqrt{2}}, \frac{L_\theta}{\sqrt{2}}, -\frac{L_\theta}{\sqrt{2}}\right\},
\end{gathered} \tag{4.28}$$

$$\left\{-\frac{L_\theta}{\sqrt{2}}, -\frac{L_\theta}{\sqrt{2}}, \frac{L_\theta}{\sqrt{2}}\right\}, \left\{-\frac{L_\theta}{\sqrt{2}}, -\frac{L_\theta}{\sqrt{2}}, -\frac{L_\theta}{\sqrt{2}}\right\}$$

As an example consider the case $u_1 = u_3 = u_5$, i.e. when

$$sin(\alpha_i + \beta - \gamma_i) = \frac{L_\theta}{\sqrt{2} r_{O_i}}, i = 1,3,5$$

or

$$sin(\alpha_i + \beta - \gamma_i) = -\frac{L_\theta}{\sqrt{2} r_{O_i}}, i = 1,3,5.$$

Only two of eight combinations $\{\alpha_3 - \alpha_1, \alpha_5 - \alpha_1\}$ satisfy the conditions (4.25), (4.26) in this case:

1) $\alpha_3 = \alpha_1 - \frac{2\pi}{3}, \alpha_5 = \alpha_1 + \frac{2\pi}{3};$

2) $\alpha_3 = \alpha_1 + \frac{2\pi}{3}, \alpha_5 = \alpha_1 - \frac{2\pi}{3}.$

Fig.6a demonstrate the configurations corresponding to the first, and Fig.6b correspond to the second solutions in symmetric case when

$$r_{O_1} = r_{O_3} = r_{O_5} = \pm \frac{L_\theta}{\sqrt{2}\sin(\alpha_1 + \beta - \gamma_1)};$$

$$\gamma_3 - \gamma_1 = \alpha_3 - \alpha_1;$$

$$\gamma_5 - \gamma_1 = \alpha_5 - \alpha_1.$$

For $\gamma_1 = \frac{\pi}{3}$,

1) for the first solution, $\gamma_3 = \gamma_1 - \frac{2\pi}{3} = -\frac{\pi}{3}; \gamma_5 = \gamma_1 + \frac{2\pi}{3} = \pi.$

2) and for the second solution $\gamma_3 = \gamma_1 + \frac{2\pi}{3} = \pi;\ \gamma_5 = \gamma_1 - \frac{2\pi}{3} = -\frac{\pi}{3}.$

Note that the second configuration can be obtained from the first by swapping leg mechanisms with numbers 3 and 5.

And for $\gamma_1 = -\frac{\pi}{3}$,

1) the first solution is $\gamma_3 = -\pi;\ \gamma_5 = \frac{\pi}{3}$,

2) and the second is $\gamma_3 = \frac{\pi}{3};\ \gamma_5 = -\pi,$

i.e. swapped are the legs with numbers 1 and 3.

When choosing α_1, γ_1, it is necessary that $sin(\alpha_i + \beta - \gamma_i), i = 1,3,5$ have the same signs. In the example above, this follows from condition (4.1):

$$\alpha_1 + \beta - \gamma_1 = \alpha_3 + \beta - \gamma_3 = \alpha_5 + \beta - \gamma_5.$$

for the first solution,

$$\gamma_3 = \gamma_1 - \frac{2\pi}{3} = -\frac{\pi}{3}.$$

As can be seen in the Figure 4.3, in the isotropic configuration the lines P_iS_i form an equilateral triangle. Another advantage is that the center of mass of body C is located in the center of the supporting triangle $\Delta S_1S_3S_5$, which ensures “equal” movement (the same ability of movement) in all directions and an equal margin of stability.

Remark. There is a disadvantage in these two configurations. Let's call "the main movement" the uniform translational motion of the WR. During the main movement, when the main engines rotate uniformly and the angular speeds $\omega_1, \omega_3, \omega_5$ reach the nominal value ω_{nom},, the robot operates in an energy-optimal mode. During such a movement, the guides P_iS_i of our model will be parallel (Figure 4.2a). And if $\beta_1 = \beta_3 = \beta_5$ and $a_1 = a_3 = a_5$, then the lines O_iS_i will be parallel, which means that the mechanism is in a singular position. To avoid the singularity, a_5 *can be chosen* differently: $a_5 \neq a_1, a_5 \neq a_3$. But a more advantageous solution is the case $\beta_3 = \beta_1, \beta_5 = -\beta_1$ (Figure 4.2b) or $\beta_3 = -\beta_1, \beta_5 = \beta_1$.

Thus, the expressions are obtained that determine the parameters P=$\gamma_3, \gamma_5, \alpha_3, \alpha_5, r_{O_1}, r_{O_3}, r_{O_5}$ for given values of X=$\alpha_1, \gamma_1, \beta_1, \beta_3, \beta_5, a$. As noted earlier, during the movement of the robot, two conditions must be maintained: the absence of a singularity, as well as the stability of the robot (the center of mass of the WR body should be inside the support triangle). After numerical studies of different solutions of the isotropy equations, for each solution were found the boundary values of the generalized coordinates satisfying both mentioned conditions. The step length of the WR is defined as $L_0 = \min(|q_1^* - q_1^{**}|, |q_3^* - q_3^{**}|, |q_5^* - q_5^{**}|)$. The optimal solution corresponds to $L_0 \to max$. Such a solution is $u_1 = u_3 = u_5$, $\{\alpha_3 - \alpha_1, \alpha_5 - \alpha_1\}$= $\left\{-\frac{2\pi}{3}, -\frac{\pi}{3}\right\}$. E.g., with the given parameters

$$\beta_0 = \beta_{1_0} = \beta_{3_0} = \beta_{5_0} = \frac{\pi}{4}, \gamma_1 = \frac{\pi}{3}, a_1 = 10\ cm, a_3 = 10\ cm, a_5 = 7\ cm,$$

$$r_{O_i} = \frac{L_\theta}{\sqrt{2}\, sin(\alpha_1 + \beta - \gamma_1)}, L_\theta = 0.1\ m;$$

the step length can be up to L_{0max}=*3.610688817* m. This indicates that the solution ensures a sufficient “remoteness” from singularity and instability.

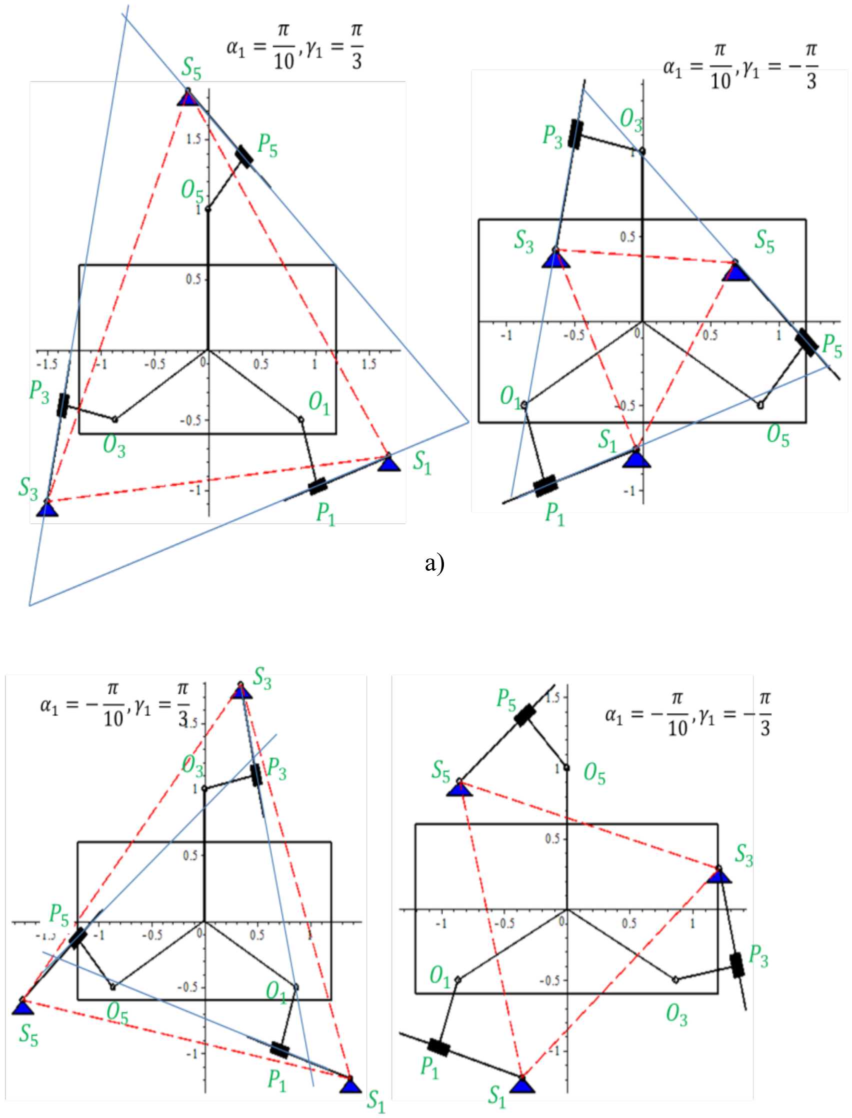

Figure 4.3 – Isotropic configurations: $r_{O_i} = 1, a_i = 0.5, i = 1,3,5.$

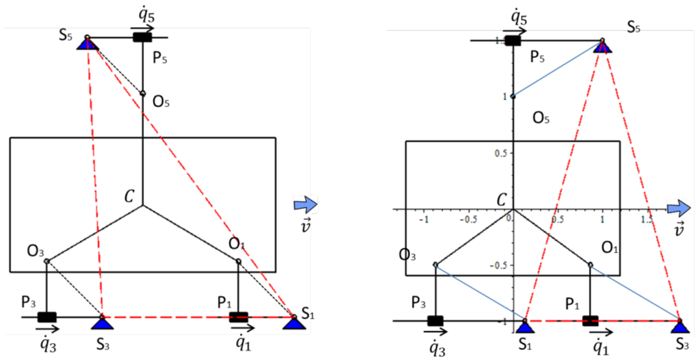

a) b)

Configurations at the main movement:
a) $\beta_1 = \beta_3 = \beta_5$; b) $\beta_1 = \beta_3 = -\beta_5$

Search for more symmetric solutions is provided in [Ibrayeva, 2019] and according to numerical studies was concluded that the above solutions are the furthest from singularity.

4.3 Conclusions on Section 4

Turning modes of the WR were studied and a parametric synthesis of the turning mechanism has provided. The rotation of the WR is carried out due to the difference in the velocities of the main drives. The method of synthesis of parallel manipulators based on the isotropy criterion is applied for optimization of the WR turning mechanism. The isotropy conditions for robots with orthogonal propulsion are derived. Solutions of isotropy equations are defined. The analysis of the solutions of the isotropy equations was carried out and on their basis the metric parameters of the robot were obtained, which ensure the optimal transmission of forces and motion. One of the symmetric solutions ensures the stability and absence of singularity for the step length 3.6 m, while the characteristic length of the robot is 10 cm.

5 Design of the Adaptation Mechanism to Uneven Surface

Based on the solution of the aforementioned multi-criteria optimization task, an SLM with optimal dimensions has been developed. The solution to the problem and the work with the Test Tables to obtain a compromise solution considering multiple criteria are described in Appendix B. The final dimensions of the mechanism with the best accuracy and motion transmission are shown in Tables 1 and 2, respectively. A 3D model of the AWR, developed using the SolidWorks software suite, and a working prototype of the ultimately selected SLM are shown in Figure 5.1. The construction of the prototype showed that in this mechanism, the *EF* link moves in a straight-line reciprocating motion uniformly with the uniform rotation of the crank.

A mechanism for adaptation to uneven terrain has been developed. The adaptation system was tested on the developed robot prototype (Figure 5.2). The adaptation is performed through the coordination of the main engine, which rotates the crank of the AWR's primary movement, and additional engines responsible for lifting and lowering the foot through the adaptation mechanism (Figure 5.2). During the transfer phase, i.e., at certain crank rotation angles φAB where $\varphi_0 + \Phi_{SUP} \leq \varphi_{AB} \leq \varphi_1$, where $\varphi_1 = \varphi_0 + 360^0$, the adaptation engine raises the foot to the maximum height. At the rotation angle $\varphi_1 = \varphi_0 + 360^0$, the leg enters the support phase and the foot begins to lower, and upon contact with the support surface, the foot contact sensor is triggered and sends a signal to the adaptation engine to "lock the engine," i.e., in the support phase, the adaptation engine is locked, ensuring linear motion of the body.

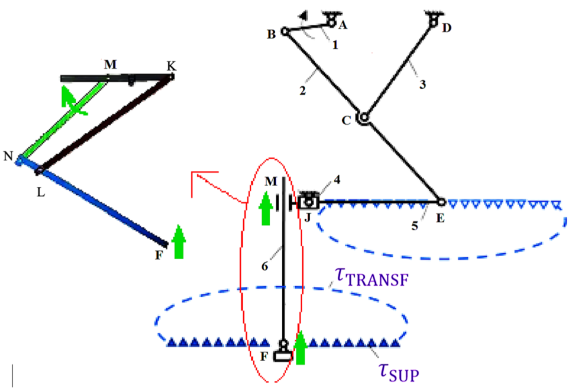

Figure 5.1 – Kinematic Scheme of the SLM of the AWR and the Adaptation Mechanism

The metrical values of the adaptation mechanism **normalized** (not real) by the crank (*MN*) length are following. *MN = 1, KL = 1.37126, NN' = 0.10591, N'L = 0.36312, LF = 0.63167, MK=0.52718,* where *N'* is the projection of the point (joint center) *N* to the line *FL.*

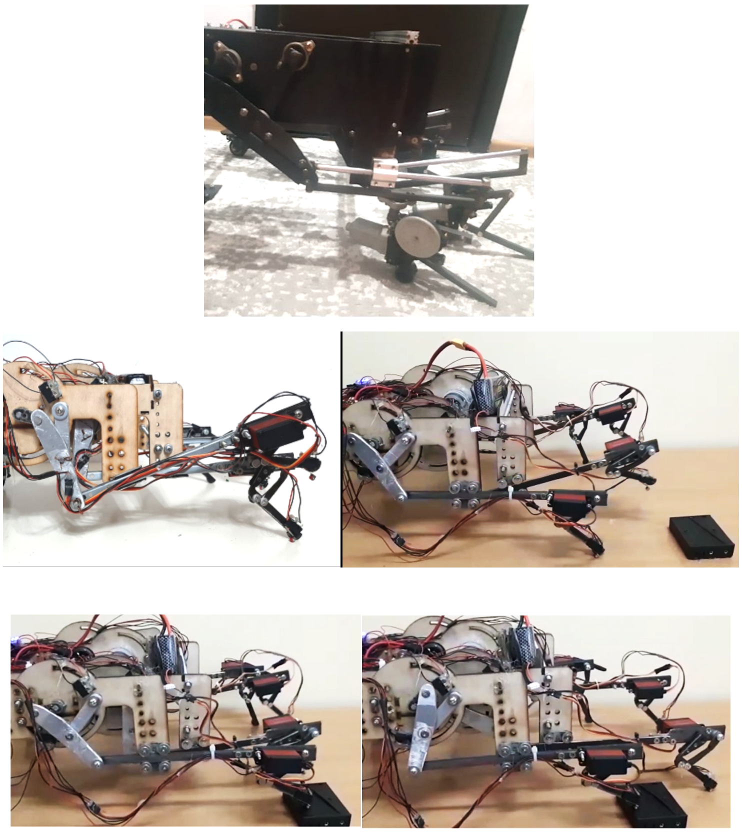

Figure 5.3 – Testing the adaptation mechanism of the WR

6 AWR Prototype Design and Experimental Validation

The aim of this experimental study is to develop a functional prototype of the AWR (Autonomous Walking Robot), with the following objectives:

- To test the effectiveness of implementing the new AWR scheme on a physical robot, especially in terms of forward movement and turning capabilities.
- To evaluate the functionality of the SLM (System of Parametric Measurements) of the AWR.
- To test the robot's control system.
- To identify any shortcomings in the proposed scheme.
- To conduct an energy consumption analysis: determining the duration of the robot's operation on a single full charge.
- Within the scope of this experimental research, an analysis of the turning mechanism will also be conducted: determining the optimal local angular positions of the robot's feet during the transfer phase relative to the body to ensure maximum turning angle of the body (Fig. 6.1).
- To study the robot's stability during movement: stability is achieved by ensuring the movement of the robot in which the projection of the center of mass constantly lies within the area supported by the robot's feet.

General Description of the Robot: For the purpose of conducting experimental research, three iterations of prototypes were developed, each manufactured with consideration of the shortcomings identified in previous experimental models.

For enhanced stability and safety of movement, an eight-legged design was chosen for the first two prototypes. During movement, four legs are constantly in the support phase while the other four are in the transfer phase, alternating in this pattern. The third stage tested a 'tripod gait' in a six-legged robot. The body and SLM (System of Parametric Measurements) of the prototypes were made of aluminum.

Controller. A readily available universal controller, the REV Robotics Control Hub, was used, the advantage of which is that it provides all the necessary interfaces for projects in robotics and mechatronics with multiple programming language options.

The Control Hub is specifically designed to withstand the harsh conditions of various experiments and research, thanks to its protection against electrostatic discharge and reverse polarity. The use of the Android operating system gives the Control Hub flexibility in managing both basic and advanced robots, as well as the ability to be updated on-site as new features are developed.

The Control Hub operates under the control of the Robot Controller application version 5.0 or higher and must be paired with the Driver Station application version 5.0 or higher.

Figure 6.1 REV Robotics Control Hub

Specifications
- Actuator interfaces
    - Control position and velocity of DC motors
    - Small and easy to control actuators
    - 4 - DC motor ports with built-in encoder ports
    - 6 - Servo motor ports
- Sensor and device interfaces
    - 8 - Digital input/output ports
    - 4 - Analog input ports
    - 4 - Independent I2C ports
    - 1 - Internal 9-axis IMU
- Additional expansion interfaces
    - Additional Expansion Hubs to add more actuator and sensor ports
    - 2 - RS485 ports
- Supported programming languages
    - Blocks
    - OnBot Java
    - Java

Software. The REV Hardware Client—a software designed to make managing REV devices easier for the user—is utilized. This Client automatically detects connected devices, downloads the latest software for those devices, and allows for seamless updating of the devices.

Features:
- Automatically detect supported devices when connected via USB
- Connect a REV Control Hub via Wi-Fi
- One Click update of all software on connected devices
- Pre-download software updates without a connected device
- Back up and restore user data from Control Hub
- Install and switch between DS and RC applications on Android Devices

- Access the Robot Control Console on the Control Hub
- Auto-update to latest version of the REV Hardware Client
- Display devices connected via RS485
- Includes all software less than 1MB in size in the REV Hardware Client installer
- Adds alternative installers for offline use that bundle all available software, or all software that applies to just FTC or just FRC

Enhancements:
- Makes it so that downloading software and checking for updates now apply to all users on a computer
- Improves performance when checking for updates with large software updates downloaded
- Improves SPARK MAX fault names

Bug fixes:
- Fixes issue where SPARK MAX limit switch polarities would be displayed incorrectly
- Fixes issue where selecting a DFU device's type would not work
- Fixes issue where non-CAN devices would not disappear when unplugged
- Fixes issue where the recovery device type selection menu was not working
- Improves error message when checking for REV Hardware Client updates while offline

Primary motors. For the primary motors, the HD Hex Motor with the UltraPlanetary Gearbox reducer has been selected. The REV UltraPlanetary Gearbox. The REV UltraPlanetary Gearbox (Figure 6.2) is the entry point into using the REV UltraPlanetary System. UltraPlanetary Cartridges allows to support six different final gear reductions ranging from nominally 3:1 to 60:1 ensuring the right amount of torque for the application at hand. A pinion already pressed onto the motor and pre-assembled cartridges for designers to begin testing and iterating on their design.

The UltraPlanetary System is a cartridge based modular gearbox designed to handle the rigors of the competition and the classroom. The UltraPlanetary System includes an input stage and pinion gear that works the REV HD Hex Motor and other 550 class motors. Building on the ability to iterate and adjust designs easily using the REV Building System, the UltraPlanetary System consists of pre-assembled and lubricated cartridges allowing for swapping gear ratios on the fly and with ease. Users can configure a single-stage planetary using one of three different reduction cartridges, build multi-stage gearboxes through stacking individual cartridges together, and choose two different ways for transferring power: either through face mounting directly on the output stage or choosing the length of 5mm hex shaft best suited for the application. It has a variety of options for mounting with four different brackets available for mounting to REV 15mm Extrusion, REV C Channel, or REV U Channel. The UltraPlanetary 550 Motor Pinion Gear (REV-41-1608) is pressed on to an HD Hex Motor (REV-41-1291).

Gearbox Specifications
- Module: 0.55
- Pressure Angle: 20°

- Materials: Sintered Steel, Glass Fiber Reinforced PA66 Nylon
- Weight(s):
    - UltraPlanetary w/3 Cartridges and HD Hex Motor, no hardware: 441.5 g (0.973 lbs)
    - UltraPlanetary w/3 Cartridges, no motor and no hardware: 206.5 g (0.456 lbs)
    - UltraPlanetary Output Cartridge: 66.5 g (0.147 lbs)
    - UltraPlanetary Mounting Plate: 33.5 g (0.074 lbs)
    - UltraPlanetary 3:1 Cartridge: 35.5 g (0.078 lbs)
    - UltraPlanetary 4:1 Cartridge: 34.0 g (0.075 lbs)
    - UltraPlanetary 5:1 Cartridge: 36.0 g (0.079 lbs)

HD Hex Motor Specifications - No Cartridges

- Body Diameter: 37mm
- Voltage: 12V DC
- No-Load Current: 400mA
- Stall Current: 8.5A
- Free Speed: 6000 rpm
- Stall Torque: .105 Nm
- Max Output Power: 15W
- Encoder Counts per Revolution
    - at the motor - 28 counts/revolution

Driver. The BTS7960 motor driver was used to control the main motors; it allows control of a single brushed DC motor rated for voltages from 5.5 to 27.5 volts DC up to 43 A. However, as the terminal block installed on the board is not rated for such currents, motors with a consumption current of up to 10 A were used for long-term operation.

Characteristics:

- Motor supply voltage: from 5.5 to 27.5 V DC (outside this range, the driver will enter protection mode).
- Logic supply voltage: 5 V DC.
- Maximum permissible motor current: 43 A (short-term).
- Maximum permissible motor current: 10 A (long-term).
- Maximum PWM frequency on control outputs: 25 kHz.
- Voltage of logic levels on control outputs: 3.3 or 5 V.

Connections:

- "M+" and "M-" - Outputs for connecting the motor.

"M-" Output of the left arm of the H-bridge (chip U3).
"M+" Output of the right arm of the H-bridge (chip U2).

- "S+" and "S-" - Motor power supply.
- "Vcc" and "GND" - Logic power supply.
- "L_IS" - Output state of the left arm of the H-bridge (chip U3).

This output serves as an error flag (if present), or otherwise, it can measure the voltage level proportional to the current flowing through the motor, thus controlling the force of the load applied to the motor.

- "R_IS" - Output state of the right arm of the H-bridge (chip U2).

Similar to "L_IS", this output serves as an error flag or for measuring the voltage level proportional to the current through the motor.

- "L_EN" - Input for enabling the operation of the left arm of the H-bridge (chip U3).

Reset to 0 - disables the "M-" motor output (puts it in a high impedance state).
Set to 1 - enables the "M-" motor output.

- "R_EN" - Input for enabling the operation of the right arm of the H-bridge (chip U2).

Reset to 0 - disables the "M+" motor output (puts it in a high impedance state).
Set to 1 - enables the "M+" motor output.

- "L_PWM" - Input for setting the potential at the output of the left arm of the H-bridge (chip U3).

Reset to 0 - sets the potential at the "M-" output to that of the "S-" output.
Set to 1 - sets the potential at the "M-" output to that of the "S+" output.

The description you've provided is about a motor driver (like the BTS7960) and how to control it using 2 wires. Here's the translation into English:

"Setting the potentials of 'S+' or 'S-' at the output 'M-' is possible only if a 1 is set on the input 'L_EN'.

'R_PWM' - Input for setting the potential at the output of the right arm of the H-bridge (chip U2).

Reset to 0 - sets the output 'M+' to the potential of the output 'S-'.

Setting to 1 - sets the output 'M+' to the potential of the output 'S+'.

Setting the potentials 'S+' or 'S-' at the output 'M+' is possible only if a 1 is set on the input 'R_EN'.

The motor is connected to the 'M+' and 'M-' terminals. The motor supply voltage (5.5 - 27.5 V DC) is applied to the 'S+' and 'S-' terminals. The logic part supply voltage (5 V DC) is applied to the 'Vcc' and 'GND' terminals.

The driver can be controlled by 2, 3, or 4 wires:

2-wire motor driver connection:

The 'L_EN' and 'R_EN' outputs of the driver are connected together and connected to 'Vcc' (do not participate in control).

The 'L_PWM' output is connected to any Arduino pin supporting PWM.

The 'R_PWM' output is connected to any Arduino pin supporting PWM.

2-wire motor driver control:

Forward motion with speed control: 'L_PWM' = 0, 'R_PWM' = PWM (the higher the PWM, the higher the speed).

Forward motion with speed control: 'L_PWM' = PWM, 'R_PWM' = 1 (the higher the PWM, the lower the speed).

Reverse motion with speed control: 'L_PWM' = PWM, 'R_PWM' = 0 (the higher the PWM, the higher the speed).

Reverse motion with speed control: 'L_PWM' = 1, 'R_PWM' = PWM (the higher the PWM, the lower the speed).

Braking: 'L_PWM' = 'R_PWM' = 0 or 1 (maximum braking).

Advantages and disadvantages of the 2-wire control scheme:

The obvious advantage of the scheme is the minimal number of Arduino pins used.

Since 'L_EN' and 'R_EN' are constantly set to 1 (they are connected to 'Vcc'), it means the motor outputs 'M+' and 'M-' do not go into a high impedance state (do not disconnect), therefore, it is possible to brake by speed (reducing speed leads to braking). This fact can also be considered a disadvantage of the scheme, as it does not allow the motor to be freed, with the 'M+' and 'M-' outputs always having the potentials 'S+' and/or 'S-'."

Setting the potentials of 'S+' or 'S-' at the output 'M-' is possible only if a 1 is set on the input 'L_EN'.

- 'R_PWM' - Input for setting the potential at the output of the right arm of the H-bridge (chip U2).
- Reset to 0 - sets the output 'M+' to the potential of the output 'S-'.
- Setting to 1 - sets the output 'M+' to the potential of the output 'S+'.
- Setting the potentials 'S+' or 'S-' at the output 'M+' is possible only if a 1 is set on the input 'R_EN'.

The motor is connected to the 'M+' and 'M-' terminals. The motor supply voltage (5.5 - 27.5 V DC) is applied to the 'S+' and 'S-' terminals. The logic part supply voltage (5 V DC) is applied to the 'Vcc' and 'GND' terminals.

The driver can be controlled by 2, 3, or 4 wires: 2-wire motor driver connection: The 'L_EN' and 'R_EN' outputs of the driver are connected together and connected to 'Vcc' (do not participate in control). The 'L_PWM' output is connected to any Arduino pin supporting PWM. The 'R_PWM' output is connected to any Arduino pin supporting PWM.

2-wire motor driver control: Forward motion with speed control:

'L_PWM' = 0, 'R_PWM' = PWM (the higher the PWM, the higher the speed).

Forward motion with speed control: 'L_PWM' = PWM, 'R_PWM' = 1 (the higher the PWM, the lower the speed).

Reverse motion with speed control: 'L_PWM' = PWM, 'R_PWM' = 0 (the higher the PWM, the higher the speed).

Reverse motion with speed control: 'L_PWM' = 1, 'R_PWM' = PWM (the higher the PWM, the lower the speed).

Braking: 'L_PWM' = 'R_PWM' = 0 or 1 (maximum braking).

Advantages and disadvantages of the 2-wire control scheme: The obvious advantage of the scheme is the minimal number of Arduino pins used. Since 'L_EN' and 'R_EN' are constantly set to 1 (they are connected to 'Vcc'), it means the motor outputs 'M+' and 'M-' do not go into a high impedance state (do not disconnect), therefore, it is possible to brake by speed (reducing speed leads to braking). This fact can also be considered a disadvantage of the scheme, as it does not allow the motor to be freed, with the 'M+' and 'M-' outputs always having the potentials 'S+' and/or 'S-'.

3-wire motor driver connection:

The 'L_EN' and 'R_EN' outputs of the driver are connected together and connected to any Arduino pin supporting PWM.

The 'L_PWM' output is connected to any Arduino pin.

The 'R_PWM' output is connected to any Arduino pin.

3-wire motor driver control:

Forward motion with speed control: 'L_PWM' = 0, 'R_PWM' = 1, 'EN' = PWM (the higher the PWM, the higher the speed).

Reverse motion with speed control: 'L_PWM' = 1, 'R_PWM' = 0, 'EN' = PWM (the higher the PWM, the higher the speed).

Free rotation: 'L_PWM' and 'R_PWM' do not matter, 'EN' = 0 (motor is electrically disconnected).

Braking: 'L_PWM' = 'R_PWM' = 0 or 1, 'EN' = PWM (the higher the PWM, the stronger the braking).

Advantages and disadvantages of the 3-wire control scheme:

Despite more wires, the control scheme seems simpler: 'L_PWM' and 'R_PWM' control direction, and 'EN' controls speed. If 'L_PWM' and 'R_PWM' have the same logic level, then 'EN' controls braking.

There is the ability to adjust the level of braking using PWM without applying voltage (potential difference) to the motor.

When a logical 0 is applied to the 'EN' input, the motor is electrically disconnected from the circuit. For example, if a device powered by the motor is on a hill and 1 is set on all 'L_PWM', 'R_PWM', and 'EN' inputs, it won't move, but as soon as the level on the 'EN' input is dropped to 0, the motor is freed, and the device will roll down the hill. Another example is saving electricity: after reaching the required speed, drop the level on the 'EN' input to a logical 0, and the device will continue moving by inertia, then set logical 1 on the 'EN' input, accelerate, and drop to 0 again.

A disadvantage of the 3-wire connection scheme is that speed braking is not provided in the scheme.

Power Supply. The motor supply voltage (5.5 - 27.5 V DC) is applied to the 'S+' and 'S-' terminals.

The logic part supply voltage (5 V DC) is applied to the 'Vcc' and 'GND' terminals.

The driver is built on an H-bridge assembled from two half-bridges using BTS7960 chips. These BTS7960 chips support PWM up to 25 kHz (for instance, the Arduino UNO only supports a PWM frequency of 0.5 kHz) and are equipped with protection circuits against short-circuiting, overheating, overvoltage (on the S+ and S- terminal outputs), and voltage drops below 5.5 V (on the S+ and S- terminal outputs). The BTS7960 chips feature an "IS" output, where the voltage changes proportionally to the current flowing through the motor, allowing for the monitoring of motor load. In case of errors, the "IS" output acts as an error detection flag, switching to logical "1". On the board, the "IS" outputs of the chips are connected to GND through a 10 kΩ resistor and are linked to the board's "L_IS" and "R_IS" outputs. A bus driver based on the 74HC244 chip is installed on the driver board, which isolates the logic levels of control signals between the "L_EN", "R_EN", "L_PWM", "R_PWM" inputs and the BTS7960 chip inputs. Thanks to the bus driver, the motor driver can be controlled by both 3.3 V and 5 V logic levels.

In our experimental studies, a three-wire control scheme is used for the motor driver. The Arduino pin numbers are defined in the first three lines of the sketch:

```
const uint8_t EN = 1; // pin number connected to the driver's L_EN and R_EN inputs.
const uint8_t L_PWM = 2; // pin number connected to the driver's L_PWM input.
const uint8_t R_PWM = 3; // pin number connected to the driver's R_PWM input.

void setup() {
  pinMode(EN, OUTPUT); // Configuring the EN pin as an output (driver input)
  pinMode(L_PWM, OUTPUT); // Configuring the L_PWM pin as an output (driver input)
  pinMode(R_PWM, OUTPUT); // Configuring the R_PWM pin as an output (driver input)
}

void loop() {
  // Forward movement at 50% speed:
  digitalWrite(L_PWM, LOW); // Set logical 0 on the L_PWM driver input, thus M- output of the driver will be at S- potential
  digitalWrite(R_PWM, HIGH); // Set logical 1 on the R_PWM driver input, thus M+ output of the driver will be at S+ potential
  analogWrite(EN, 127); // Set 50% PWM on the L_EN and R_EN driver inputs for speed control, adjustable from 0 (0%) to 255 (100%).
  delay(2800); // Wait for 2800 ms. PWM and logic levels remain unchanged, hence the motor continues to rotate at the set speed and direction.

  // Forward movement at maximum speed:
  digitalWrite(L_PWM, LOW); // Set logical 0 on the L_PWM driver input, thus M- output of the driver will be at S- potential
  digitalWrite(R_PWM, HIGH); // Set logical 1 on the R_PWM driver input, thus M+ output of the driver will be at S+ potential
  analogWrite(EN, 255); // Set 100% PWM on the L_EN and R_EN driver inputs for speed. If the set value is 255, this function can be replaced with digitalWrite(EN, HIGH);
```

delay(2800); // Wait for 2800 milliseconds. PWM and logic levels remain unchanged, hence the motor continues to rotate at the set speed and direction.

// Free rotation:
digitalWrite(EN, LOW); // Set logical 0 on the L_EN and R_EN driver inputs, thus M+ and M- outputs will transition to high impedance state and the motor will be electrically disconnected.
}
delay(2800); // Wait for 2800 milliseconds. The logic levels at the driver's L_PWM and R_PWM inputs are irrelevant (they can be any value).
// Reverse at 50% speed:
digitalWrite(L_PWM, HIGH); // Set logic level 1 at the driver's L_PWM input, meaning the driver's M- output will be set to the S+ potential.
digitalWrite(R_PWM, LOW); // Set logic level 0 at the driver's R_PWM input, meaning the driver's M+ output will be set to the S- potential.
analogWrite (EN, 127); // Set 50% PWM at the driver's L_EN and R_EN inputs, which controls the speed, adjustable from 0 (0%) to 255 (100%).
delay(2800); // Wait for 2800 milliseconds. The PWM and logic levels will remain unchanged, so the motor will continue rotating at the set speed and direction.
// Reverse at 100% speed:
digitalWrite(L_PWM, HIGH); // Set logic level 1 at the driver's L_PWM input, meaning the driver's M- output will be set to the S+ potential.
digitalWrite(R_PWM, LOW); // Set logic level 0 at the driver's R_PWM input, meaning the driver's M+ output will be set to the S- potential.
digitalWrite(EN, HIGH); // This function performs the same action as analogWrite(EN, 255);
delay(2800); // Wait for 2800 milliseconds. The logic levels will remain unchanged, so the motor will continue rotating at the set speed and direction.
// Braking with 50% force:
digitalWrite(L_PWM, HIGH); // Set logic level 1, but you can also set logic level 0, the important thing is that the levels at the driver's L_PWM and R_PWM inputs match.
digitalWrite(R_PWM, HIGH); // Set logic level 1, but you can also set logic level 0, the important thing is that the levels at the driver's L_PWM and R_PWM inputs match.
analogWrite (EN, 127); // Set 50% PWM at the driver's L_EN and R_EN inputs, which controls the braking force, adjustable from 0 (0%) to 255 (100%).
delay(2800); // Wait for 2800 milliseconds. During this time, the motor will stop.
}

Adaptation mechanism. The mechanism for adapting the suspension response to the irregularities of the supporting surface is controlled using a 16-channel, 12-bit PWM/Servo module based on PCA9685 (see Figure 4). The PCA9685 is a 16-channel, 12-bit controller. The PWM frequency can be adjusted within a range of 40 to 1000

Hz. This PWM controller can be used to control various devices that use a PWM signal as the control signal.

The controller is managed via the I2C bus. This board features two sets of I2C bus connectors on both sides, allowing multiple boards to be connected in series to the bus or to connect other devices to the I2C bus. Most modules have only one group of contacts, sometimes necessitating the use of splitters. This problem is eliminated in this device. On the board, there are jumpers that can be used to set a device address different from the default. Therefore, if 16 channels are not enough, several such boards can be connected in series, setting a unique address for each using the jumpers.

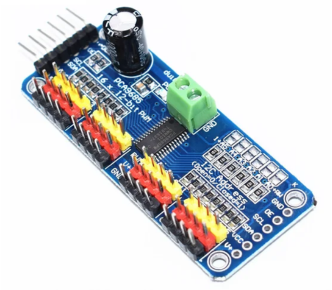

Figure 6.4 16-channel, 12-bit controller PCA9685

ANNIMOS 60 digital servo motors, installed on each leg, are responsible for adjusting the robot's feet, ensuring smooth horizontal movement of the robot's body when traversing rough terrain. This significantly reduces energy consumption due to the absence of vertical movement of the body. The DS5160SSG is known for its high quality, featuring a CNC-machined aluminum middle case for better heat dissipation, and dual ball bearings on the output shaft to reduce friction. It is lightweight, offers high-speed torque, is waterproof, sensitive, has a short response time, operates quietly, and more. The stainless-steel gear provides higher speed and precision, as well as a longer lifespan. It is also powerful, strong, and stable.

Features include:

- High-precision metal gear.
- Durable SS metal gear.
- Dual ball bearing.
- Programmable digital amplifier with Mosft Drive.
- Axial mounting hole on the bottom side.
- Orientation angle: up to 270 degrees.
- Mechanical angle: 360 degrees (plug/output wheel/radio control system, compatible with Futaba JR Hitec).

Speed:

- 0.17 sec/60 degrees at 6V
- 0.15 sec/60 degrees at 7.4V
- 0.13 sec/60 degrees at 8.4V

Torque:

- 58 kg.cm at 6V
- 65 kg.cm at 7.4V
- 70 kg.cm at 8.4V

Operating voltage: 6V-8.4V Connector wire length: 17.7 inches (450 mm) Gear ratio: 279 Pulse width range: 500～2500μs Deadband width: Microseconds Waterproof rating: IP67

The following hardware parts are used:

- 1 piece of digital metal robotic servo motor mounted on the robot's "knee" using the following elements: long aluminum holder, short aluminum holder, round 18T holder, round holder, and screws.

The mechanism for adapting/regulating the height of the feet works in coordination with the linear guide mechanisms, responsible for horizontal movement. During the transition to the swing phase, i.e., at certain crank angles φ_{AB} where $\varphi_0 + \Phi_{SUP} \leq \varphi_{AB} \leq \varphi_1$, and $\varphi_1 = \varphi_0 + 360^0$, the adaptation motor raises the foot to its maximum height. At the angle $\varphi_1 = \varphi_0 + 360^0$, the leg enters the support phase, and the foot begins to descend. Upon contacting the support surface, the foot contact sensor is triggered, sending a signal to the adaptation motor to "lock," ensuring the motor is fixed during the support phase for straight-line movement of the body. The angular position of the linear guide mechanism's crank is measured by an AS5600 encoder (12-bit), a precision magnetic induction angle measurement sensor module from the brand ENDSTOP, model AS5600 (see Figure 6.5).

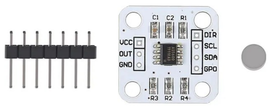

Figure 6.5 - model AS5600

The AS5600 encoder, referred to in Figure 5, is characterized by the following specifications:

- VCC: 3.3 V
- GND: Power ground
- Output: PWM/Analog voltage output
- DIR: Rotation direction (Grounding increases value clockwise; VCC decreases value clockwise)
- SCL: I2C communication line (Clock)
- SDA: I2C communication line (Data)
- GPO: Mode selection (internal pull-up for programming mode)

The rotation of the hexapod robot's body is achieved through differential speeds of the main motors. When rotating the body of the hexapod robot without translational movement, the maximum rotation angle of the body is 60 degrees. Meanwhile, the rotation angle of the legs in the swing phase around the vertical axis relative to the main direction of the body at that moment is 120, 120, and 60 degrees. It's important to note that when there is translational movement of the body, the rotation angle is not limited. The robot, weighing 5.7 kg, can move in the main direction on a full charge of a 7A Li-Po battery for 2.5 hours, which is significantly longer than existing experimental models. It should be taken into account that the robot was manufactured under laboratory conditions. Therefore, it is expected that the energy efficiency will be greater when the quality of manufacturing is improved in commercial robot production under factory conditions.

Figure 6.6 illustrates the latest experimental prototype:

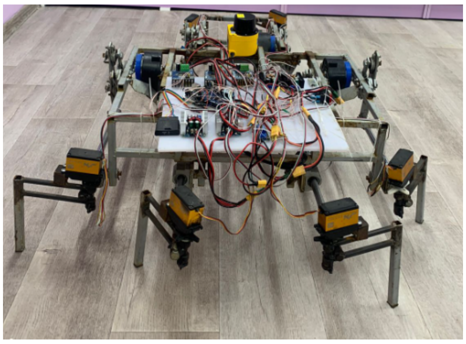

Figure 6.6 – Experimental prototype of the WR

CONCLUSIONS

1. In this (PhD) research, an alternative design principle for adaptive walking robots is developed, moving away from the traditional insectomorphic (insect-like) designs in favor of optimizing the robot's operational characteristics in terms of mechanics and control. The optimal synthesis of support and locomotion mechanisms, along with the functional separation of structural modules and their corresponding motors, has led to simplified control systems and minimized energy consumption during movement across uneven terrain.

2. Methods for the synthesis have been developed and optimal structural-metric parameters of AWR were determined based on the decomposition of the robot's movement and functional separation of the motors. This allowed:
    a. Simplifying the coordination of legs and achieving movement with a minimal number of motors, with the least energy consumption, and using the simplest control system;
    b. Solving the problem of adapting each leg to the irregularities of the support surface individually and independently from the main control unit;
    c. Solving the problem of redundant connections in existing designs and eliminating parasitic loads on the motors associated with multiple static indeterminacies;
    d. Eliminating additional energy consumption for leg slippage and reducing reactions in leg joints during turns.
3. An analysis of the main types of propulsion systems was conducted and the rational structural synthesis of AWR was justified based on functionally independent structural modules.
4. A method for multicriterial synthesis was developed, and optimal metric parameters of SLM with linear-translational movement of the supporting limb were determined, with an unlimited range of limb adaptation to terrain irregularities, and an adaptation system was developed.
5. Modes of turning were investigated, and structural-parametric synthesis of AWR for optimal turning was carried out using the isotropy criterion.
6. Prototypes were manufactured, and an experimental laboratory model of AWR was developed, demonstrating the full functionality of the design and the validity of the main hypotheses.

LITERATURE

1. Antonov, A.V., Vorotnikov, S.A.: Reshenie zadach kinematiki i dinamiki dlya trexopornogo kolesno-shagayushhego robota. Izvestiya vy`sshix uchebny`x zavedenij. Mashinostroenie. 3, 684 (2018).
2. Ignat`ev, M.B., Vladimirov, S.V., Sapozhnikov V.I., Sergeev M.B.: Shagayushhie roboty` – problemy` i perspektivy`. Innovatika i e`kspertiza. 2 (17), 128 – 137 (2016).
3. Cherny`shev, V.V., Ary`kancev, V.V.: Shagayushhaya opora transportny`x sredstvpovy`shennoj proxodimosti dlya vodonasy`shhenny`x gruntov. UM 177594 Russian Federation. IPC B62D57/032 (2018).
4. Ceccarelli, M.: Historical and Modern Perspective of Walking Robots (2016).
5. Wang, G., Riaz, A., Balachandran, B.: Computational Studies on Interactions between Robot Leg and Deformable Terrain. The 10th International Conference on Structural Dynamics, EURODYN 2017. Procedia Engineering. 199, 2439 –2444 (2017)
6. Antonov A.V., Vorotnikov S.A. "Solving the problems of kinematics and dynamics for a three-support wheel-walking robot." Proceedings of the Higher Education Institutions: series Mechanical Engineering. - №3 (684). – 2018.
7. Briskin E.S., Kalinin Ya.V., Miroshkina M.V. "About energy-efficient modes of movement of mobile robots with orthogonal walking propulsors when overcoming obstacles." News of the Russian Academy of Sciences. Theory and Control Systems. – 2020. - № 2. – Pp. 75-82.
8. Briskin E.S., Sharonov N.G. "On the control of the movement of mechanical systems with an excess number of control actions." News of the Russian Academy of Sciences. Theory and Control Systems. – 2019. - № 3. – Pp. 48-54.
9. Briskin E.S., Sharonov N.G., Barsov V.S. "About energy-efficient modes of motion of robots with rotary-jamming propulsors." Mechatronics, Automation, Control. – 2018. - № 2. – Pp. 100-103.
10. Briskin E.S., Sharonov N.G., Serov V.A., Penshin I.S. "Controlling the motion of an underwater mobile robot with anchor-rope propulsors." Robotics and Technical Cybernetics. – 2018. - № 2(19). – Pp. 39-45.
11. Military Robot of VNIISignal. – 2017. – URL: www.vniisignal.ru (accessed on 15.09.2021)
12. RU №166237 A1, 2010.10.15.
13. Ibraev S.M., Aidashova G.A., Dzhamalov N.K., Ibraev A.S., Mukhambetkalieva G.M. "New adjustable straight-line guiding mechanisms for the drive of the leg of walking robots." Proceedings of the XII All-Russian Congress on Fundamental Problems of Theoretical and Applied Mechanics. – Ufa: Publishing Center of Bashkir State University, 2019. – Vol. 1. – Pp. 563-564.
14. Ibraev S.M., Aidashova G.A., Dzhamalov N.K., Ibraev A.S., Mukhambetkalieva G.M. "Optimization synthesis of the leg mechanism for a walking machine." Bulletin of the Kazakh-British Technical University. – 2019. - №16 (2). – Pp. 102-107.

15. Ignatyev M.B., Vladimirov S.V., Sapozhnikov V.I., Sergeev M.B. "Walking robots - problems and prospects." Innovatics and Expertise. – 2016. - №2 (17). – Pp.128 -137.
16. Kalinin Ya.V. "On the mechanical effects arising during the interaction of propulsors of walking robots with the support surface." Proceedings of the XII All-Russian Congress on Fundamental Problems of Theoretical and Applied Mechanics. - Ufa: Publishing Center of Bashkir State University, 2019. – Vol. 1. – Pp. 530-532.
17. Catalog of ground-based military robots of various purposes. – 2018. -URL: http://robotrends.ru/robopedia/rys (accessed on 14.07.2021).
18. Lepetukhin, K.Y., Maloletov, A.V., Briskin, E.S. On the criteria for optimizing the movement of sections of a circular action rain machine when processing fields of complex shapes // News of Volgograd State Technical University. – 2018. - No. 8 (218). – P. 117-121.
19. Miroshkina, M.V., Briskin, E.S., Smirnaya, L.D. On the optimal modes of walking machines movement when moving on uneven ground // Progress of vehicles and systems: Materials of the international scientific-practical conference. – Volgograd: FSTC "Titan–Barricades", 2018. – P. 142-144.
20. Lynx-UGV. The newest Russian walking robot. – 2017. – URL: http://savepearlharbor.com (accessed on 12.04.2021)
21. Serov, V.A., Ustinov, S.A., Maksimenko, V.I. Onboard control system of special-purpose mobile robots // News of Tula State University. Technical sciences. – 2019. - No.1. – P. 32-39.
22. Serov, V.A., Kovshov, I.V., Ustinov, S.A. Tasks of technological robotic walking platforms in the development of underwater (under-ice) mineral deposits // News of SFU "Technical Sciences". – 2017. - No.9 (194). – P. 181-191.
23. Tolstov, K.M., Pismennaya, E.V. Lower limb exoskeleton mechanisms ensuring natural human movements // Materials of the XII All-Russian Congress on Fundamental Problems of Theoretical and Applied Mechanics. – Ufa: RIC BashSU, 2019. – P.114-119.
24. Tuleshov, A.K., Ibraev, S.M., Ibraeva, A.S., Dzhomartov, A.A. Development of robots and manipulators with parallel topology // Machine Science. – 2020. - No.2(10). -P.10-19.
25. Chernyshev, V.V., Arykantsev, V.V. Walking support of all-terrain vehicles for water-saturated soils.– Patent No. 177594 Russian Federation, IPC B62D57/032, 2018.
26. RU 195402 U1, 24.01.2020.
27. RU 177594 A, 27.02.2009.
28. RU 180262 U1, 07.06.2018.

29. Babu, N., Sujatha, S., Narayanan, S., and Balamurugan, V. Novel Hybrid Leg-Track Locomotion Robot and its Stability Analysis Using a Unified Methodology // Procedia Computer Science. – 2018. - No.133. – P. 486–493.
30. Briskin E.S., Kalinin Y., Maloletov A. On energetically effective modes of walking robot's movement // CISM International Centre for Mechanical Sciences, Courses and Lectures. – 2019. – Vol.584. – P.425-432.
31. Briskin E.S., Sharonov N.G. On Motion Control of Mechanical Systems with an Excessive Number of Control Actions // International Journal of Computer and Systems Sciences. – 2019. – Vol. 58. – P.374–381.
32. Song Shin-Min, Waldron Kenneth J. Machines that Walk: The Adaptive Suspension Vehicle. – Cambridge: MIT Press. – 1989. – 226 p.
33. Ceccarelli M. Historical and Modern Perspective of Walking Robots. – 2016. – URL: www.academia.edu (обращения 24.05.2021).
34. Genta G. Introduction to the Mechanics of Space Robots // Springer: Berlin, Germany. – 2012. – P.112-125.
35. Chen Gang, Jin Bo, Chen Ying. Tripod gait-based turning gait of a six-legged walking robot // Journal of Mechanical Science and Technology. -2017. – Vol.31(3). – P.1401-1411.
36. Comănescu A., Comănescu D.M., Dugăeşescu I., Ungureanu L.M. Structural and Constructive Design of Some Bi-mobile Leg Mechanisms // Proceedings of the 14th IFToMM World Congress. – 2015. –P.387-392.
37. Da Gou. China's Robot Dog Takes a Walk // Popular Science. – 2017. –P. 56-71.
38. Ding L.H. Key Technology Analysis of Big Dog Quadruped Robot // Journal of Mechanical engineering. – 2015. – Vol.51. – P. 1-23.
39. Fernandez Jose de Gea, Mronga Dennis, Günther Martin, Stock Sebastian, Niemann Nils, Wiese Hendrik, Menon Rohit, Kirchner Elsa Andrea, Stiene Stefan. Towards Contextual Robots for Collaborative Manufacturing // Workshop "Human-Robot Cooperation and Collaboration in Manipulation: Advancements and Challenges" at 2018 IEEE/RSJ International Conference on Intelligent Robots and Systems (IROS 2018). – 2018. – P. 221-228.

40. Gao J., Li M., Li Y., Wang B. Singularity Analysis and Dimensional Optimization on a Novel Serial-Parallel Leg Mechanism // 13th Global Congress on Manufacturing and Management. – 2016. - №174. – P. 45 – 52.
41. Geonea I., Tarnita D., Carbone G., Ceccarelli M. Design and Simulation of a Leg Exoskeleton Linkage for Human Motion Assistance // In New Trends in Medical and Service Robotics. Springer. – 2019. – P. 93-100.
42. Geonea I. D., Tarnita D. Design and Evaluation of a New Exoskeleton for Gait Rehabilitation // Mechanism Science. – 2017. - № 8. – P.307-321.
43. Ghassaei Amanda. Design and Synthesis of Six Legged Walking Robot Using Single Degree Of Freedom Linkage // Imperial Journal of Interdisciplinary Research (IJIR). – 2016. -Vol. 2. – P. 112-125.
44. The Ghost Minitaur: Ghost Q-UGVs are Superior to Wheels and Tracks on Unstructured Terrain. – 2019. -URL: https://www.ghostrobotics.io/ (дата обращения 15.09.2021)
45. Hadizadeh S., Kafash S., Nahvi A. Optimal synthesis of four-bar path generator linkages using circular proximity function // Mech. Mach. Theory. – 2017. – Vol. 115. – P.18–34.
46. Hu N., Li S., Huang D., Gao F. Modeling and Optimal Control of Rescue Quadruped Robot with High Payload // Mechanism and Machine Science. – 2016. – P. 521-535.
47. Ibrayev S., Jamalov N., Ibrayeva A., Mukhambetkaliyeva G. Optimal structural synthesis of agricultural legged robot with minimal damage on soil // E3S Web of Conferences. – 2019. - №135. – P. 21-27.
48. Ibrayev S., Jomartov A., Tuleshov A., Jamalov N. Synthesis of Four-Bar Linkage with Adjustable Crank Length for Multi-Path Generation // International Journal of Mechanical Engineering and Robotics Research. – 2020. -Vol. 9 (4). – P.489-495.
49. Ibrayev S.M., Jamalov N.K., Ibrayeva A.S., Mukhambetkaliyeva G.M. Optimization of the Structure and Modelling of the Turning of Legged Robot //

Proc.of the International Conference “Actual Problems of Informatics, Mechanics and Robotics. – 2018. – P.87-88.
50. Kim Sangbae, Wensing Patrick. Design of Dynamic Legged Robots // Foundations and Trends in Robotics. – 2017. – Vol.5. – P.117-190.
51. Komoda K, Wagatsuma H. Energy-efficiency comparisons and multibody dynamics analyses of legged robots with different closed-loop mechanisms // Multibody System Dynamics. -2017. - №40 (2). – P. 123-153.
52. Lin R., Guo W., Li M. Novel Design of Legged Mobile Landers with Decoupled Landing and Walking Functions Containing a Rhombus Joint // Journal of Mechanisms and Robotics. – 2018. - №10 (6). – P 61-75.
53. Lin R., Guo W., Li M., et al. Novel design of a legged mobile lander for extraterrestrial planet exploration // International journal Advanced Robotic Systems. – 2017. - №14 (6). – P. 118-126.
54. Ma Z.L., Zhu Y.F., Liu Y.Ch. Design and Analysis of New Energy-Efficient Legs for Quadruped Robots // J. NORTHEAST UNIV. – 2016. - №37. – P.543-553.
55. Mantis Hexapod. – 2019. – URL: http://www.mantisrobot.com (дата обращения 25.09.2021)
56. Pop F., Lovasz E. C., Pop C. Dimensional synthesis of a leg mechanism // Materials Science & Engineering Conference Series. – 2016. - № 147 (1). – P. 225-240.
57. Savin S., Jatsun S., Vorochaeva L. Trajectory generation for a walking in-pipe robot moving through spatially curved pipes // 12th International Scientific-Technical Conference on Electromechanics and Robotics “Zavalishin’s Readings”, MATEC Web of Conferences 113. – 2017. – P.156-161.
58. Selvi Ö., Ceccarelli M. Design and Optimization of a Walking Over-Constrained Mechanism // Proceedings of the 15th IFToMM World Congress on Mechanism and Machine Science. – 2020. – P. 61-687.

59. Selvi Özgün, Samet Yavuz. Design and Dimensional Optimization of a Novel Walking Mechanism with Firefly Algorithm // International Workshop on Computational Kinematics, Springer. – 2017. – P.188 200.
60. Semini C., Tsagarakis N.G. Design and Experimental Evaluation of the Hydraulically Actuated Prototype Leg of the HyQ Robot // IEEE/RSJ Int.Conference on Intelligent Robots and Systems (IROS). – 2010. – P. 352-365.
61. Shao Y., et. Al. Conceptual design and dimensional synthesis of cam-linkage mechanisms for gait rehabilitation // Mech. Mach. Theory. – 2016. - №104. – P. 31–42.
62. Sharbafi M. A., In Seyfarth A. Bioinspired legged locomotion: Models, concepts, control and applications // Butterworth-Heinemann. – 2017. – P 114-121.
63. Shen Z., Tan T., Allison G., Cui L. A Customized One-Degree-of-Freedom Linkage Based Leg Exoskeleton for Continuous Passive Motion Rehabilitation // Mechanism and Machine Science 68, Advances in Italian Mechanism Science, Springer. – 2019. – P. 518-526.
64. Shen Z., Allison G., Cui L. An integrated type and dimensional synthesis method to design one degree-of-freedom planar linkages with only revolute joints for exoskeletons // J. Mech. Des. – 2018. - №140 (9). – P. 172-190.
65. Soh J.S., Mc Carthy J.M. Dimensional Synthesis of Six-Bar Linkage as a Constrained RPR Chain // Int. Journal Mechanism and Machine Theory. – 2015. – P147-160.
66. Sun T., Xiang X., Su W., et al., A transformable wheel-legged mobile robot: Design, analysis and experiment. // Rob. Autom. Syst. – 2017. - №98. – P. 30–41.
67. Noriaki Takasugi, Kunio Kojima, Shunichi Nozawa, Kei Okada, Masayuki Inaba: 3D walking and skating motion generation using divergent component of motion and gauss pseudospectral method // IROS. – 2017. – P. 503-510.

68. Tsuge B.Y., Plecnik M.M., McCarthy J.M. Homotopy directed optimization to design a six-bar linkage for a lower limb with a natural ankle trajectory // J. Mech. Robot. – 2016. - №8 (6). – P.254-269.
69. Tuleshov A. K., Jomartov A. A., Ibrayev S., Jamalov N. K., Halicioglu R. Optimal synthesis of planar linkages // News of the Academy of Sciences of the Republic of Kazakhstan: Series of geology and technical sciences. – 2020. -Vol. 1 (439). – P. 172-180.
70. He, J., Gao, F. Mechanism, Actuation, Perception, and Control of Highly Dynamic Multilegged Robots: A Review. Chin. J. Mech. Eng. 33, 79 (2020). https://doi.org/10.1186/s10033-020-00485-9
71. Yohei Kakiuchi, Masayuki Kamon, Nobuyasu Shimomura, Sou Yukizaki, Noriaki Takasugi, Shunichi Nozawa, Kei Okada, Masayuki Inaba: Development of life-sized humanoid robot platform with robustness for falling down, long time working and error occurrence // IROS. – 2017. – P. 689-696.
72. Veerendrakumar, C.M., Math V.B. Kinematic Synthesis of Planar Adjustable Six-Bar Mechanism for Specified Output // International Journal of Research in Engineering and Technology. – 2016. – Vol. 05 (13). – P. 2321-7308.
73. Wang C.Y., Hou J.H. Analysis and Applications of Theo Jansen's Linkage Mechanism. Theo Jansen's Linkage Mechanism on Kinetic Architecture // Proceedings of the 23rd CAADRIA Conference. – 2018. – P.359–368.
74. Wang G., Riaz A., Balachandran B. Computational Studies on Interactions between Robot Leg and Deformable Terrain // The 10th International Conference on Structural Dynamics, EURODYN 2017, Procedia Engineering. – 2017. – Vol.199. – P.2439–2444.
75. World Robotics 2017: Industrial Robots & Service Robots 2017. – International Federation of Robotics. – 2017. – P. 245-272.
76. Xu K., Liu H., Xingqiao Zhu X., Song Y. Kinematic analysis of a novel planar six-bar bionic leg // Advances in Mechanism and Machine Science, Proceedings of the 15th IFToMM World Congress on Mechanism and Machine Science. – 2020. - №73. – P.13-21.

77. Yang Zh., Gu W., Zhang J., Gui L. Force Control Theory and Method of Human Load Carrying Exoskeleton Suit. – Springer. – 2017. – P. 200- 218.
78. Zang H.B., Shen L.G. Research and Optimization Design of Mechanism for Theo Jansen Bionic Leg // Journal of Mechanical Engineering. – 2017. - №53(15). – P.101-109.
79. Ibrayev S.M. Approximate Synthesis of Planar Cartesian Manipulators with Parallel Structures // Int. Journal Machine and Mechanism Theory. – 2002. - №37. – P. 877-894.
80. https://www.google.com/url?sa=i&url=https%3A%2F%2Frobotsguide.com%2Frobots%2Fspot&psig=AOvVaw3DYBHSARdOABsZryOFC9_L&ust=1697723131468000&source=images&cd=vfe&opi=89978449&ved=0CBEQjRxqFwoTCLi4ntbd_4EDFQAAAAAdAAAAABAD
81. http://army-guide.com/eng/product.php?prodID=5963&printmode=1
82. https://laughingsquid.com/mantis-robotic-walking-machine/
83. Mosher R. S. Exploring the potential of a quadruped //SAE Transactions. – 1969. – C. 836-843.
84. A. Takanishi, M. Ishida, Y, Yamazaki and I. Kato, “The Realization of Dynamic Walking by the Biped Walking Robot WL-10RD” // International Conference on Advanced Robotics, pp. 459~466, 1985.
85. Shigemi S., Goswami A., Vadakkepat P. ASIMO and humanoid robot research at Honda //Humanoid robotics: A reference. – 2018. – C. 55-90.
86. Omarov, B., Ibrayev, S., Amanov, B., & Momynkulov, Z. Optimal Leg Linkage Design for Horizontal Propel of a Walking Robot Using Non-dominated Sorting Genetic Algorithm // IEEE Access, 2024.
87. Ibrayev, S., Jamalov, N., Ibrayev, A., Ualiyev, Z., & Amanov, B. "Optimal synthesis of walking robot leg." // Mechanics Based Design of Structures and Machines, 1-21, 2023.
88. Ibrayev, S., Jamalov, N., & Patel, S. H. "Optimization of the Walking Robot Parameters on the Basis of Isotropy Criteria." IEEE Access, 10, 113969-113979, 2022.
89. Ibrayev, S., Rakhmatulina, A., Amanov, B., & Imanbayeva, N. "Multicriteria Optimization of Lower Limb Exoskeleton Mechanism." Applied Sciences 13, no. 23 (2023): 12781. https://doi.org/10.3390/app132312781
90. Rakhmatulina, A., Ibrayev, S., Imanbayeva, N., & Tolebayev, N. "Kinematic and kinetostatic analysis of the six-link straight-line generating converting mechanism of the unbalanced sucker rod pumper drive." Eastern-European Journal of Enterprise Technologies, 6(7), 108, 2020. (Scopus, Web of Science)
91. Rakhmatulina, A., Ibrayev, S., & Imanbaeva, N. "Synthesis of the transforming mechanism of the rocking machine." KazNU Bulletin. Mathematics, Mechanics, Computer Science Series, 2022, 116(4), pp. 46–57.

92. Ibrayev, S.M., Jamalov, N.K., Kamal, A., Ibrayev, A. S., & Abduraimov, A. E. "Walking mechanism of a vehicle." Patent No. 35852, RGNIIS RK, 2021.
93. Ibrayev, S.M., Sakenova, A.M., Karim, A.T., & Amanov, B. "Optimal Synthesis Of Upper And Lower Limb Exoskeleton Mechanisms." SIJC "Future Mechanics", 1 - 5 March, 2021, Almaty, p.93 – 103.
94. Ibrayev, S., Jamalov, N., Tuleshov, A., & Bissembayev, K. "Walking Robot Leg Design Based on Translatory Straight-Line Generator." In: Venture G., Solis J., Takeda Y., Konno A. (eds) ROMANSY 23 - Robot Design, Dynamics and Control. ROMANSY 2020. CISM International Centre for Mechanical Sciences (Courses and Lectures), vol 601. Springer, Cham.
95. Tuleshov, A., Ibrayev, S., & Jomartov, A. "Development of Robots and Manipulators with Parallel Topology." Machinery Researching, 2019, 2(10), p. 10-19.
96. Ibrayev, S., Jamalov, N., & Mukhambetkaliyeva, G. "Optimal structural synthesis of agricultural legged robot with minimal damage on soil." In E3S Web of Conferences (Vol. 135, p. 01027), 2019. EDP Sciences.
97. Ibrayev, S., Jamalov, N., Mukhambetkaliyeva, G., & Aidasheva, G. "Optimization of the structure and modelling of the turning of legged robot." International Conference "Science World of al-Farabi", Almaty, Kazakhstan, 8-10.04.2019.
98. Ibraev S.M., Jamalov N.K., Ibraeva A.S., & Mukhambetkaliyeva G.M. "Obosnovanie struktury i modelirovanie povorota shagayushchego apparata s dvizhitelyami ortogonal'nogo tipa." Sbornik tezisov Mezhdunarodnoy nauchno-prakticheskoy konferentsii «Aktual'nye problemy informatiki, mekhaniki i robototekhniki. Tsifrovye tekhnologii v mashinostroenii», g. Almaty. 4-5 oktyabrya 2018 g., S. 83-84.
99. Ibrayev, S., Ibrayeva, A., & Ibrayev, A. "Walking Robot with decoupled motion. Optimal design and synthesis." KAUST Research Conference on Robotics and Autonomy 2022, KSA.

APPENDIX A

Fragments of Truncated Tables

N	LPT	rAB	BC	CD	XDnew	YDnew	fi_0	x_BP	y_BP	Sx	Sy	Kcos	Ksin	ε	μ_e
1	22207	0,2335	0,4926	0,5037	-0,4243	0,0301	245	0,9568	0,0271	2,0543	1,8465	-2,3449	-0,1666	**0,0049**	22,2
2	23023	0,2347	0,4889	0,4982	-0,4278	0,0382	244	0,9523	0,0514	2,0063	1,8550	-2,3193	-0,2069	**0,0050**	22,7
3	12127	0,2304	0,4904	0,5025	-0,4199	0,0248	248	0,9603	0,0180	2,0699	1,8570	-2,3735	-0,1404	**0,0050**	22,0
4	26783	0,2277	0,4869	0,4889	-0,4160	0,0150	249	0,9683	0,0279	2,1232	1,8539	-2,4010	-0,0867	**0,0051**	22,3
5	9071	0,2286	0,4950	0,5017	-0,4184	0,0149	248	0,9712	0,0085	2,1298	1,8461	-2,3869	-0,0853	**0,0051**	22,0
6	4639	0,2345	0,4816	0,4910	-0,4267	0,0436	246	0,9449	0,0685	1,9668	1,8674	-2,3195	-0,2367	**0,0051**	**23,0**
7	7423	0,2389	0,4938	0,5050	-0,4324	0,0434	241	0,9475	0,0484	1,9986	1,8363	-2,2896	-0,2298	**0,0051**	22,6
8	25775	0,2323	0,4912	0,5026	-0,4248	0,0317	246	0,9585	0,0332	2,0344	1,8581	-2,3408	-0,1748	**0,0051**	22,4
9	21983	0,2375	0,4858	0,5050	-0,4301	0,0523	244	0,9380	0,0553	1,9282	1,8628	-2,2910	-0,2786	**0,0051**	22,7
10	29431	0,2340	0,4930	0,5031	-0,4294	0,0370	244	0,9582	0,0453	2,0092	1,8566	-2,3115	-0,1989	**0,0052**	22,8
…	…				… … … …							…			
137	**10995**	**0,2390**	**0,4854**	**0,4946**	**-0,4456**	**0,0739**	**242**	**0,9380**	**0,1282**	**1,7979**	**1,8819**	**-2,1843**	**-0,3622**	**0,0057**	**25,1**
…	…				… … … …							…			
201	4123	0,2377	0,4811	0,4860	-0,4410	0,0677	243	0,9372	0,1300	1,8290	1,8827	-2,2153	-0,3400	0,0058	**24,9**
…	…				… … … …							…			
278	7211	0,2454	0,4904	0,5055	-0,4532	0,0891	237	0,9263	0,1306	1,7475	1,8603	-2,1243	-0,4177	0,0059	**25,1**
…	…				… … … …							…			

Table A1. Fragments of the truncated Test Table with the best accuracy ε

N	LPT	rAB	BC	CD	XDnew	YDnew	fi_0	x_BP	y_BP	Sx	Sy	Kcos	Ksin	ε	μ_e
1	2675	0,2445	0,4867	0,5002	-0,4531	0,0925	238	0,9230	0,1457	1,7207	1,8693	-2,1189	-0,4327	0,0060	**25,5**
2	21267	0,2423	0,4925	0,4993	-0,4534	0,0802	239	0,9388	0,1367	1,7818	1,8664	-2,1386	-0,3782	0,0060	**25,4**
3	27955	0,2363	0,4841	0,4819	-0,4432	0,0632	243	0,9464	0,1391	1,8490	1,8840	-2,2115	-0,3155	0,0060	**25,3**
4	15107	0,2360	0,4895	0,4966	-0,4463	0,0672	243	0,9520	0,1225	1,8200	1,8906	-2,1907	-0,3299	0,0060	**25,2**
5	4811	0,2360	0,4774	0,4789	-0,4396	0,0665	244	0,9378	0,1419	1,8235	1,8925	-2,2240	-0,3362	0,0060	**25,2**
6	26059	0,2415	0,4820	0,4949	-0,4470	0,0846	241	0,9253	0,1390	1,7484	1,8794	-2,1598	-0,4086	0,0059	**25,2**
7	22667	0,2445	0,4854	0,5063	-0,4515	0,0953	239	0,9197	0,1347	1,7031	1,8725	-2,1203	-0,4477	0,0059	**25,2**
8	14131	0,2447	0,4893	0,5115	-0,4535	0,0951	238	0,9241	0,1283	1,7063	1,8702	-2,1121	-0,4427	0,0059	**25,1**
9	7211	0,2454	0,4904	0,5055	-0,4532	0,0891	237	0,9263	0,1306	1,7475	1,8603	-2,1243	-0,4177	0,0059	**25,1**
10	**10995**	**0,2390**	**0,4854**	**0,4946**	**-0,4456**	**0,0739**	**242**	**0,9380**	**0,1282**	**1,7979**	**1,8819**	**-2,1843**	**-0,3622**	**0,0057**	**25,1**
11	17123	0,2414	0,4971	0,5083	-0,4530	0,0758	239	0,9464	0,1154	1,8023	1,8663	-2,1476	-0,3592	0,0060	**25,0**
…	…				… … … …							…			
128	20759	0,2358	0,4869	0,4941	-0,4339	0,0492	244	0,9492	0,0822	1,9381	1,8672	-2,2753	-0,2580	**0,0052**	23,6
…	…				… … … …							…			
173	12151	0,2334	0,4846	0,4862	-0,4284	0,0384	245	0,9542	0,0769	1,9964	1,8636	-2,3154	-0,2075	**0,0052**	23,4
…	…				… … … …							…			
244	4639	0,2345	0,4816	0,4910	-0,4267	0,0436	246	0,9449	0,0685	1,9668	1,8674	-2,3195	-0,2367	**0,0051**	23,0
…	…				… … … …							…			

Table A2. Fragments of the truncated Test Table with the best pressure angle μ_e

N	LPT	rAB	BC	CD	XDnew	YDnew	fi_0	x_BP	y_BP	Sx	Sy	Kcos	Ksin	ε	μ_e
1	20759	0,2358	0,4869	0,4941	-0,4339	0,0492	244	0,9492	0,0822	1,9381	1,8672	-2,2753	-0,2580	**0,0052**	23,6
2	9031	0,2350	0,4850	0,4920	-0,4342	0,0511	244	0,9491	0,0899	1,9189	1,8760	-2,2715	-0,2675	**0,0053**	23,9
3	20623	0,2382	0,4900	0,4954	-0,4354	0,0484	242	0,9479	0,0786	1,9597	1,8496	-2,2685	-0,2524	**0,0054**	23,4
4	**29755**	0,2370	0,4841	0,4914	-0,4390	0,0615	243	0,9427	0,1097	1,8639	1,8787	-2,2340	-0,3132	**0,0054**	**24,4**
5	25015	0,2374	0,4805	0,4932	-0,4338	0,0600	244	0,9354	0,0934	1,8756	1,8754	-2,2617	-0,3130	**0,0054**	23,7
6	26807	0,2339	0,4830	0,4792	-0,4298	0,0393	245	0,9533	0,0935	1,9934	1,8621	-2,3072	-0,2112	0,0055	23,7
7	6231	0,2389	0,4828	0,4931	-0,4375	0,0633	242	0,9351	0,1027	1,8666	1,8698	-2,2392	-0,3238	0,0055	24,0
8	7327	0,2376	0,4776	0,4832	-0,4309	0,0543	244	0,9338	0,0998	1,9164	1,8660	-2,2846	-0,2881	0,0055	23,6
9	**23207**	0,2388	0,4885	0,4943	-0,4397	0,0579	241	0,9442	0,0988	1,9013	1,8607	-2,2356	-0,2944	0,0055	**24,0**

10	8119	0,2396	0,4883	0,4953	-0,4382	0,0567	241	0,9417	0,0915	1,9147	1,8544	-2,2444	-0,2905	0,0055	23,7
11	**10823**	0,2407	0,4871	0,4978	-0,4427	0,0686	241	0,9360	0,1079	1,8441	1,8652	-2,2059	-0,3419	0,0055	**24,3**
12	31419	0,2319	0,4901	0,4944	-0,4317	0,0387	246	0,9636	0,0706	1,9827	1,8737	-2,2980	-0,2060	0,0056	23,6
13	24175	0,2341	0,4746	0,4777	-0,4264	0,0464	246	0,9401	0,0969	1,9437	1,8754	-2,3178	-0,2523	0,0056	23,6
…	…				… … … …							…			
27	**10995**	0,2390	0,4854	0,4946	-0,4456	0,0739	242	0,9380	0,1282	1,7979	1,8819	-2,1843	-0,3622	0,0057	**25,1**

Table A3. Truncated Test Table: Best Accuracy Solutions with Pressure Angle Limitation μ_e>23.5 deg.

N	LPT	rAB	BC	CD	XDnew	YDnew	fi_0	x_BP	y_BP	Sx	Sy	Kcos	Ksin	accuracy	Transm. angle
1	**10995**	**0,2390**	**0,4854**	**0,4946**	**-0,4456**	**0,0739**	**242**	**0,9380**	**0,1282**	**1,7979**	**1,8819**	**-2,1843**	**-0,3622**	**0,0057**	**25,1**
2	4123	0,2377	0,4811	0,4860	-0,4410	0,0677	243	0,9372	0,1300	1,8290	1,8827	-2,2153	-0,3400	0,0058	**24,9**
3	14027	0,2338	0,4851	0,4887	-0,4371	0,0531	245	0,9539	0,1060	1,8972	1,8865	-2,2544	-0,2736	0,0057	**24,5**
4	**29755**	0,2370	0,4841	0,4914	-0,4390	0,0615	243	0,9427	0,1097	1,8639	1,8787	-2,2340	-0,3132	**0,0054**	**24,4**
5	21415	0,2403	0,4815	0,4928	-0,4403	0,0712	242	0,9294	0,1162	1,8242	1,8723	-2,2132	-0,3580	0,0057	24,3
6	20071	0,2376	0,4826	0,4833	-0,4371	0,0568	242	0,9412	0,1150	1,9008	1,8677	-2,2496	-0,2922	0,0057	24,3
7	**10823**	0,2407	0,4871	0,4978	-0,4427	0,0686	241	0,9360	0,1079	1,8441	1,8652	-2,2059	-0,3419	**0,0055**	24,3
8	31451	0,2453	0,4971	0,5167	-0,4519	0,0808	237	0,9346	0,0979	1,7969	1,8512	-2,1444	-0,3833	0,0057	24,3
9	29659	0,2318	0,4793	0,4822	-0,4311	0,0474	247	0,9525	0,1021	1,9199	1,8916	-2,2919	-0,2519	0,0057	24,2
10	5223	0,2415	0,4817	0,5012	-0,4413	0,0781	241	0,9242	0,1085	1,7877	1,8739	-2,1974	-0,3887	0,0057	24,2
11	28039	0,2471	0,4918	0,5196	-0,4509	0,0918	237	0,9206	0,1011	1,7424	1,8551	-2,1294	-0,4333	0,0057	24,1
12	23879	0,2448	0,4965	0,5110	-0,4494	0,0737	237	0,9370	0,0962	1,8381	1,8452	-2,1667	-0,3551	0,0057	24,1
13	3223	0,2351	0,4832	0,4766	-0,4330	0,0435	243	0,9513	0,1080	1,9731	1,8611	-2,2861	-0,2298	0,0057	24,1
14	**23207**	0,2388	0,4885	0,4943	-0,4397	0,0579	241	0,9442	0,0988	1,9013	1,8607	-2,2356	-0,2944	**0,0055**	**24,0**
…	…				… … … …							…			
22	9031	0,2350	0,4850	0,4920	-0,4342	0,0511	244	0,9491	0,0899	1,9189	1,8760	-2,2715	-0,2675	**0,0053**	23,9
…	…				… … … …							…			
39	20759	0,2358	0,4869	0,4941	-0,4339	0,0492	244	0,9492	0,0822	1,9381	1,8672	-2,2753	-0,2580	**0,0052**	23,6

Table A4. Truncated Test Table: Best Pressure Angle Solutions with Accuracy Limit ε<0.0058.